SUBSURFACE FRACTURE ANALYSIS USING FMI LOGS: IMPLICATIONS FOR REGIONAL STATE OF STRESS PREDICTION IN THE BLACK WARRIOR BASIN, ALABAMA

by

AYCAN YILDIRIM

ANDREW M. GOODLIFFE, COMMITTEE CHAIR

İBRAHİM ÇEMEN
DELORES ROBINSON
TONY SMITHSON

A THESIS

Submitted in partial fulfillment of the requirements
for the degree of Master of Arts
in the Department of Geological Sciences
in the Graduate School of
The University of Alabama

TUSCALOOSA, ALABAMA

2014

ABSTRACT

The Black Warrior Basin is a Paleozoic foreland basin located at the southern tip of the exposed northeast-trending Alleghanian fold-thrust belt. It is bounded by the northwest-trending Ouachita fold-thrust belt to the southwest. The eastern Black Warrior Basin is broken by a multitude of thin-skinned normal faults that generally strike northwest, parallel to the Ouachita trend and perpendicular to the Alleghanian trend. However, little is known about the regional state of stress in the Black Warrior Basin. This study uses FMI (Fullbore Formation MicroImager) and other conventional open hole logs to define the orientation of subsurface natural fractures. Using well log data from the Gorgas #1, the present-day stress orientation was interpreted from induced fractures (borehole breakouts and drilling-induced tensile fractures), indicating a maximum horizontal stress orientation (S_{Hmax}) of N 65°E. The image log interpretation revealed three sets of conductive and resistive fractures with strikes of (i) 45°-75°, (ii) 300°-320°, and (iii) 0°-10°. Fracture sets (i) and (ii) were interpreted as a part of the previously identified and documented regional east-northeast (ENE) joint system and the cross-fold joint system, respectively. Fracture set (iii) consists of only resistive (healed) fractures detected in the Lower Pottsville and older strata. It is postulated that the origin of these NNE oriented fractures, on the basis of the subsidence pattern of the Pennsylvanian strata in the basin and the similarity with the regional joint system observed in the Arkoma basin, is the Ouachita orogeny. The interpreted NNE Ouachita convergence direction indicates that thin-skinned normal faults in the Pottsville Formation are not related to the Ouachita thrust belt system, but

are instead related to the NE-SW oriented extensional stress field created at a right angle to the northwest-converging Alleghanian orogeny.

DEDICATION

This thesis is dedicated to my parents for making me who I am, and my wife and brother for supporting me all the way.

LIST OF ABBREVIATIONS AND SYMBOLS

ft	Feet
in	Inch
m	Meter
mi	Mile
km	Kilometer
Ga	Billion years
Ma	Million years
BWB	Black Warrior Basin
DITF	Drilling-induced tensile fracture
ECS	Elemental Capture Spectroscopy Sonde
FMI	Fullbore Formation MicroImager
WSM	World Stress Map
2–D	Two-dimensional
3-D	Three-dimensional
±	Plus or minus (range indicator)
°	Degree
%	Percentage
~	Approximately equal to

ACKNOWLEDGMENTS

I would first like to extend a special thanks to my advisor, Dr. Andrew Goodliffe, for allowing me the opportunity to work on this project. It has been a great learning experience and has provided me with a skill set that I will continue to use in my career as a professional geologist. I would also like to thank all of my committee members, Dr. İbrahim Çemen, Dr. Delores Robinson, and Tony Smithson for their invaluable input, careful review, and support of both the thesis and my academic progress.

This research would not have been possible without the support of my family and wife who never stopped encouraging me to persist. I also express my gratitude toward all the fellow graduate students, faculty, and staff of the Department of Geological Sciences at The University of Alabama that overlapped their presence here with mine. Thanks to each one of you for creating such a warm and supportive environment for both personal growth and scientific progress. Thanks to Heather Black for her final touch-ups on my grammar in this thesis.

I want to express my appreciation to Turkish Petroleum Corporation (TPAO) for their financial support. Data collection would not have been possible without the financial support of an American Recovery and Reinvestment Act grant issued by the Department of Energy and the National Energy Technology Lab.

TABLE OF CONTENTS

LIST OF TABLES

LIST OF FIGURES

1. INTRODUCTION

The Black Warrior Basin, located in northwestern Alabama and northeastern Mississippi, is a 90,000 km^2 Paleozoic foreland basin (Thomas, 1977; Hatch and Pawlewicz, 2007; Figure 1). The basin has a triangular outline that is bounded to the southwest by the northwest-trending Ouachita thrust front, to the east and southeast by the northeast-trending Alleghanian thrust front, and to the north by the Nashville dome (Horsey, 1981; Thomas, 1988; Figure 1). The eastern

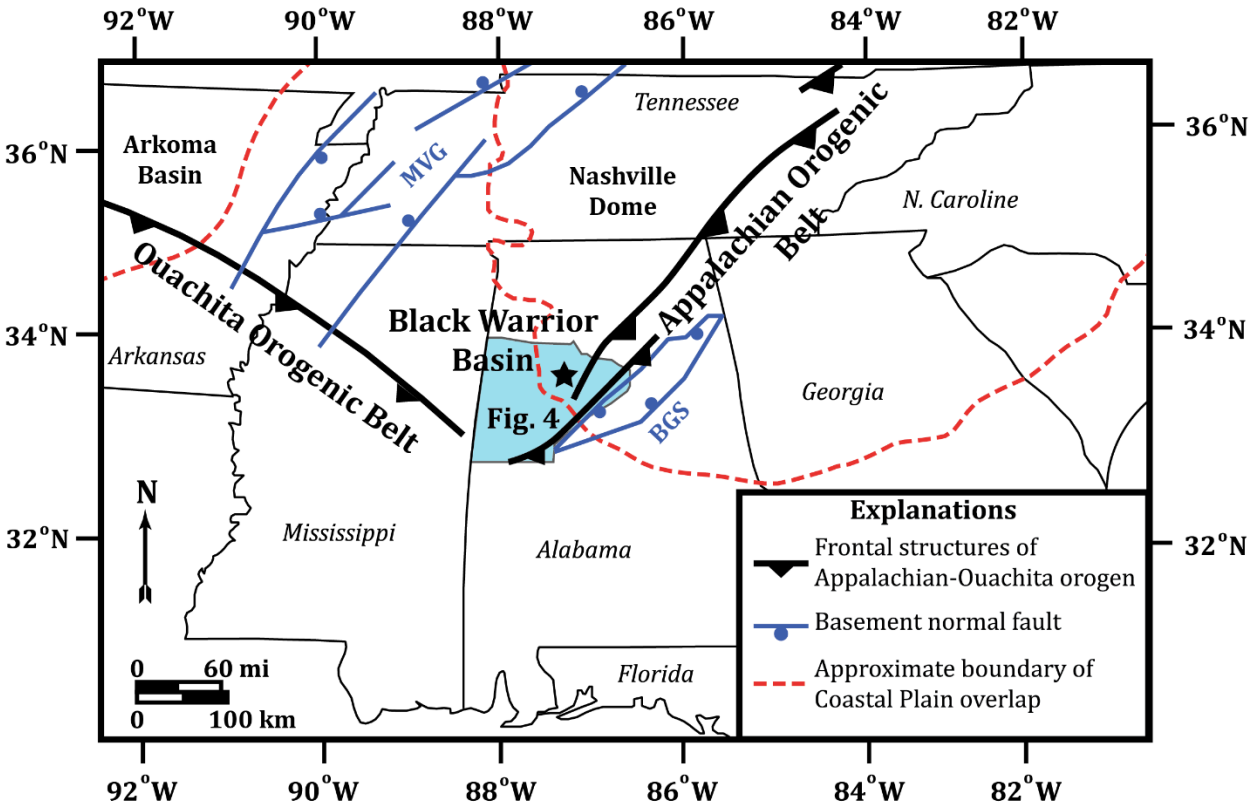

Figure 1: Tectonic map showing the location of the Black Warrior Basin and the Gorgas #1 well (black star) in relation to the Ouachita and Alleghanian fold-thrust belts and the regional graben systems (modified from Groshong et al., 2010). The blue shaded area refers to the location of Figure 4. BGS, Birmingham graben system; MVG, Mississippi Valley graben.

portion of the basin outcrops in north-central Alabama. The western part of the basin is buried below the Mesozoic-Cenozoic strata of the Gulf Coastal Plain, which unconformably overlies the Paleozoic sequence (Mellen, 1947; Whiting and Thomas, 1995). In the northeast, the basin is separated from the Appalachian Basin by a low, indistinct arch that plunges southeastward from the Nashville dome. In the west, the basin is separated from the Arkoma Basin by the Mississippi Valley graben (Thomas, 1988). The Sequatchie anticline, a large fault bend fold, is the frontal structure of the exposed Alleghanian thrust belt. The amplitude and the fault displacement of this anticline decreases gradually southwestward.

The Black Warrior Basin has a polyphase tectonic history and collected sediment throughout the Late Paleozoic Alleghanian-Ouachita orogenesis and Mesozoic rifting. All structures are pre-Cretaceous in age in the basin and are truncated by the unconformity at the base of Gulf of Mexico coastal plain sediments (Groshong *et al.,* 2010). Located at the junction of the frontal structures, trends of the Ouachita and Alleghanian thrust belts converge nearly at right angles within the basin. The relation of the two orogens is incompletely determined. The diverse structures types formed in the Black Warrior basin suggest a heterogeneous distribution of compressional and extensional strain related to basin-forming processes.

The Black Warrior Basin is economically important due to the oil and gas reserves in the multiple Paleozoic reservoirs and extensive coal and coalbed methane resources in the Pennsylvanian section. There is current commercial coalbed methane production from 20 coalbed gas fields discovered in the Pennsylvanian Pottsville Formation in Alabama (Hatch and Pawlewicz, 2007). Commercial and noncommercial hydrocarbon exploration has taken place or is ongoing in the Mississippian and Pennsylvanian sandstones, the Mississippian limestones, the Devonian cherty limestones, and the Ordovician limestones (Epsman, 1987). Asphaltic rocks of

the Mississippian tar sands crop out in north-central and northwest Alabama, and the widespread Hartselle Sandstone is considered to have the best potential for future hydrocarbon exploration operations (Hatch and Pawlewicz, 2007). Multiple shale gas plays in Cambrian, Devonian, and Mississippian strata of the southern Appalachian thrust belt of Alabama have good economic potential.

Increasing greenhouse gas emissions related to the coal-fired power facilities and the need for enhanced methane recovery from coal beds, has led to a number of CO_2 sequestration projects in the Black Warrior Basin. The downhole logs used in this study originate from one of these projects in the vicinity of Gorgas Power Plant, Walker County, Alabama (Rutter, 2012).

In this study we will test the follow hypotheses: 1) the paleostress state can be derived in the Black Warrior Basin by interpreting the structural features from resistivity image logs; 2) the Pottsville Formation thin-skinned normal faults in the northeast part of the Black Warrior Basin are developed in response to the northwest-vergent Alleghanian thrust belt. The main objectives of this study are to: (1) determine the geometry of subsurface natural fracture systems within the Black Warrior Basin by interpreting structural features from FMI resistivity image logs; (2) determine the contemporary stress field affecting the basin; (3) determine the architecture of the state of (paleo) stress field related to faults and fractures; (4) determine if any structural influence from the Ouachita thrust belt is observed in the basin. This is the first study to estimate the paleostress field based on FMI log fracture analysis. The FMI fracture analysis presented here provides insight into the spatial and temporal variations of Ouachita- and Alleghanian-related structural features within the basin.

1.1. Fracture Systems in the Black Warrior Basin

Faults and fractures provide a useful tool for the study of regional tectonics and have a significant impact on conventional oil and gas exploration and carbon sequestration reservoir quality. In large part driven by coalbed methane production (Pashin *et al.*, 1991, 1995; Pashin and Groshong, 1998; Groshong *et al.*, 2010), map-scale structures have been extensively documented in the Black Warrior Basin, especially in the Pennsylvanian section. Numerous northwesterly trending normal faults cutting the Pennsylvanian Pottsville Formation sediments have been observed within the basin (Wang *et al.*, 1993; Cates and Groshong, 1999). Fracture systems associated with the Alleghanian orogeny were also recognized in outcrops and coal mines (Ward *et al.*, 1984; Groshong *et al.*, 2009).

The origin and evolution of structural features in a basin is strongly controlled by the changes in the lithospheric stress fields (Angelier, 1994; Michael, 1984; Engelder, 1993; Delvaux *et al.*, 1995, 1997; Brandes *et al.*, 2013; Tripathy and Saha, 2013). The orientation of new fractures and faults in a sedimentary basin is systematically related to the orientation of the regional contemporary stress field (Brandes *et al.*, 2013). The present-day state of stress is described by the stress tensor, comprising three orthogonal principle stresses, each with a magnitude and orientation. In many sedimentary basins, it is assumed that one principal stress acts vertically (Anderson, 1951; Figure 2). Therefore, the stress tensor is simplified to consist of four components, the magnitudes of the vertical (S_V), maximum horizontal (S_{Hmax}) and minimum horizontal stresses (S_{hmin}) in addition to the orientation of the maximum horizontal stress (Bell, 1996; Tingay *et al.*, 2009). The vertical stress can be the greatest, the intermediate, or the least principal stress (Figure 2).

Different paleostress inversion methods have been developed that use the orientation of beds, faults, fractures, styolites, and slickensides on these surfaces (Etchecopar *et al.*, 1981; Angelier *et al.*, 1982; Michael, 1984; Angelier, 1990; Pollard *et al.*, 1993). Fractures, including

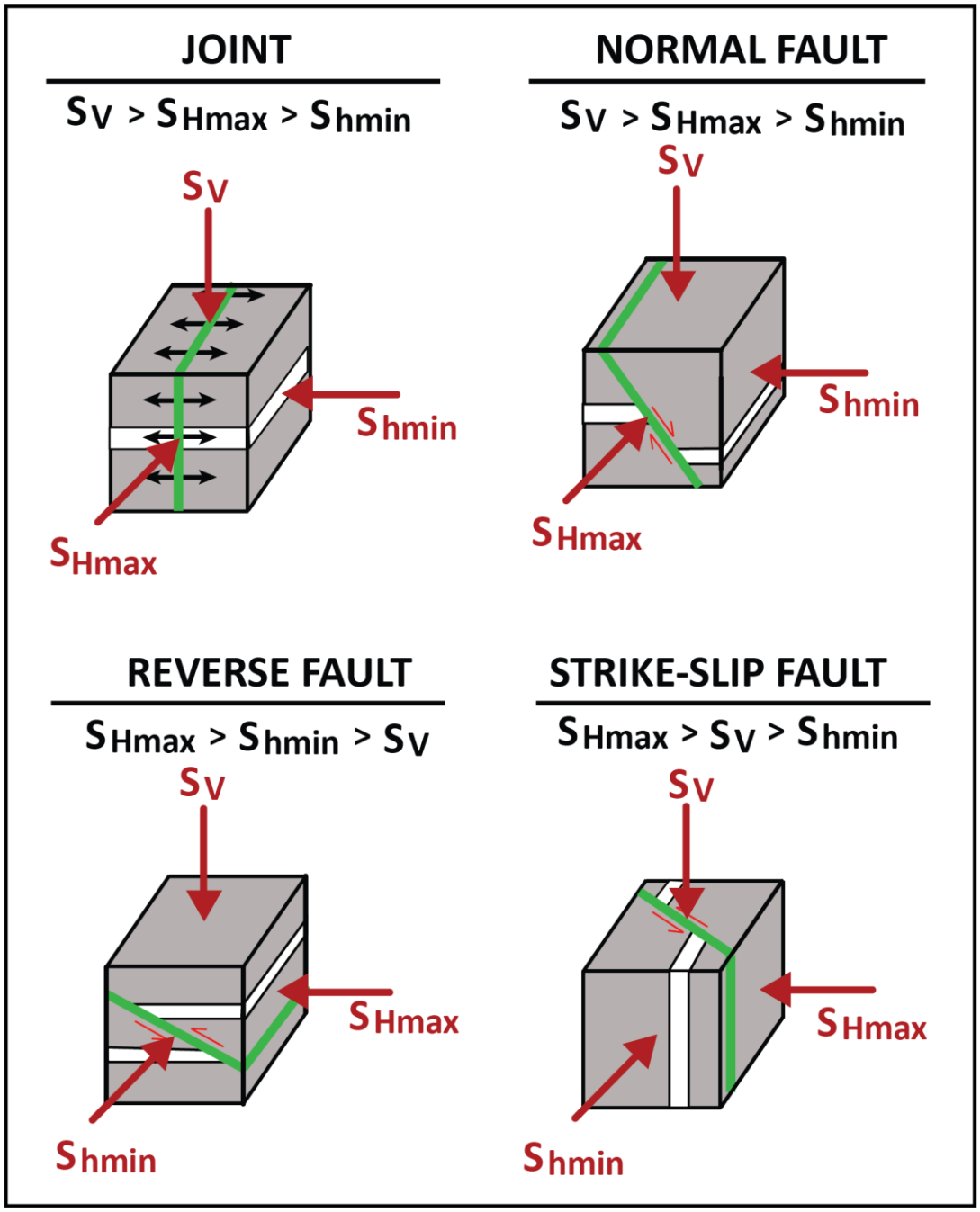

Figure 2: Common fracture styles, displacements and orientations relative to principal stress directions in the Earth's crust. The relative magnitudes of the stresses dictate the type of faulting in a given region (modified from Narr et al., 2006). S_V, vertical stress; S_{Hmax}, maximum horizontal stress; S_{hmin}, minimum horizontal stress.

natural and induced fractures, are the most abundant visible structural features formed in the Earth's upper crust in response to brittle failures. Natural fractures are those related to natural deformation of the rock including faults, joints, veins, and stylolites. Joints, which show no displacement, are extensional fractures that form in tension (Figure 2). Faults are shear fractures which experience later shearing displacement. Shearing displacement is the main characteristic used to discriminate faults from joints (Narr *et al.*, 2006; Figure 2). Induced fractures are those induced artificially including by core handling, coring, drilling, fluid injection (Ameen, 2003).

Fracture systems in the Black Warrior Basin include joints, cleats, and fault-related shear fractures (Pashin *et al.*, 2004). In outcrops and underground coal mines, the siliciclastic rocks are dominated by an orthogonal joint system consisting of planar systematic joints, orthogonal cross joints, and face and butt cleats in coal (Ward *et al.*, 1984; Pitman *et al.*, 2003). Systematic joints and face cleats strike northeast (Figure 3). The regional ENE joint and cleat set has been recognized to be part of an Appalachian-wide stress field (AWSF) trend (Engelder and Whitaker, 2006). The early stages of convergence between Gondwana and Laurentia, during the final assembly of Pangea, generated the AWSF and related fracturing with the shortening direction aligned ENE, indicating minimum stress (σ_3) to be oriented NNW-SSE, parallel to the convergence direction (Engelder and Whitaker, 2006). The other fracture set consists of a northwest-striking system that is superimposed on the regional joint and cleat systems and restricted to Alleghanian folds (Ward *et al.*, 1984; Figure 3). In the Pottsville Formation systematic joints of the regional joint system strike with a vector-mean azimuth of N47°E, and face cleats strike an average N62°E. In comparison, cross-fold joints and cleats strike with a vector-mean azimuth of N64°W and N36°W, respectively (Pitman *et al.*, 2003).

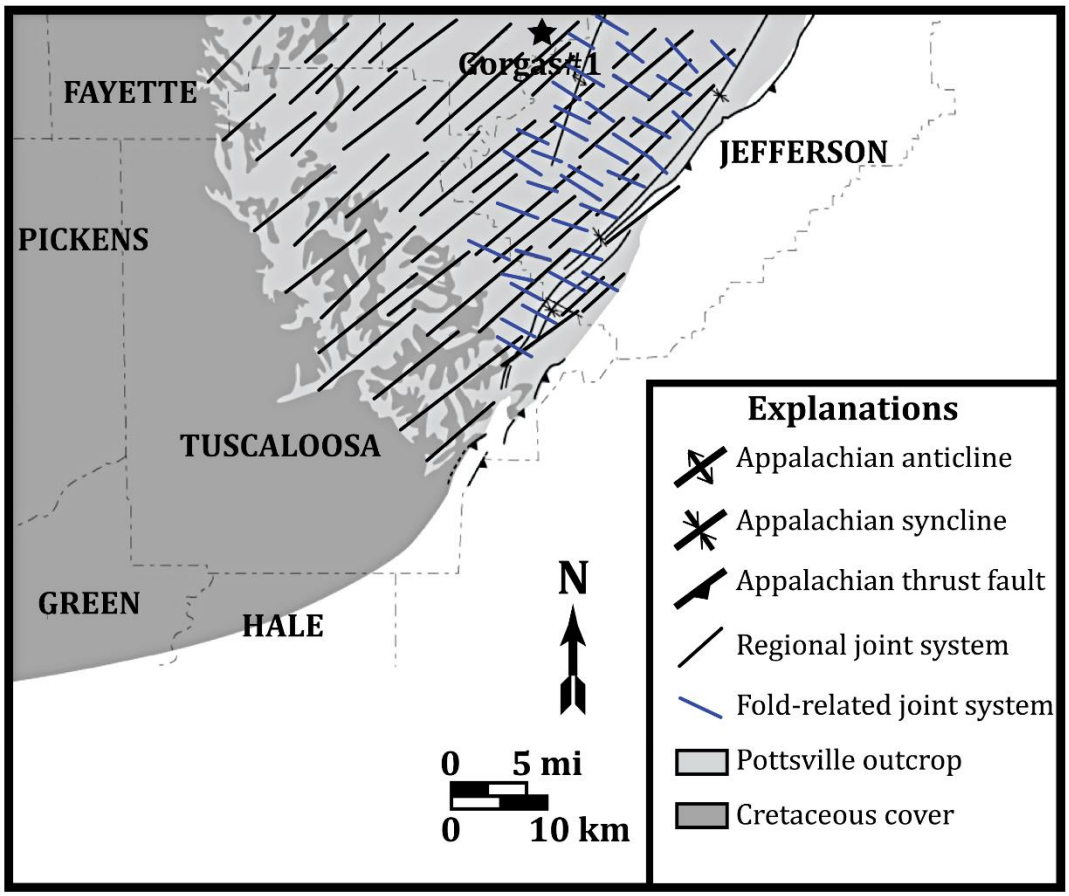

Figure 3: Generalized map showing joint systems in the eastern Black Warrior Basin (modified after Pashin et al., 2004).

1.2. Regional Tectonic Evolution

Starting in the Cambrian the region underwent a transition from clastic units to Cambrian-Ordovician stable shelf carbonate ramp facies (Thomas, 1985; Raymond *et al.*, 1988), continuing as a passive margin for 200 million years until the Mississippian (Thomas, 1976; Pashin and Gastaldo, 2009). By Mid-Cambrian time, closure of the Iapetus Ocean east of the continent had begun with the establishment of an arc-trench system offshore (Miall and Blakey, 2008). The oblique collision of arcs with the southwestern side of the Alabama Promontory forced an accretionary prism onto the former transform margin (Thomas, 1976; Viele and

Thomas, 1989; Robinson *et al.*, 2012). The Black Warrior Basin first formed as a foreland basin in response to the obduction of a Ouachita accretionary prism in the Mid- to Late Mississippian (Thomas 1976, 1991). The southern margin of the Alabama Promontory is commonly interpreted as an ancient transform margin related to Iapetus seafloor spreading. This transform offset the Blue Ridge rift to the Ouachita rift along the Alabama-Oklahoma transform fault. The Birmingham graben and Mississippi Valley syn-rift intracratonic fault systems are part of the same system (Thomas, 1991, 2011; Figure 1). Other workers, based on the absence of a geophysical signature and expected structural features (Robinson et al., 2012) have debated the presence of this transform.

On the eastern margin of Laurentia, a series of Paleozoic mountain-building events, the Middle Ordovician to Early Silurian Taconic, Devonian-Mississippian Neoacadian, and Pennsylvanian-Permian Alleghanian orogenies, ended with the closure of the Iapetus Ocean and formation of Pangea (Ettensohn, 2008). No stratigraphic record of the Taconic or Acadian orogenies is recognizable west of the Alabama Promontory (Robinson *et al.*, 2012). The basin was sheltered from Appalachian tectonic activity and sediment sources by the Birmingham graben until the Early Pennsylvanian (Pashin, 2004). The Alleghanian orogeny is comprised of northeast-striking, northwest-vergent thrust faults and associated folds bounded by undeformed strata on the northwest and by the Talladega slate belt and Appalachian Piedmont on the southeast (Bayona et al., 2003). By the end of this mountain-building period, the Black Warrior Basin was confined to its present location and formed as a faulted homocline that dips southwest in response to two separate converging thrust and sediment loads: (1) the Ouachita accretionary prism along the southwest side of the basin, and (2) thrust-imbricated passive-margin rocks in

the Alleghanian thrust belt along the southeast side of the basin (Thomas, 1977; Hines, 1988; Whiting and Thomas, 1994; Figure 1).

The Late Paleozoic through Early Triassic marked thermal reequilibration, uplift, and erosion during a tectonically quiescent period prior to the onset of Late Triassic Gulf of Mexico extensional deformation at ~215 Ma (Huerta and Harry, 2012). Rifting triggered the basin downwarping to the southwest and deposition of the Mesozoic cover sequence (Mancini *et al.*, 1983). Deposition and lithification of the Gulf of Mexico coastal plain occurred from the Cretaceous to present.

Within the Black Warrior Basin, a multitude of northwest-trending normal faults form horst, graben, and half graben structures (Figures 4, 5). Late Precambrian through Pennsylvanian normal faults were episodically active in the region (Figure 5). None of the extensional faults in the Black Warrior Basin offset the Cretaceous section. In the southwest deeper deformational features and multiple normal fault sets have been interpreted by Groshong *et al.* (2010). Many small planar faults offset the top of basement and die out near the top of the Rome and Conasauga Formations (Figure 5). These faults are coeval with the Rome and Conasauga sedimentation and are likely associated with the Iapetan rifting. Some faults offset basement and die out near the top of the Knox carbonate section (Figure 5). This Middle Cambrian to Lower Ordovician growth faulting is the product of Rheic rifting (Groshong *et al.*, 2010). Faults penetrating the complete Paleozoic section (Figure 5) were reactivated as a result of subsidence of the foreland basin associated with the Appalachians during Taconic, Acadian, and Alleghanian orogenies.

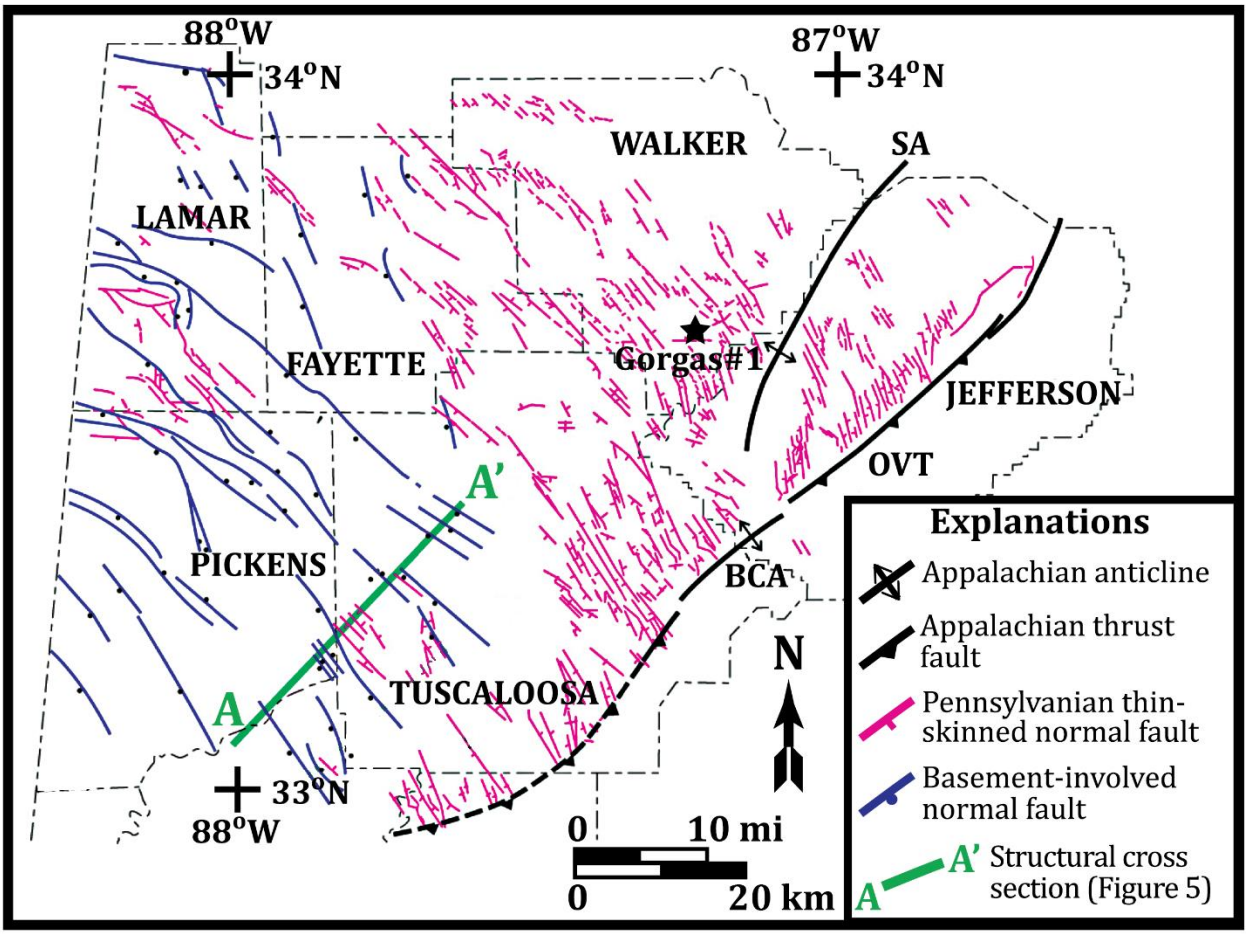

Figure 4: Structural map of the Black Warrior Basin showing the relationship among frontal Alleghanian structures and normal faults in the Black Warrior Basin (modified from Groshong et al., 2010). BCA, Blue Creek anticline; OVT, Opossum Valley thrust; SA, Sequachie anticline. Black star shows the location of the Gorgas #1 well.

The Birmingham graben system trends NE-SW and is overlain by the frontal part of the Alleghanian fold and thrust belt (Thomas, 1985, 1989; Figure 1). The Birmingham graben system has been interpreted as a faulted half graben that consists of multiple faults with a master fault on the southeastern side and active Late Precambrian to Middle Cambrian faults associated with Iapetus rifting (Groshong *et al.*, 2010).

Toward the northeastern part of the Black Warrior Basin, deformation is dominated by ramp-flat style thin-skinned faulting with faults maintaining planar 60°-70° dips until joining the

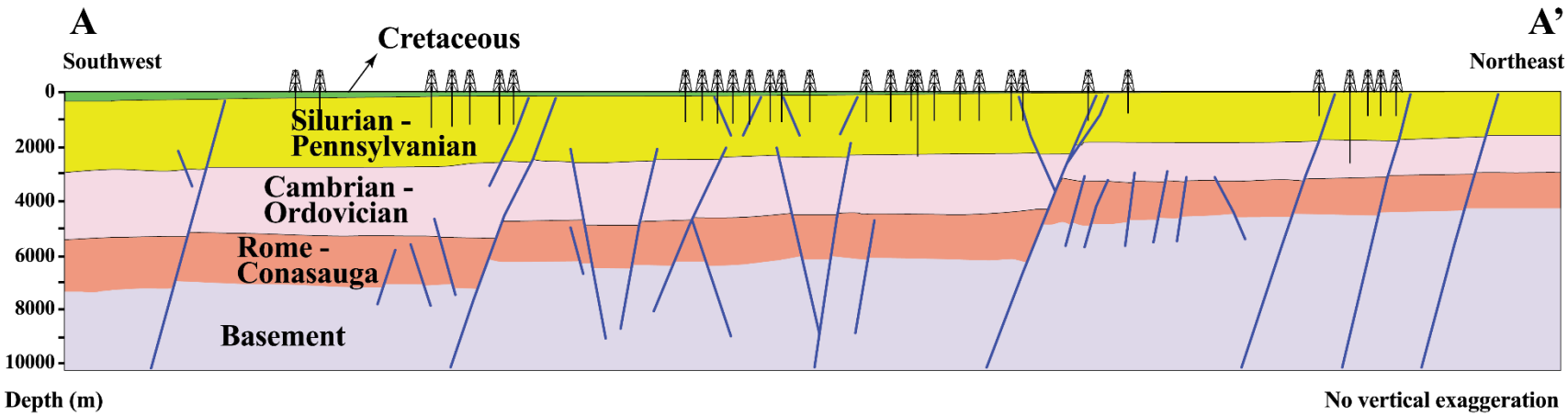

Figure 5: Structural cross section showing thin-skinned and basement involved growth faults in the Black Warrior Basin (modified from Groshong et al., 2010). See Figure 4 for location.

lower Pottsville detachment (Wang *et al.*, 1993). The strike of these faults is perpendicular to the Alleghanian trend and sub-parallel with the Ouachita trend (Figure 4).

Brittle deformation features on the Pottsville Formation thin-skinned normal faults indicate post-depositional deformation after lithification (Groshong *et al.*, 2009). The age of these faults is not well studied in the Black Warrior Basin. Bradley and Kidd (1991) and Cates *et al.*, (2004) have interpreted these faults as a result of Ouachita flexural extension due to similarities with the Arkoma Basin. Based on such studies, researchers have argued that the stratigraphic and structural architecture of the Black Warrior Basin has been affected mostly by the Ouachita orogeny (Thomas, 1989; Cates *et al.* 2004; Groshong *et al.*, 2010). An intersection between the northwest-trending Ouachita thrust belt and the northeast-trending Alleghanian thrust belt under the Gulf coastal plain sediments in central Alabama has been inferred (e.g., Branan, 1968, Thomas, 1991, 2004). In contrast, Robinson *et al.* (2012) failed to find interference structure that would support this hypothesis. A total effective subsidence study (Pashin, 2004) of the Pottsville Formation depositional cycles of Alabama showed that prior to the Pottsville deposition, subsidence increased toward the southwest, suggesting development of a Ouachita foreland basin with little effect from Alleghanian tectonism. The same study also concluded that the basal contact of the Pottsville Formation coincides with initiation of the depocenter adjacent to the Alleghanian thrust belt to the southeast. This was fully developed by end of the Early Pennsylvanian.

1.3. Stratigraphy

Stratigraphic descriptions and thicknesses are derived from the Gorgas #1 well data in conjunction with interpreted seismic reflection profiles and well logs (Thomas and Bayona,

2002; Groshong *et al.*, 2010; Robinson *et al.*, 2012; Rutter, 2012). The Black Warrior Basin is predominantly composed of clastic and carbonate units that reflect the polyphase tectonic history and related paleoceanographic changes that prevailed from Cambrian through Permian age (Figure 6).

The Precambrian basement ranges in age from 750 Ma to 1 Ga and comprises igneous and metamorphic rocks that are nonconformably overlain by the oldest stratigraphic units recognized in the basin, the Cambrian rift-fill clastic sequence. This sequence consists of the ~90-300 m (295-1000 ft) thick Early Cambrian Rome Formation and the ~200-300 m (650-100 ft) thick Conasauga Formation (Neathery and Copeland, 1983; Ferrill, 1989). The Rome Formation was deposited as a shallow carbonate bank (peritidal depositional environment) and supplied clastic material from the craton to the west (Haase et al., 1985; Thomas, 2011). The Conasauga Formation was deposited in a shallow shelf environment and encompasses an upward transition from clastic to carbonate deposition (Haase et al., 1985; Thomas, 2011). These fine-grained clastic rocks act as the main detachment surface for Alleghanian thrusting (Thomas and Bayona, 2002). The great thickness of the Conasauga Formation in the Birmingham Graben and the paleobathymetric relief indicate synsedimentary fault movement on the basement faults during deposition (Nance and Linnemann, 2008; Thomas, 2011).

By the Late Cambrian, the Conasauga Formation was overlain by the westward transgression of the passive margin carbonate platform of the Knox Group across the Birmingham Graben and boundary faults, constraining the age of the end of rift-stage fault movement (Haase et al., 1985; Thomas, 1989; Thomas, 2011). Cambrian dolomites include the ~ 400-600 m (1300-2000 ft) thick dolomitic portion of the Conasauga Formation and the Ketona Dolomite (Raymond, 1991). The Cambrian-Ordovician Knox Group is typically 900-1500 m

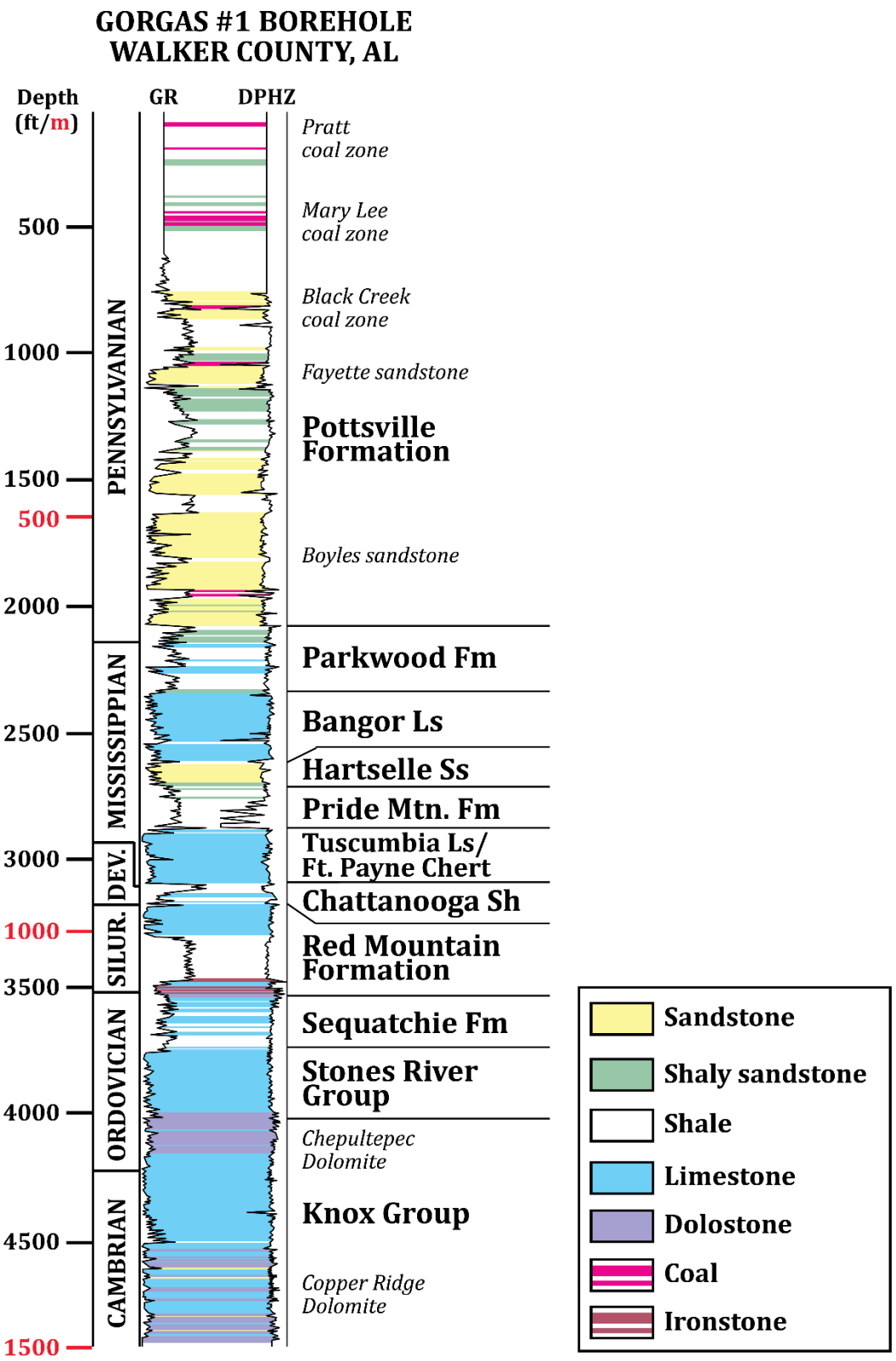

Figure 6: A stratigraphic section for the Gorgas #1 well showing formation thickness, lithology, gamma ray (GR) and density porosity (DPHZ) content (J. Pashin, personal communication, 2012).

(3000-5000 ft) thick regionally and includes, in ascending order, the Copper Ridge Dolomite, Chepultepec Dolomite, Longview Limestone, Newalla Limestone, and Odenville Limestone. The most distinctive characteristic of the Knox Group dolomite units is their chert content. The chert-free part of the group is defined as the Ketona Dolomite (Raymond et al., 1988). The Knox Group includes all five units east of the Helena thrust fault in the Alleghanian thrust belt. West of the Helena thrust fault in the Black Warrior basin, the Knox Group is subdivided into the Copper Ridge and Chepultepec Dolomites (Raymond, 1991). Units older than the Chepultepec Dolomite are not penetrated by the Gorgas well, but are present below based on previous studies (Groshong *et al.*, 2010; Robinson *et al.*, 2012). The Knox Group was reached at a depth of 1221 m (4007 ft) at the Gorgas well and includes a 150 m (493 ft) section of Chepultepec Dolomite and a 127 m (415 ft) section of Copper Ridge Dolomite above the base of the well at 1498 m (4915 ft). The Copper Ridge Dolomite contains dolomites that range from mudstones to grainstones with scattered chert beds and some siliciclastic input. The basal part of the Chepultepec Dolomite is characterized by a thick-bedded limestone. The upper part of the unit comprises thick- and thin-bedded coarse-crystalline dolomite with abundant cavernous and fossiliferous chert (Raymond et al., 1988).

The Knox Group was formed during a time of maximum transgression and the top of the unit has been interpreted as a karstic unconformity (Raymond *et al.*, 1988) overlain by the Middle Ordovician Stones River Group and Upper Ordovician Sequatchie Formation. The Stones River Group has a thickness of 80 m (261 ft) and consists of finely laminated black shale and limestone. The Sequatchie Formation is present from 1057-1142 m (3467-3746 ft). The formation contains limestone with interbedded black shale. Together with the Stones River Group it represents a varying tidal environments on the carbonate shelf.

The Silurian Red Mountain Formation extends from 952-1057 m (3124-3467 ft) and includes siltstone that fine upwards into shale, which in turn grades into limestone. The base of the formation is identified by elevated density log measurements indicating oolitic ironstone. The oolitic ironstone deposits indicate a shallow shelf or an area close to the transition from nonmarine to marine environments. On top of the Silurian strata, the Devonian Chattanooga Shale is a black fissile shale identified by an increase in gamma ray log measurements. At the Gorgas well, the Chattanooga Shale, from 941-952 m (3088-3124 ft), is calcareous and interbedded with limestone.

In the southwestern part of the Black Warrior Basin, a clastic facies of shale and sandstone comprises the Floyd Shale and Parkwood Formation. This grades northeastward into the carbonate facies in the vicinity of Birmingham, where the facies boundary is approximately perpendicular to Alleghanian structural strike (Thomas, 1972). Tongues of clastic rocks pinch out northeastward within the carbonate facies, where the stratigraphic sequence above the Fort Payne Chert comprises Tuscumbia Limestone, Pride Mountain Formation (a relatively thin tongue of Floyd Shale), Hartselle Sandstone, and Bangor Limestone (Thomas, 1972; Figure 7). The 20 m (67 ft) thick Fort Payne Chert unit comprises limestone and nodular chert that has a gradational contact with the overlying 44 m (143 ft) thick section of predominantly wackestone Tuscumbia Limestone. These Early Mississippian units indicate the persisting passive margin carbonate shelf along the southern edge of the Alabama Promontory. Synorogenic clastic wedge progradation and interfingering between siliciclastic and carbonate depositional systems have been interpreted as a result of Late Mississippian arc-continent collisions along the southeastern edge of the continent (Thomas, 1972; Pashin and Gastaldo, 2009). The 52 m (172 ft) thick Pride Mountain Formation, a heterogeneous unit with shale, limestone, and sandstone, overlies the

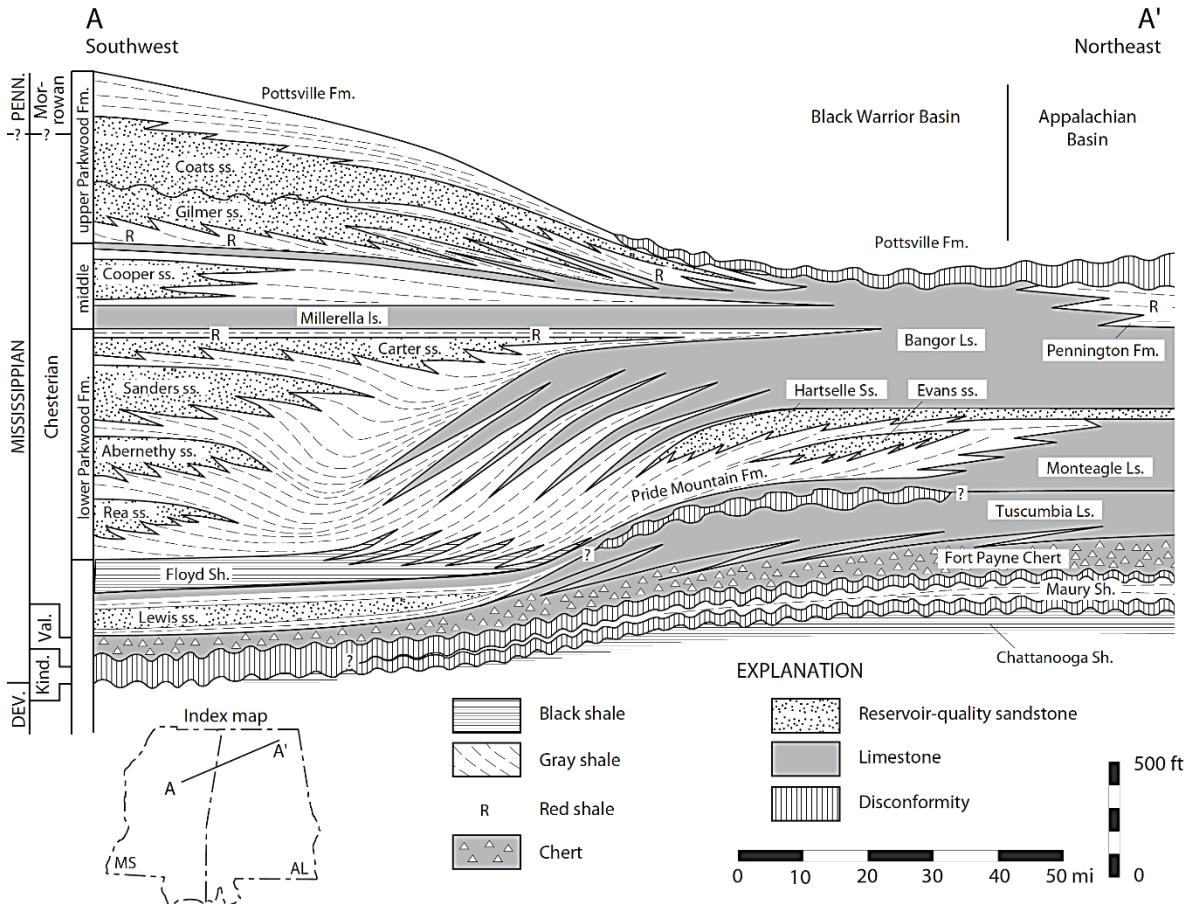

Figure 7: Generalized Mississippian stratigraphy showing facies relationships in the Black Warrior Basin (Pashin and Gastaldo, 2009).

Early Mississippian section with a disconformity. The Late Mississippian Pride Mountain Formation has a gradational contact with the 27 m (87 ft) thick Hartselle Sandstone and marks the beginning of Ouachita orogenesis. The Hartselle Sandstone is a well-sorted, fine-medium grain quartz arenite found at a depth of 797-824 m (2615-2702 ft). The Pride Mountain Formation and Hartselle Sandstone contain beach and tidal facies. The source of the siliciclastic rock is controversial; some workers favor cratonic sources (e.g., Driese et al., 1994) while others favor sources in the Ouachita orogeny (e.g., Thomas and Mack, 1982). The Late Mississippian 90 m (295 ft) thick Bangor Limestone unit has a fossiliferous limestone section in the upper part and a less fossiliferous limestone with an interbedded shale section in the lower part. The

Parkwood Formation shows a transition from marine transgression and carbonate sedimentation to siliciclastic-dominated successions indicating the beginning of the Alleghanian orogeny in the Black Warrior Basin (Pashin and Gastaldo, 2009).

The Pennsylvanian Pottsville Formation, the youngest Paleozoic sedimentary unit, reaches a depth of 631 m (2071 ft) at the Gorgas well and is exposed at the surface. The lower Pottsville Formation consists mainly of quartzose sandstone with thin coal beds and is divided into the lower Boyles, upper Boyles, and Fayette Sandstone cycles. The Gorgas well shows a thickness of 104 m (341 ft) for the lower Boyles Sandstone, 66 m (215 ft) for the upper Boyles Sandstone, and 107 m (350 ft) for the Fayette Sandstone. The upper Pottsville Formation is thicker than 325 m (1065 ft) and consists of sandstone and shale with numerous economic coal beds. The upper part of the Pottsville Formation is subdivided into depositional cycles (Pashin, 1991), and each cycle starts with a marine mudstone which grades upward into deltaic sandstone and is capped with a marginal-marine to terrestrial coal group comprised of interbedded mudstone, sandstone, and coal (Pashin, 1991; Wang, 1994). The source of the Pennsylvanian synorogenic clastic sediments has been interpreted to be the growing mountains of the Alleghanian orogeny (Pashin, 2004; Robinson *et al.*, 2012).

2. DATA AND METHODOLOGY

2.1. FMI Details and Data Processing

The Gorgas #1 well was drilled to a total depth of 1498 m (4915 ft) in the vicinity of Gorgas Power Plant in Walker County, Alabama (Figures 1, 3, and 4). A suite of open hole wireline logs including Schlumberger's FMI® (Fullbore Formation MicroImager) and ECS® (Elemental Capture Spectroscopy Sonde) were collected from the well. The gamma ray, neutron porosity, and density porosity logs were used to determine lithologic boundaries and heterogeneity within sedimentary units. The caliper logs were used to determine borehole rugosity. Mud log data covers the depth range of 10-1498 m (40-4915 ft). However, FMI, ECS, and other conventional logs have measurements from 235 m (770 ft) to 1495 m (4900 ft) as a result of surface casing from the surface to 235 m (766 ft). The log measurements have poor quality between 850 m (2785 ft) and 875 m (2875 ft) due to a major washout in the Pride Mountain Formation.

2.2. FMI Tool and Borehole Image Interpretation

Electrical borehole images are based on dipmeter technology that has been in use commercially since the 1950s (Hurley, 1994). Electrical images are best used in conjunction with other available wellbore data, such as other wireline logs, cuttings, cores, and production data. The FMI® Fullbore Formation MicroImager tool consists of two perpendicular pairs of caliper arms with the end of each arm hosting a pad and attached flap (Figure 8). The pads and flaps

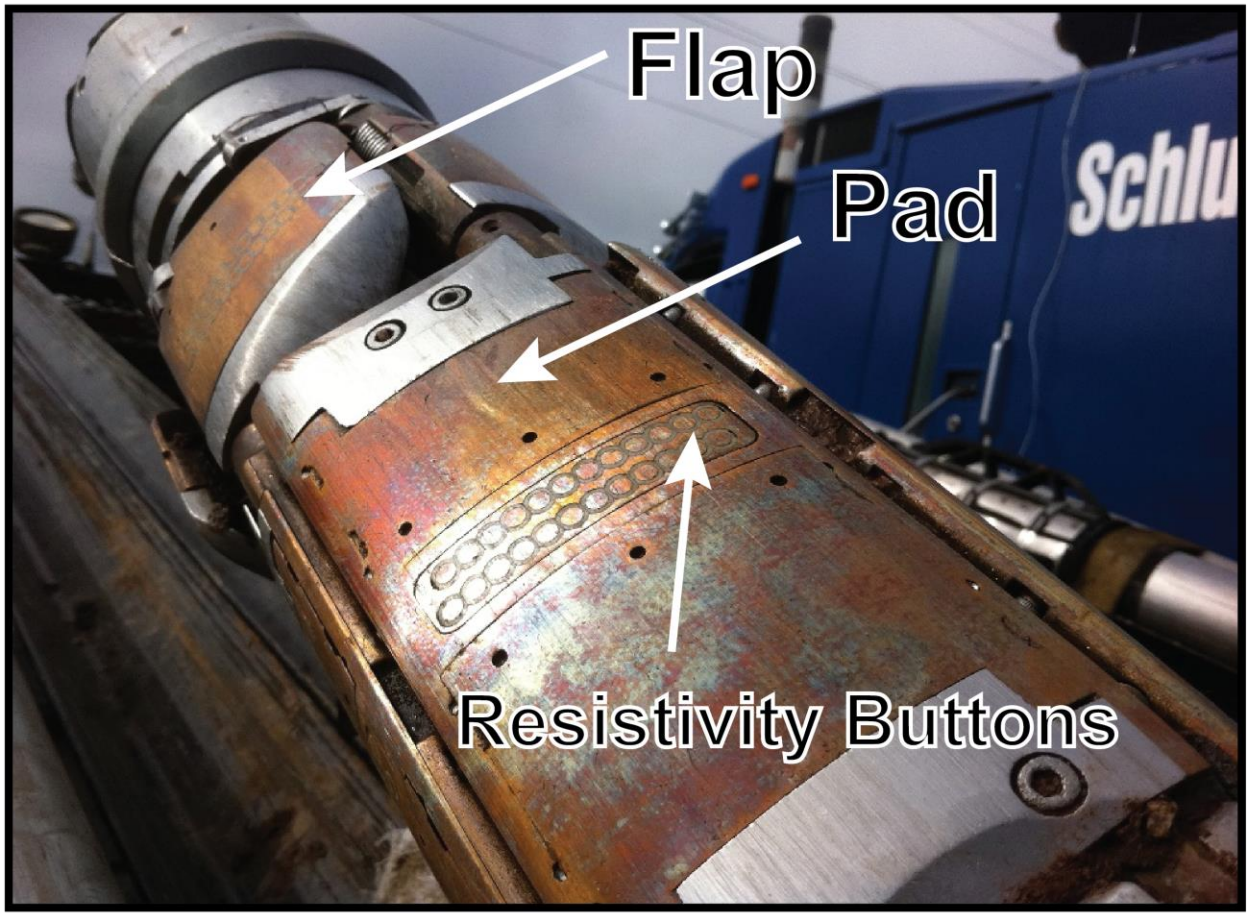

Figure 8: A close-up of the Formation MicroImager (FMI) logging tool used by Schlumberger to log the Gorgas #1 well.

contain 192 resistivity sensors (24 on each pad or flap), the data from which can be processed to build up resistivity images of the wellbore wall. The diameter of each resistivity button is 5 mm. Objects smaller than 5 mm may be visible, depending on the resistivity contrast. Characterization of a feature requires imaging by multiple sensors. Areal coverage of the FMI image is a function of borehole diameter. For an 8-inch borehole, 80% of the interior surface is imaged. If the borehole diameter increases, the borehole coverage decreases. Unimaged parts of the borehole appear as blank strips between the pads in the resultant images.

At the start of the log run, with the tool at the bottom of the drill hole, all pads and flaps are pressed against the borehole wall. The resistivity of the formation is measured by passing an

electrical current through the rock. The current passing through the rock is used to measure high- and low-resolution resistivity components. The low-resolution component is the resistivity of deeper zone in the borehole images, and appears as a gradually changing background. The high-resolution component is a result of resistivity variations in the formation directly facing the electrical sensor. This dominates the images as lithological and petrophysical variations in the rock, including texture, stratigraphic and structural features, and fractures (Schlumberger, 2002). Raw data include multiple electrode readings, caliper readings, and x-, y-, and z-axis accelerometer and compass readings. Borehole deviation and pad orientations are determined from compasses.

Data processing steps involved correcting the directional data for tool and hole azimuths and magnetic declination. Accelerometer corrections were applied and resistivity traces depth shifted such that different rows of resistivity sensors are in line where the same slice of the borehole was imaged. Color maps were assigned to the borehole images based on ranges of resistivity values. Rocks are generally resistive and water is conductive. In an FMI image, high resistivity features including, sandstone, limestone, and mineral-filled fractures, are displayed as light colors. In contrast, typically low resistivity features including water-filled open fractures and shales, are displayed as dark colors. Because it is difficult to interpret borehole images in 3-D, it is common to split the borehole along true north, then unroll the cylinder until it becomes a 2-D view (Figure 9). After the 3-D image is unrolled, dipping features that intersect the cylindrical borehole appear as sine waves (Figure 9).

The processed borehole image log was viewed in static and dynamic views while fitting sine waves to observed bed boundaries, fractures, and other geologic features (Figure 10). Static images have one contrast setting for the entire well, providing a view of relative changes in rock

resistivity throughout the borehole. Dynamic images have variable contrast applied in a moving window, providing enhanced views of features including vugs, fractures, and bed boundaries. Dynamic images bring out detailed features in rocks that have very low resistivity, such as shales, and very high resistivity, such as carbonates and crystalline rocks. Fractures in the subsurface analysis were characterized as either natural or induced features. They were also classified as conductive or resistive features, representing possibly open (water-filled) or closed (mineralized) fractures, respectively. The azimuths and dips of interpreted geologic features are presented in a tadpole plot (Figure 10). The vertical scale is depth and the horizontal scale is dip from 0°-90°.

The concentration of stress around wellbores can lead to compressive failures known as stress induced breakouts and tensile failure of the wellbore wall (Bell, 1996; Figure 11). Both borehole breakouts and drilling-induced tensile fractures form on diametrically opposite sides of the borehole wall. Borehole breakouts are parallel to the minimum horizontal stress (S_{hmin}) while drilling-induced fractures are parallel to the maximum horizontal stress (S_{Hmax}) for a vertical borehole (Figure 11). Fracture length generally varies from less than a meter to several tens of meters (Bell and Gough, 1979; Zoback *et al.*, 1985).

The perpendicular sets of caliper arms attached to the FMI tool are also be used to interpret borehole breakouts. Used in combination with FMI imaging, this can help to distinguish zones of stress-induced breakouts from other borehole enlargements, including washouts and key seats (Figure 12).

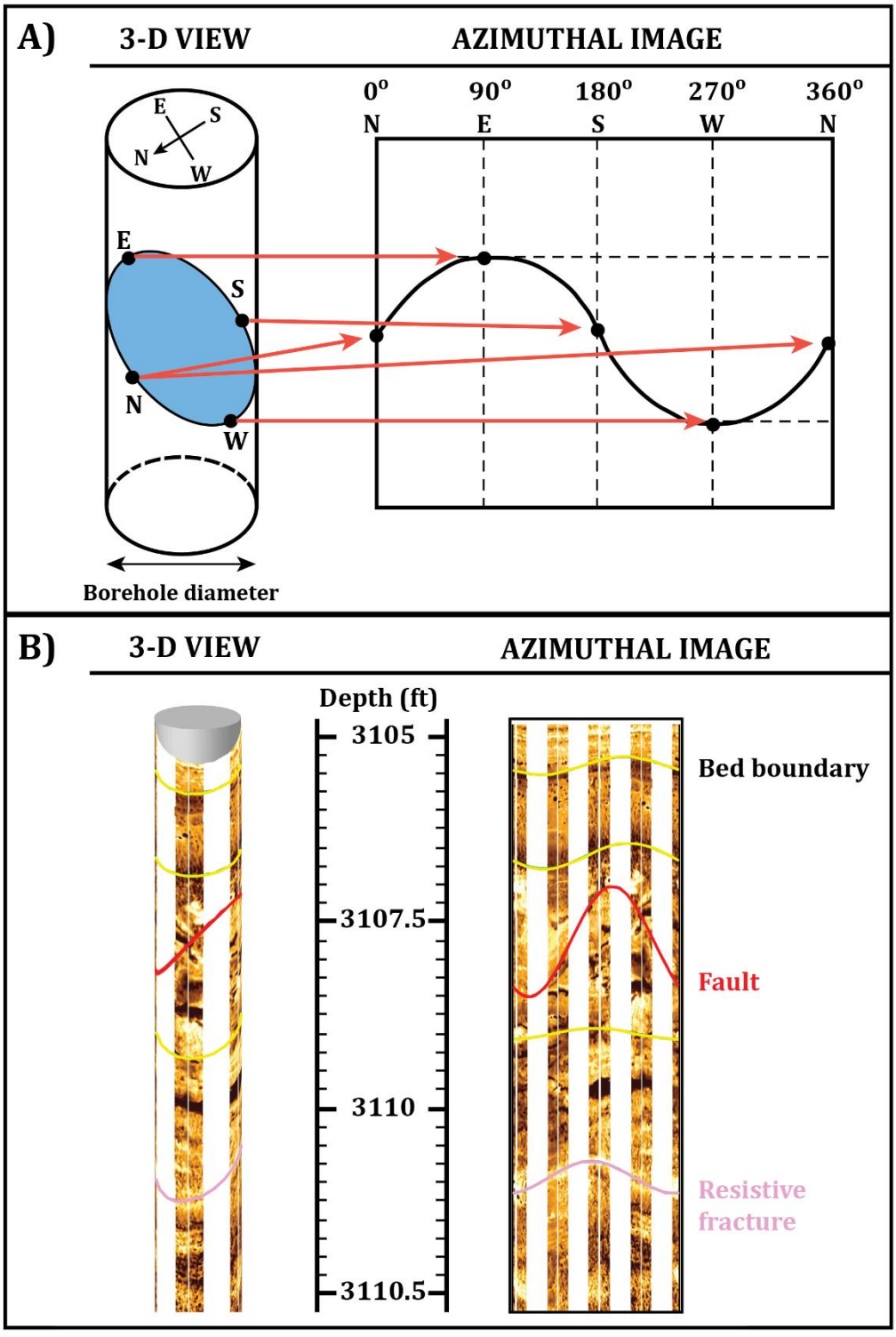

Figure 9: A) A schematic diagram of a cylindrical borehole intersected by planar features in 3-D and 2-D (azimuthal) views (modified from Donselaar and Schmidt, 2005). B) A number of planar features were interpreted and color coded within a ~1.5 m (5.5 ft) section of FMI log taken from the Gorgas Well #1. Dipping features that intersect the cylindrical borehole appear as sine waves in the azimuthal view. If the dipping angle increases the amplitude of the sine wave is also increases.

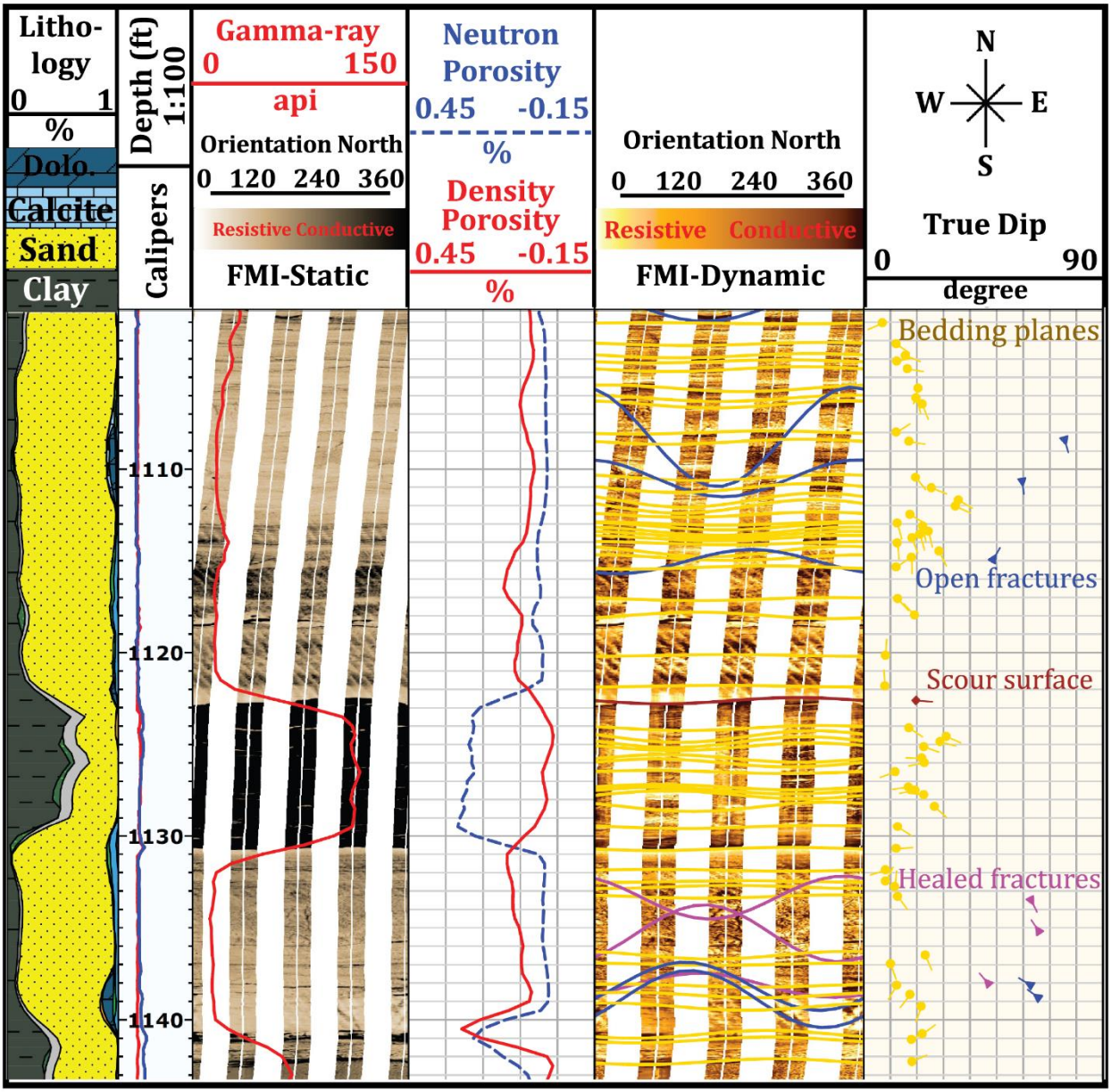

Figure 10: An example of an FMI resistivity image from the Pottsville Formation displays both open and healed fractures in a sandstone dominated depth section. Six tracks from left to right include an ELAN lithology column, caliper measurements with a depth track, a static FMI image with a GR log curve, neutron-density porosity log curves, a dynamic FMI image with interpreted features (sine waves), and a tadpole plot.

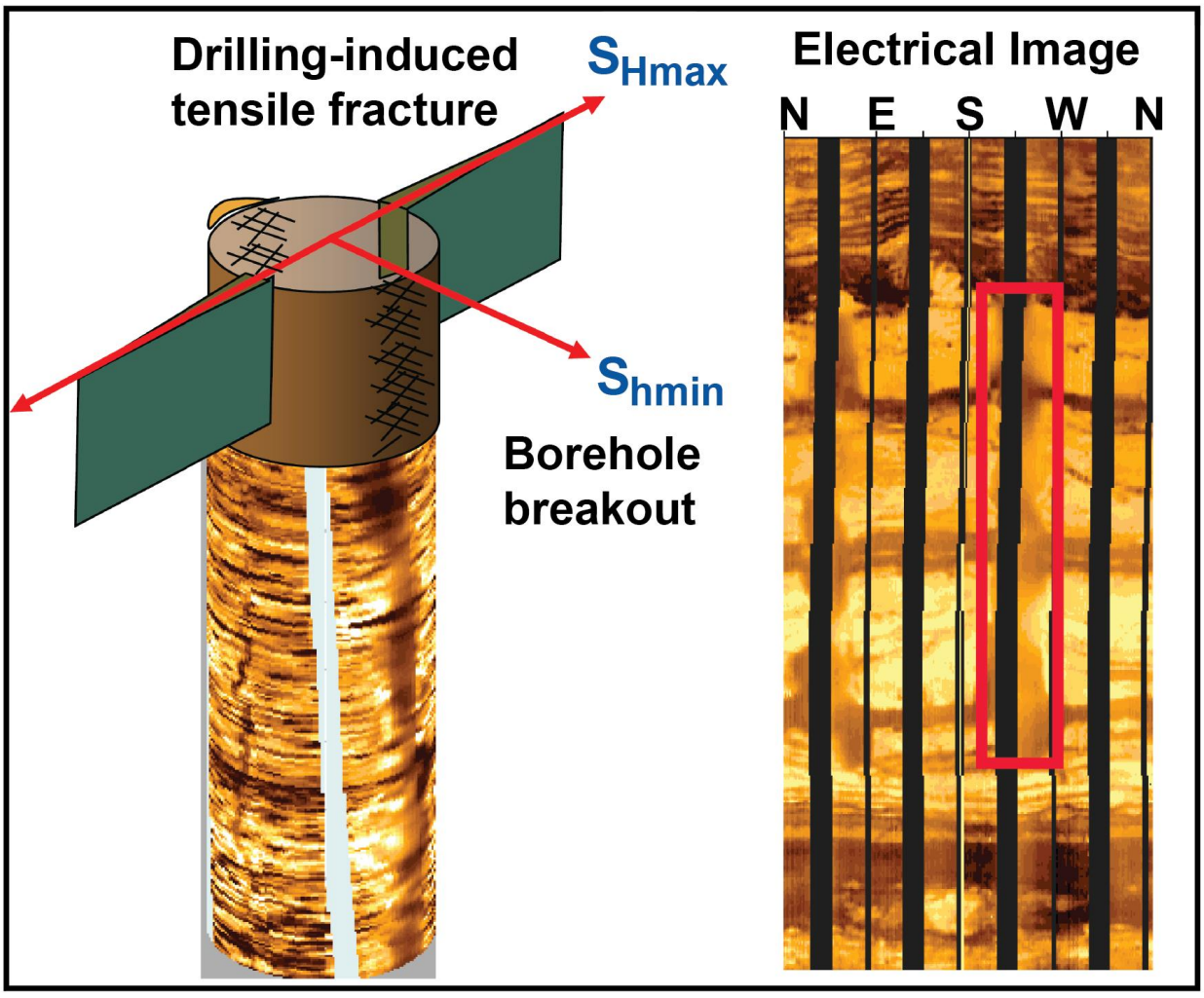

Figure 11: Examples of borehole images showing borehole breakouts (red box on the right image) and drilling-induced tensile fractures on the wellbore wall. In the case of a borehole breakout the resistivity image loses resolution as the sensors loose contact with the borehole wall. Arrows indicate the minimum and maximum horizontal stress directions (modified from Soroush, 2010).

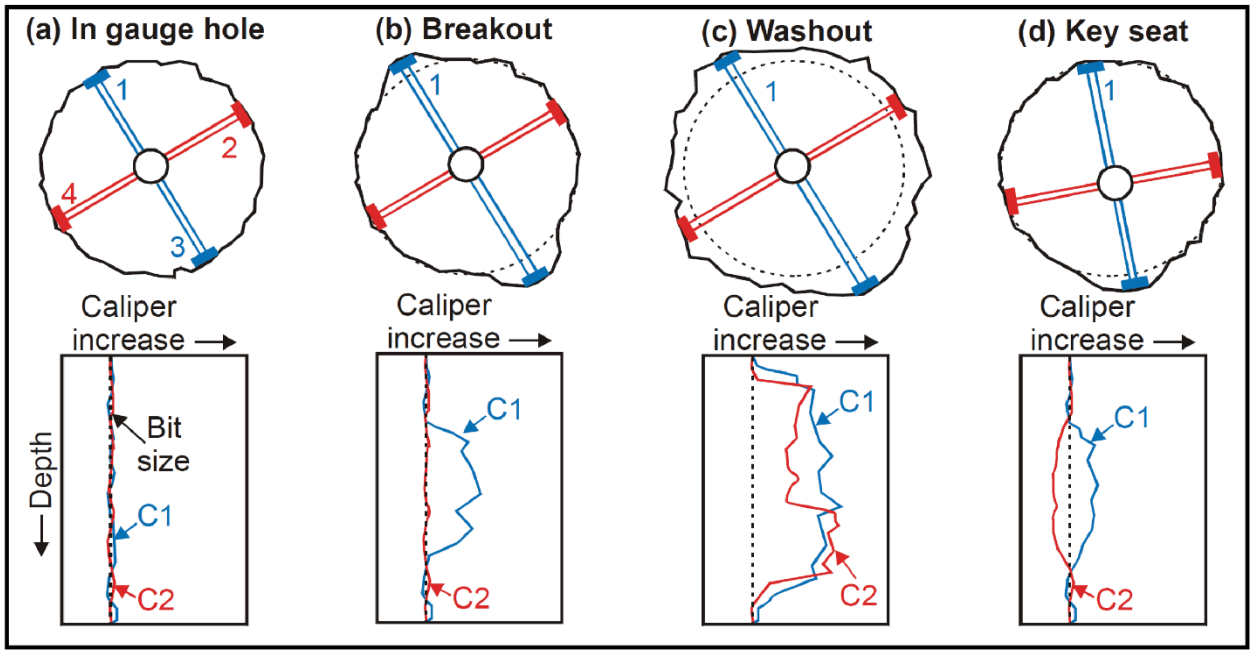

Figure 12: Common types of enlarged borehole and their caliper log responses (Reinecker et al., 2003). A key seat is formed by the drill string pressing against the side of the hole and cutting a groove. This happens when the hole is not straight.

2.3. ECS Tool and Lithology Detection

The ECS tool measures the most commonly occurring formation elements: silicon, iron, calcium, sulfur, titanium, gadolinium, chlorine, barium, and hydrogen. Lithological fractions of total clay, total carbonate, and QFM (quartz, feldspar, and mica) can be derived from the elemental measurements. ELAN (Elemental Analysis) petrophysical analysis, derived from ECS and other log measurements, were provided by Schlumberger. The ELAN model is a popular probabilistic model designed for quantitative formation evaluation of open-hole logs. Log measurements, and response parameters are used together in response equations to compute volumetric results for formation components (minerals and fluids).

2.4. Data Interpretation Methodology

All data processing and interpretations were completed using Schlumberger's Techlog® software. An example of an interpreted section of FMI log is shown in Figure 10. From left to right, six tracks were used during interpretation. Track 1 includes a lithology column derived from ELAN (Elemental Analysis) results. Track 2 contains caliper logs recorded by the FMI tool, and a depth track. Track 3 has the processed static FMI image, and a gamma-ray curve. Track 4 contains neutron and density porosity curves. Track 5 has the processed dynamic FMI image with the sinusoid traces showing the dips of interpreted geologic features. Track 6 is a tadpole plot that shows the direction and dip of beds in the formation along with tadpoles for any geological feature that may be present (Table 1).

DIP TYPE	SYMBOL	DESCRIPTION
Lamination and Bedding Plane		Sedimentological, low angle planar features (e.g. shale and sand bed boundaries).
Erosional Surface		Sedimentological, generally low angle non-planar features (unconformities).
Conductive Fracture		Structural, generally high angle planar and unhealed (open) features.
Resistive Fracture		Structural, generally high angle planar and healed (closed) features.
Shear Fracture		Structural, resistive or conductive planar features. They show minor displacement.
Fault		Structural, resistive or conductive planar features related with bedding offset.
Borehole Breakout		Conductive vertical enlargements on the wellbore wall.
Drilling-Induced Tensile Fracture		Conductive vertical planar features on the wellbore wall.

Table 1: Classification of dip types used in FMI image interpretation.

In this study, the FMI images were used for structural interpretation, with particular emphasis on the detection and orientation of fractures and faults in order to characterize the stress field trends experienced by sediments in the Black Warrior Basin. Individual fractures cannot be identified as natural or induced based solely on the fracture trace in an image log. The origin of a group of fractures can be determined from image logs because natural fractures and induced fractures have different geometries relative to the borehole. If induced fractures (borehole breakouts and drilling-induced tensile fractures) are present and if the natural fractures formed in a stress field different from the present-day stress field, then induced fractures can be easily distinguished from natural fractures (Table 1). In the case of polyphase tectonics, the orientation of the fracture sets related to each tectonic event allows a reconstruction of the successive regional paleostress patterns. The chronology of successive events is deduced from the different sets of fractures formed in the formations deposited at different times. Cross-cutting relationships of these fractures have not been observed during interpretation. To facilitate the visualization of all geological features, FMI log interpretation results were grouped over certain intervals and plotted as azimuth rose diagrams. Rose diagrams show the distribution of strike directions of the interpreted fracture sets across a 360° scale. The density of those strike directions are displayed as percentages. A useful addition to the rose diagram is a dip histogram plot in which dip angle (x-axis) is plotted against frequency (y-axis). The resultant plot shows the dominant trends of structural and sedimentary dip.

3. RESULTS

3.1. Fracture Analysis

95 conductive (open) and 89 resistive (healed) fractures were interpreted in the Gorgas #1 well. The orientation of conductive fractures can be classified into two major sets (i): 45°-75° (mode: 71°, median: 66°, standard deviation: 14°), and set (ii): 120°-140° (mode: 123°, median: 133°, standard deviation: 15°; figures 13, 14). Analysis of the dip of 95 conductive fractures shows a skewed distribution with a mean dip of 67° and a standard deviation of 13°. In comparison, resistive fractures have three orientation sets (i): 45°-75° (mode: 49°, median: 51°, standard deviation: 31°), set (ii): 120°-140° (mode: 124°, median: 131°, standard deviation: 11°), and set (iii): 0°-10° (mode: 4°, median: 4°, standard deviation: 5°; figures 15, 16). Analysis of the dip of 89 resistive fractures also shows a skewed distribution with a mean dip of 73° and a standard deviation of 8°. All fractures can be considered geologically sub-vertical or inclined. There are 16 possible faults and microfaults interpreted in the Gorgas well. The faults strike dominantly NE-SW and NW-SE.

FMI log interpretations were grouped and presented here for each stratigraphic formation drilled by the Gorgas well. Because of their thicknesses, the Pottsville Formation and Knox Group have been subdivided into depositional cycles and members, respectively, in order to show the results in more detail.

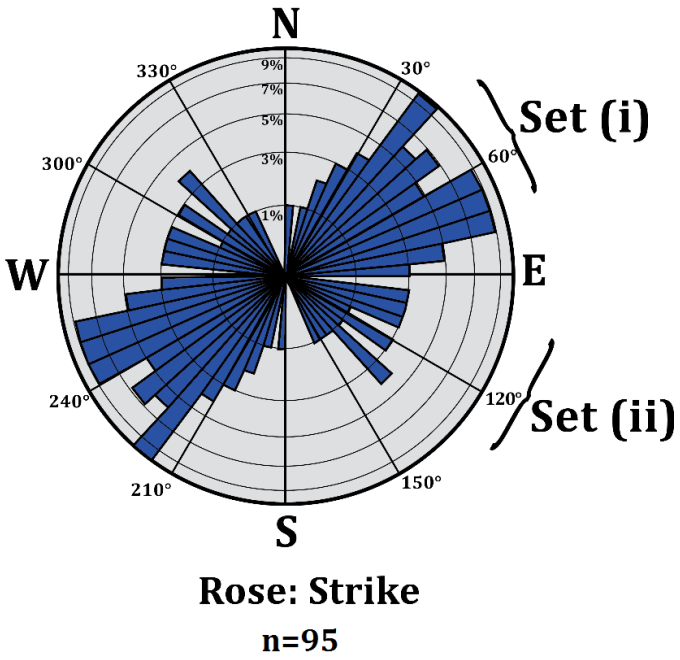

Figure 13: Bidirectional rose diagram showing the density (inner circles) of the orientations (radial scale) of all conductive (open) fractures interpreted in the Gorgas #1 well.

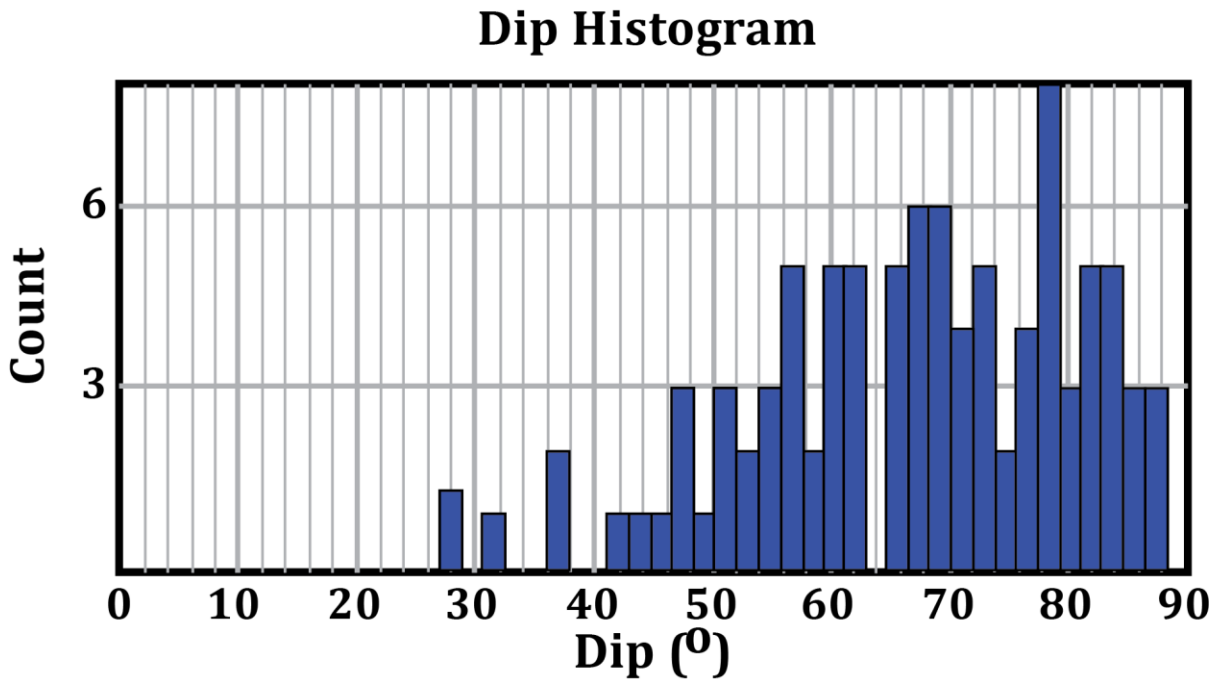

Figure 14: Dip histogram of all conductive (open) fractures in the Gorgas #1 well.

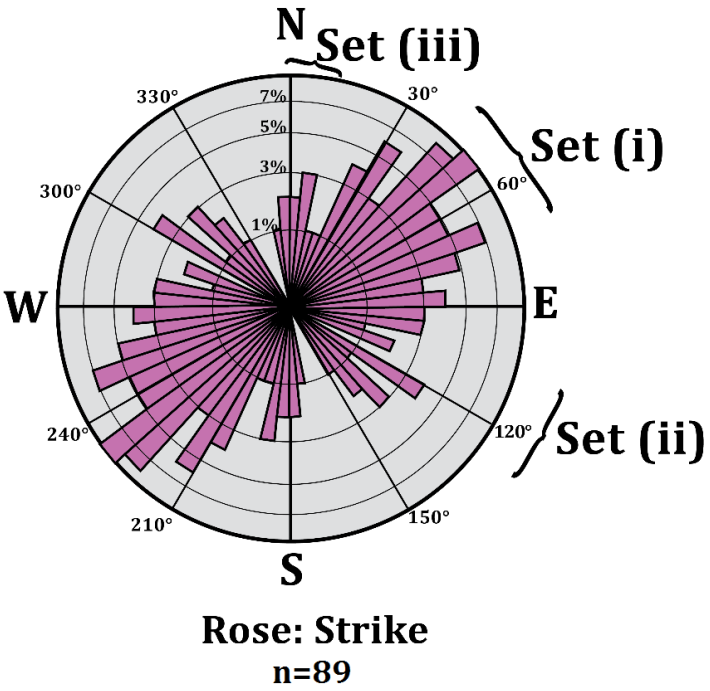

Figure 15: Bidirectional rose diagram showing the density (inner circles) of the orientations (radial scale) of all resistive (healed) fractures interpreted in the Gorgas #1 well.

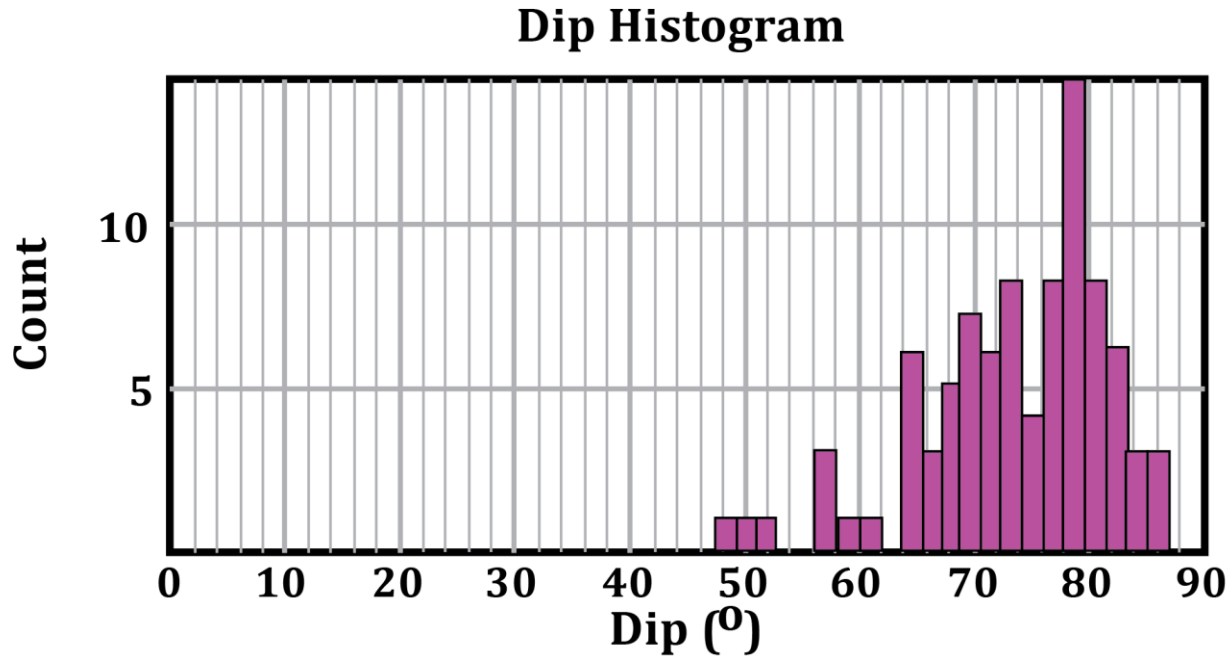

Figure 16: Dip histogram of all resistive (healed) fractures in the Gorgas #1 well.

3.1.1. Pottsville Formation 235-631 m (771-2070 ft)

3.1.1.1. Black Creek Cycle 235-322 m (771-1056.5 ft)

Thirty-two fractures, including 16 conductive (open), 2 resistive (healed), 14 shear, and 6 faults were observed in the Black Creek cycle of the Pottsville Formation (Figure 17). The distribution of the strike orientation of the fractures and faults is displayed in Figure 18. Conductive fractures have quite a bit variability but strike dominantly NE-SW and NW-SE (Figure 18). Borehole breakouts and drilling-induced fractures were not observed in the Black Creek cycle. Fractured and a faulted zones were recognized a depth of 260-265 m and 268-273 m, respectively (Figure 17). Faults and shear fractures strike dominantly NE-SW.

3.1.1.2. Fayette Cycle 322-431 m (1056.5-1414 ft)

Twenty-five total fractures, including 17 conductive (open), 3 resistive (healed), 5 shear, and 4 faults were observed in the Fayette cycle of the Pottsville Formation (Figure 19). Both conductive and resistive fractures have a dominantly NE-SW orientation (Figure 20). Borehole breakouts and drilling-induced fractures were not observed in the Fayette cycle. The sand-dominated upper part of the Fayette cycle is highly fractured. However, there is no fracture development in the shale dominated lower part (Figure 19). Faults and shear fractures strike dominantly both NE-SW and NW-SE, in contrast to the Black Creek cycle.

3.1.1.3. Upper Boyles Cycle 431-496 m (1414-1627 ft)

In the upper Boyles cycle of the Pottsville Formation, 2 conductive (open), 1 resistive (healed), 3 shear fractures, and 1 fault were observed (Figures 21, 22). Borehole breakouts and drilling-induced fractures were not observed in the upper Boyles cycle.

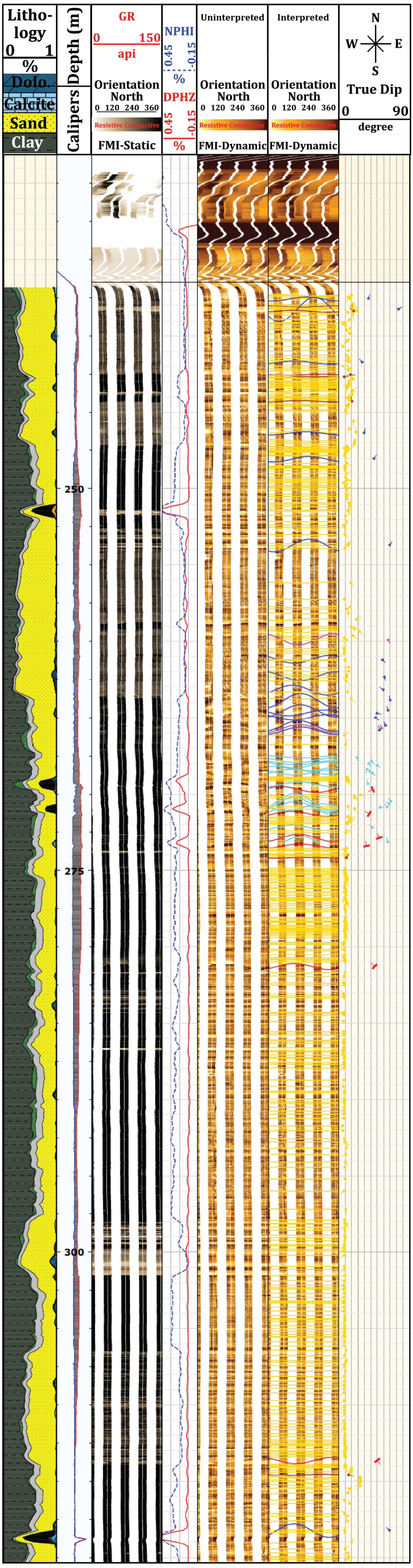

Figure 17: Interpreted log section for the Black Creek cycle of the Pottsville Formation from 235-322 m (771-1056.5 ft).

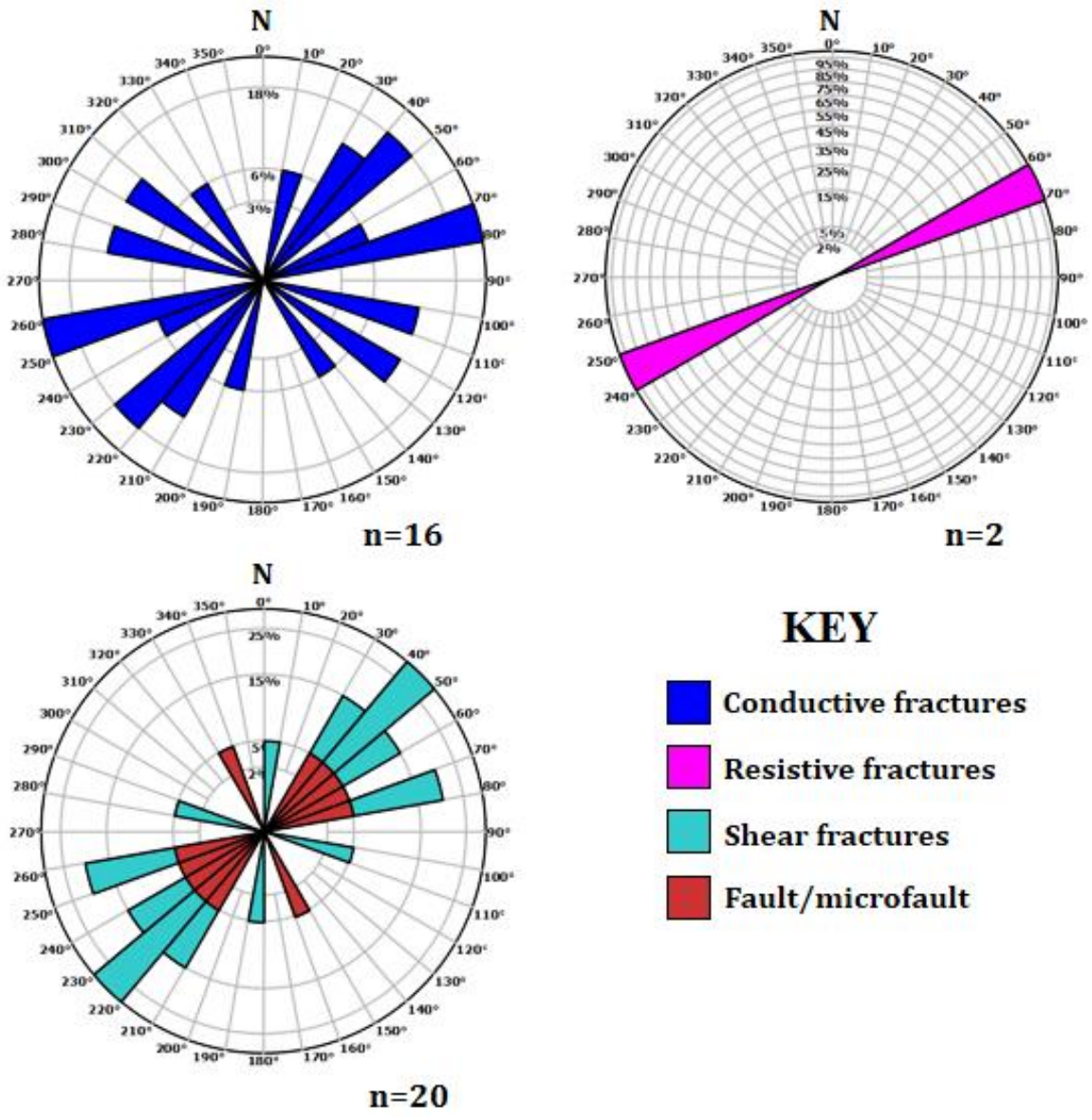

Figure 18: Rose diagrams showing the distribution of the strike orientation for the interpreted structural features in the Black Creek cycle of the Pottsville Formation.

Figure 19: Interpreted log section for the Fayette cycle of the Pottsville Formation for the depth interval 322-431 m (1056.5-1414 ft).

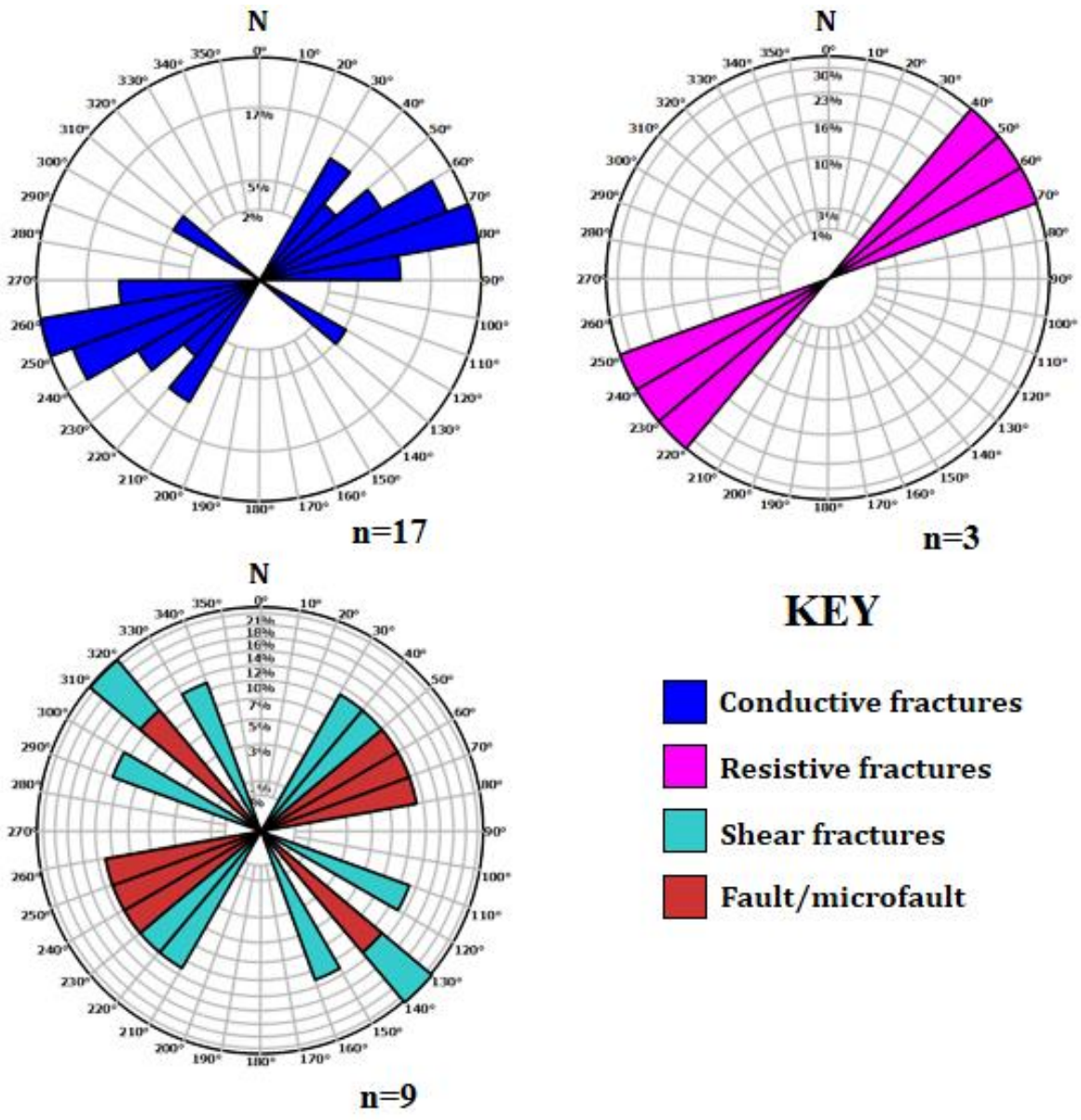

Figure 20: Rose diagrams showing the distribution of the strike orientation for the interpreted structural features in the Fayette cycle of the Pottsville Formation.

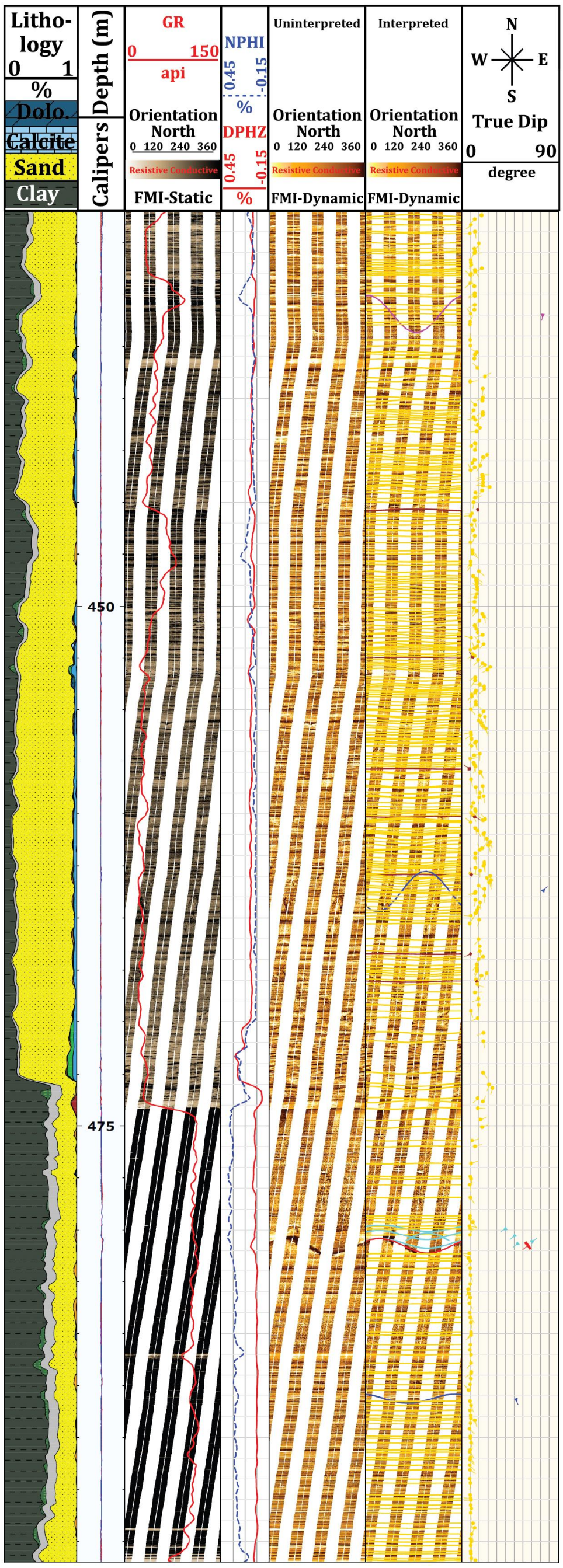

Figure 21: Interpreted log section for the upper Boyles cycle of the Pottsville Formation for the depth interval 431-496 m (1414-1627 ft).

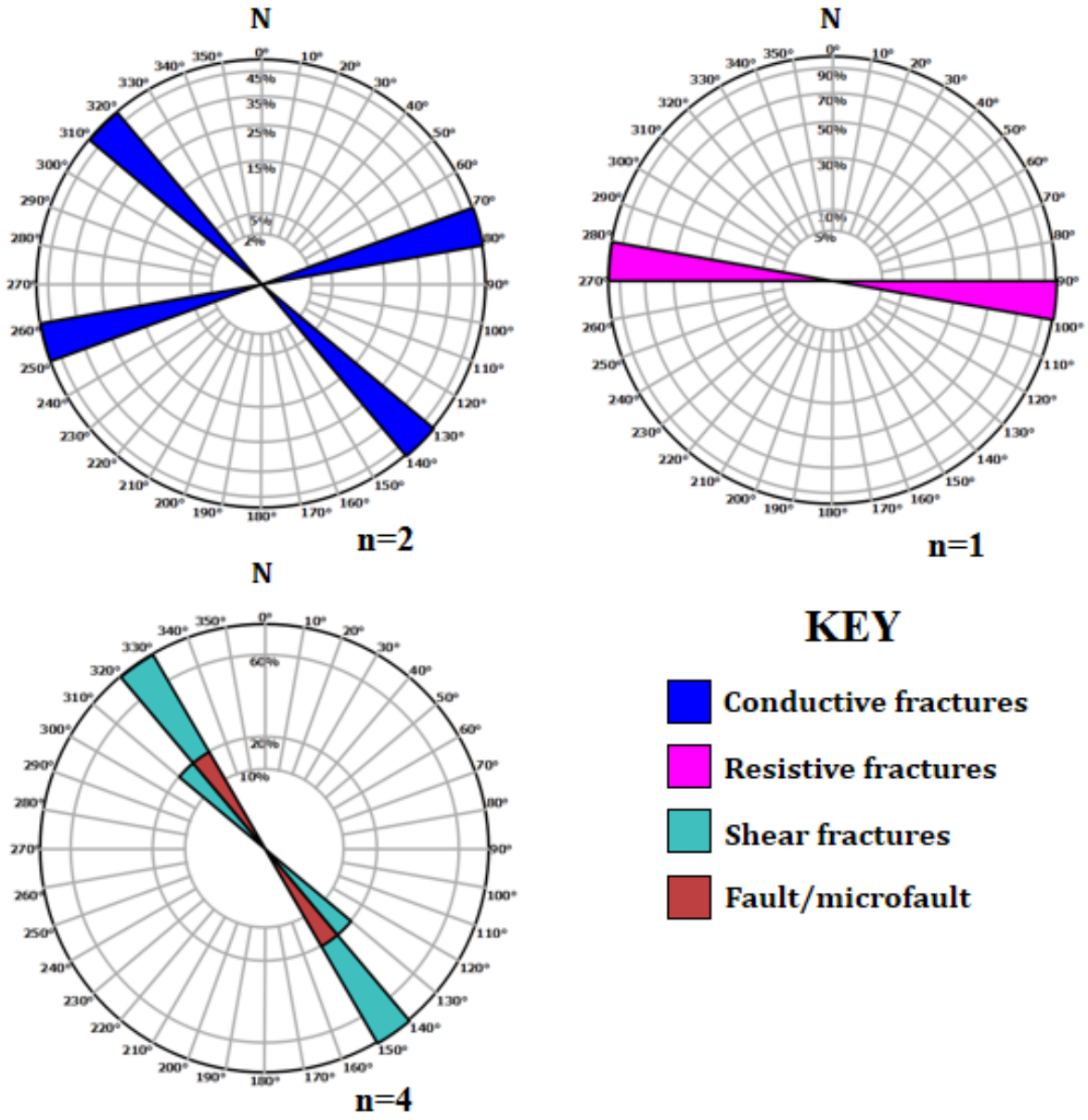

Figure 22: Rose diagrams showing the distribution of the strike orientation for the interpreted structural features in the upper Boyles cycle of the Pottsville Formation.

3.1.1.4. Lower Boyles Cycle 496-631 m (1627-2070 ft)

Seven conductive (open) and 3 resistive (healed) fractures were found in the lower Boyles cycle of the Pottsville Formation (Figure 23). Conductive fractures strike dominantly NE-SW (Figure 24). Borehole breakouts and drilling-induced fractures were not observed in the lower Boyles cycle.

3.1.2. Parkwood Formation 631-708 m (2070-2323 ft)

In the Parkwood Formation, 1 resistive (healed) fracture and 1 fault was observed (Figures 25, 26). There were also 3 sets of borehole breakouts and 1 drilling-induced tensile fracture found in the Parkwood Formation.

3.1.3. Bangor Limestone 708-794.5 m (2323-2607 ft)

One conductive (open) fracture was observed in the Bangor Limestone (Figures 27, 28). There were also 5 sets of borehole breakouts and 2 drilling-induced tensile fractures found in the formation.

3.1.4. Hartselle Sandstone 794.5-821 m (2607-2694 ft)

Three conductive (open) fractures were observed in the Hartselle Sandstone (Figures 29, 30). Conductive fractures strike dominantly NE-SW. There was also 1 set of borehole breakouts and 1 drilling-induced tensile fracture found in the formation.

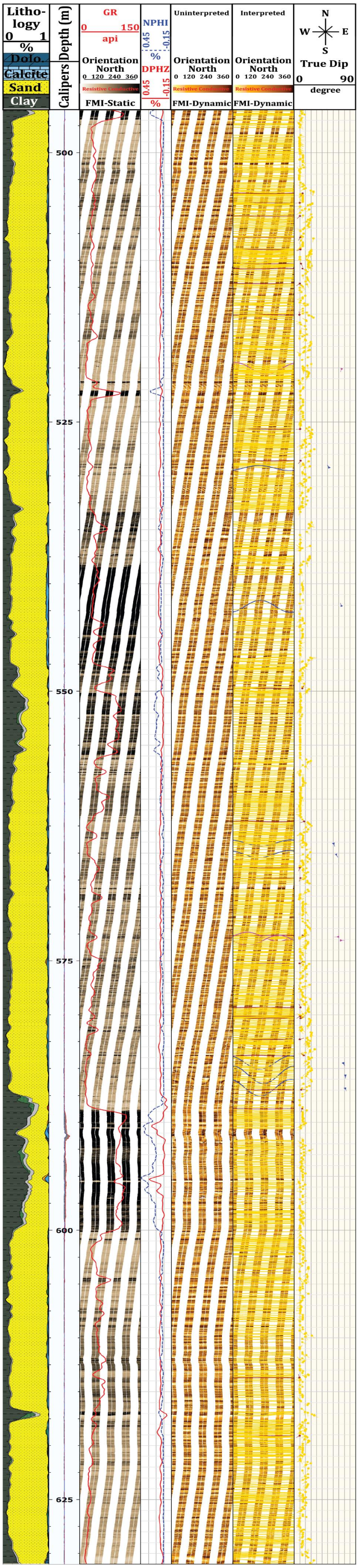

Figure 23: Interpreted log section for the lower Boyles cycle of the Pottsville Formation for the depth interval 496-631 m (1627-2070 ft).

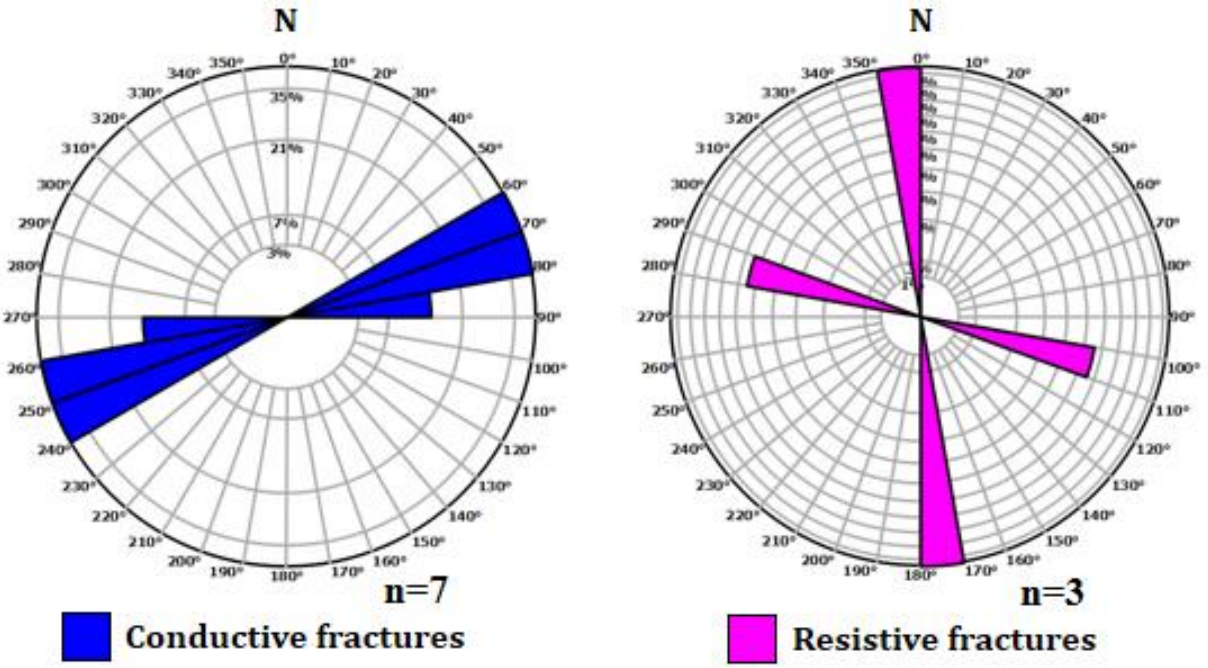

Figure 24: Rose diagrams showing the distribution of the strike orientation for the interpreted structural features in the lower Boyles cycle of the Pottsville Formation.

3.1.5. Pride Mountain Formation 821-874.5 m (2694-2869 ft)

1 conductive (open) fracture was observed in the Pride Mountain Formation (Figures 31, 32). Three sets of borehole breakouts were found in the formation. The quality of the interpretation in the lower part of the formation was not good because of a washout (Figure 31).

3.1.6. Tuscumbia Limestone 874.5-917 m (2869-3008 ft)

In the Tuscumbia Limestone, 4 conductive (open) and 6 resistive (healed) fractures were observed (Figures 33, 34). One set of borehole breakouts and 7 drilling-induced tensile fractures were found in the formation.

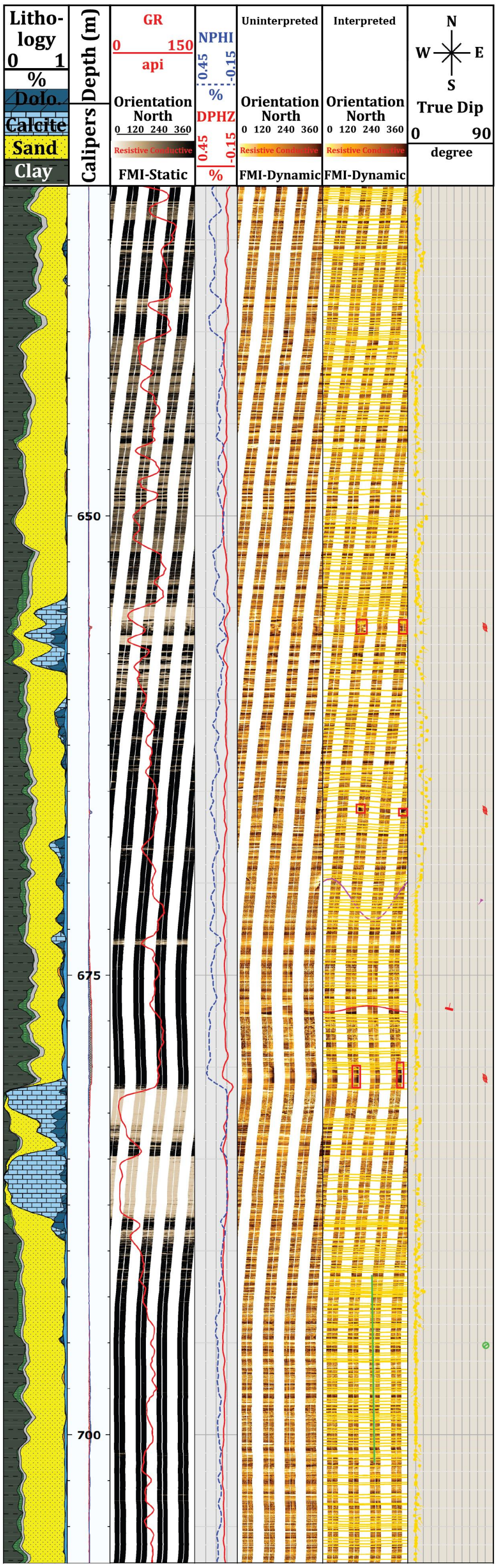

Figure 25: Interpreted log section for the Parkwood Formation for the depth interval 631-708 m (2070-2323 ft).

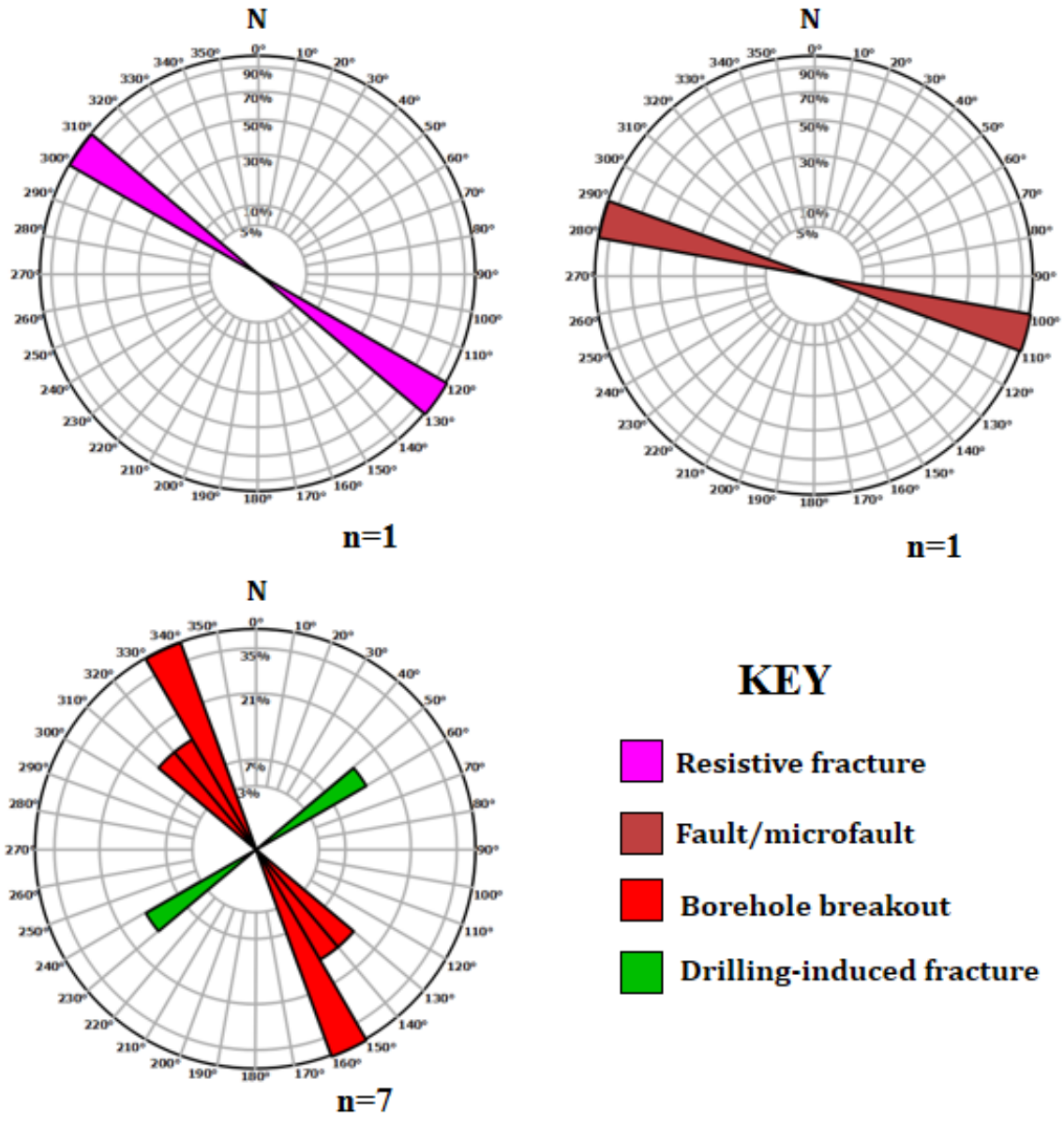

Figure 26: Rose diagrams showing the distribution of the strike orientation for the interpreted structural features in the Parkwood Formation.

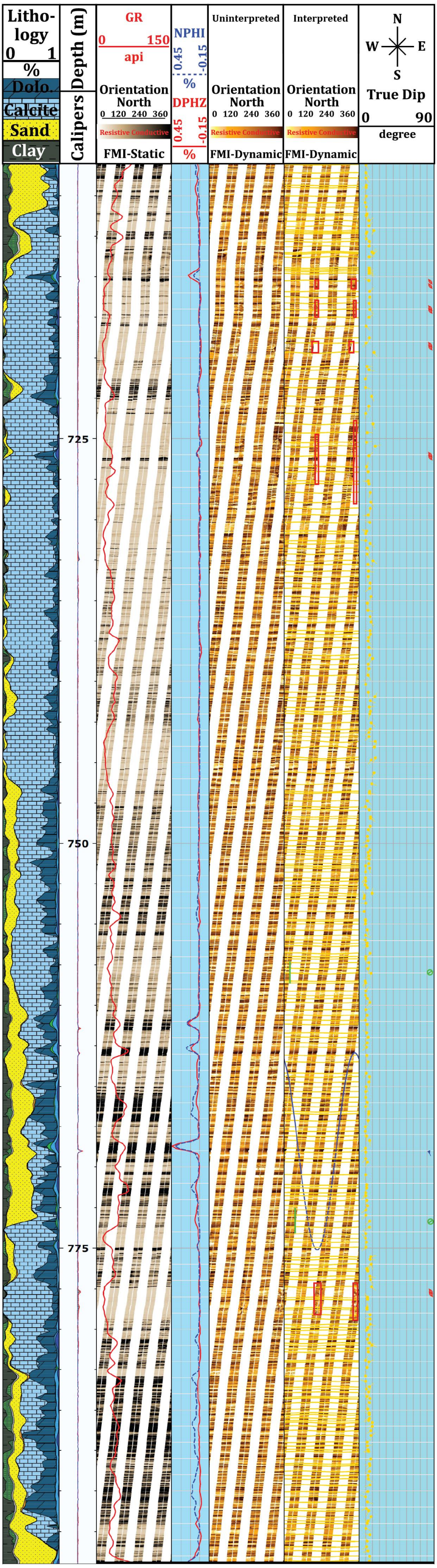

Figure 27: Interpreted log section for the Bangor Limestone over the depth interval 708-794.5 m (2323-2607 ft).

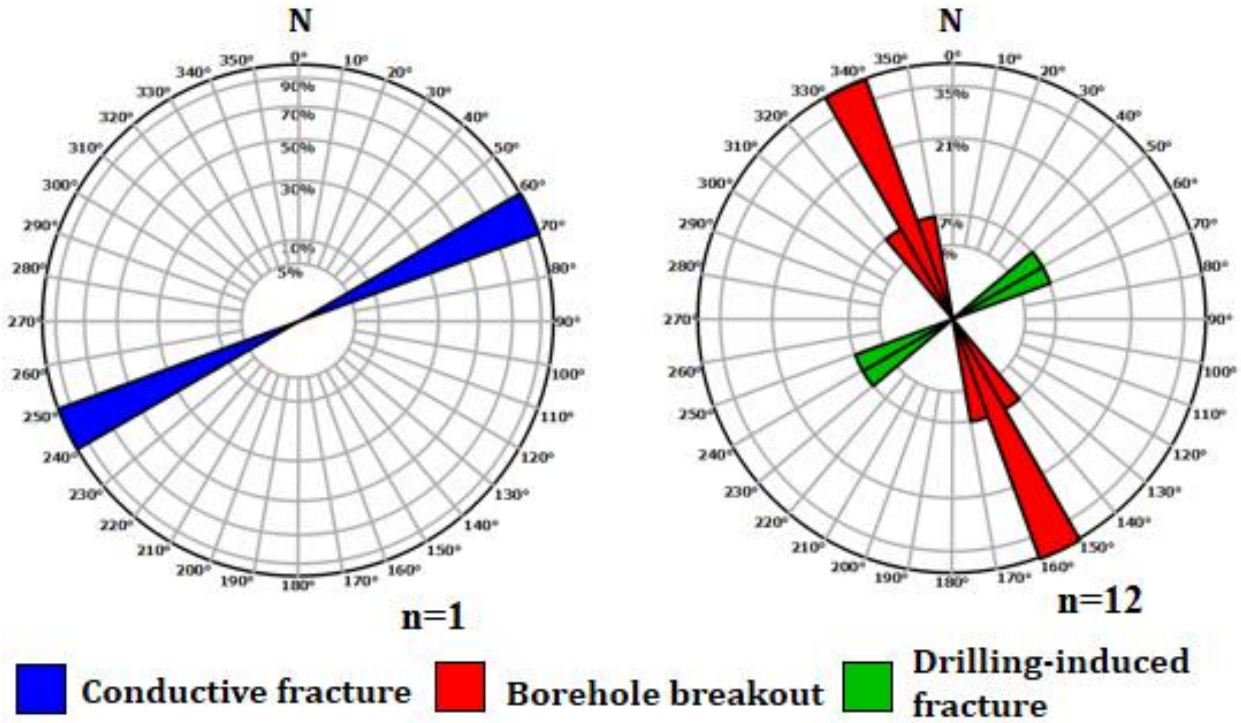

Figure 28: Rose diagrams showing the distribution of the strike orientation for the interpreted structural features in the Bangor Limestone.

3.1.7. Fort Payne Chert 917-942 m (3008-3090 ft)

One resistive (healed) fracture and 1 set of drilling-induced tensile fractures was observed in the Fort Payne Chert (Figures 35, 36).

3.1.8. Chattanooga Shale 942-966 m (3090-3169 ft)

3 conductive (open) and 2 resistive (healed) fractures were observed in the Chattanooga Shale (Figures 37, 38). Borehole breakouts and drilling-induced fractures were not found in the formation.

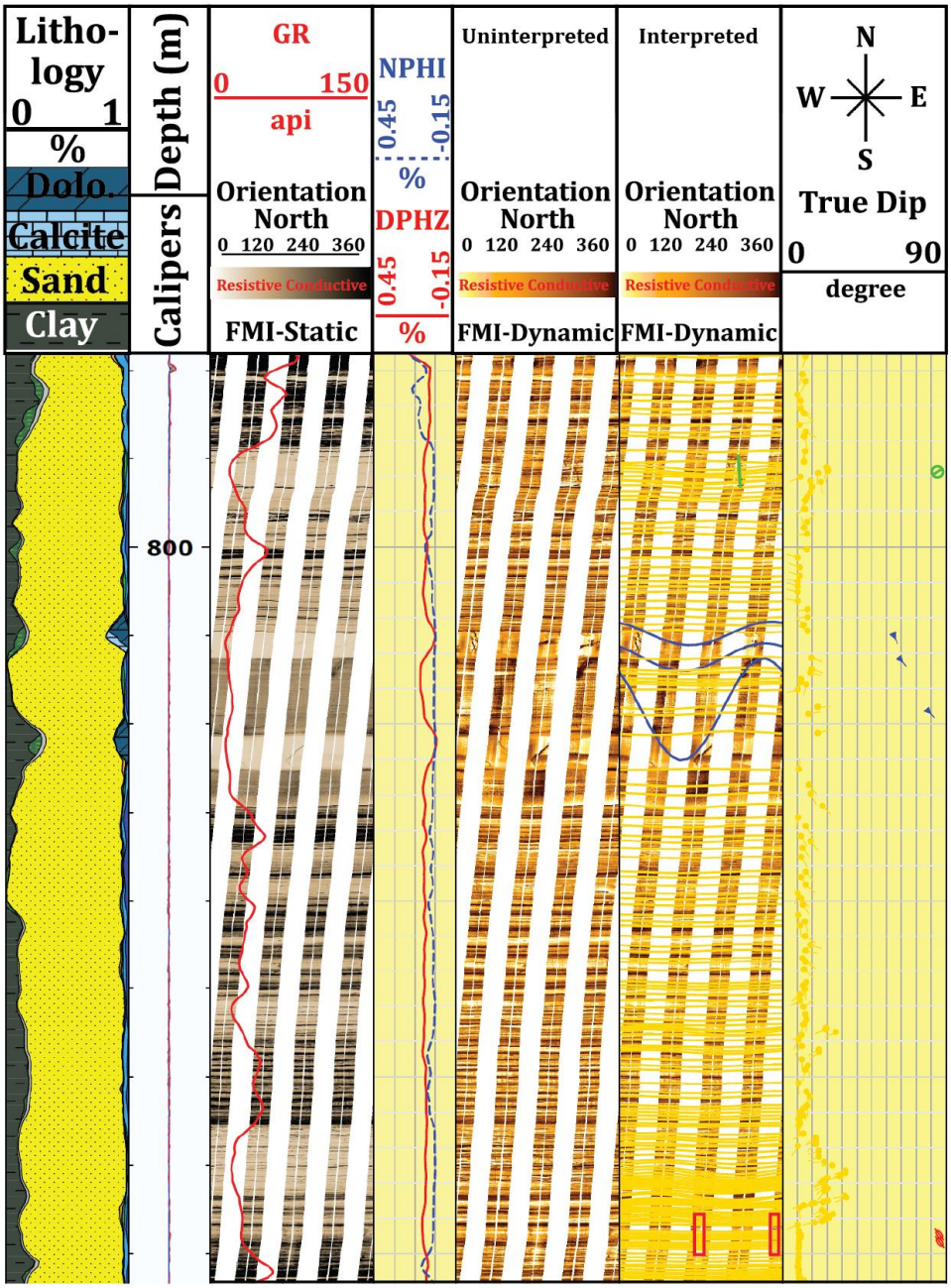

Figure 29: Interpreted log section for the Hartselle Sandstone over the depth interval 794.5-821 m (2607-2694 ft).

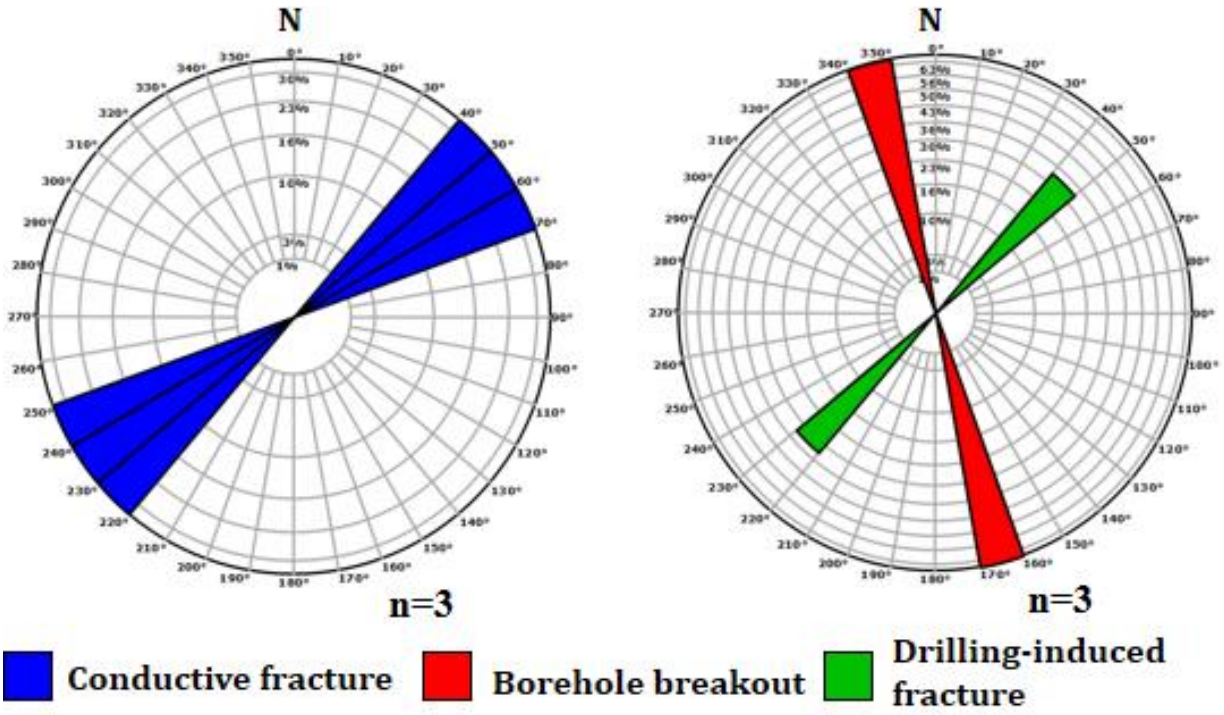

Figure 30: Rose diagrams showing the distribution of the strike orientation for the interpreted structural features in the Hartselle Sandstone.

3.1.9. Red Mountain Formation 966-1076 m (3169-3530 ft)

One conductive (open), 2 shear fractures, and 2 faults were observed in the Red Mountain Formation (Figure 39). The distribution of the strike orientation of these fractures and faults is displayed in Figure 40. Borehole breakouts and drilling-induced fractures were not observed in the formation during the interpretation.

3.1.10. Sequatchie Formation 1076-1143 m (3530-3750 ft)

Four conductive (open), 5 shear, and 1 fault was observed in the Sequatchie Formation (Figure 41). The distribution of the strike orientation of these fractures and faults is displayed in Figure 42. One set of borehole breakouts and 11 drilling-induced tensile fractures were interpreted within the formation.

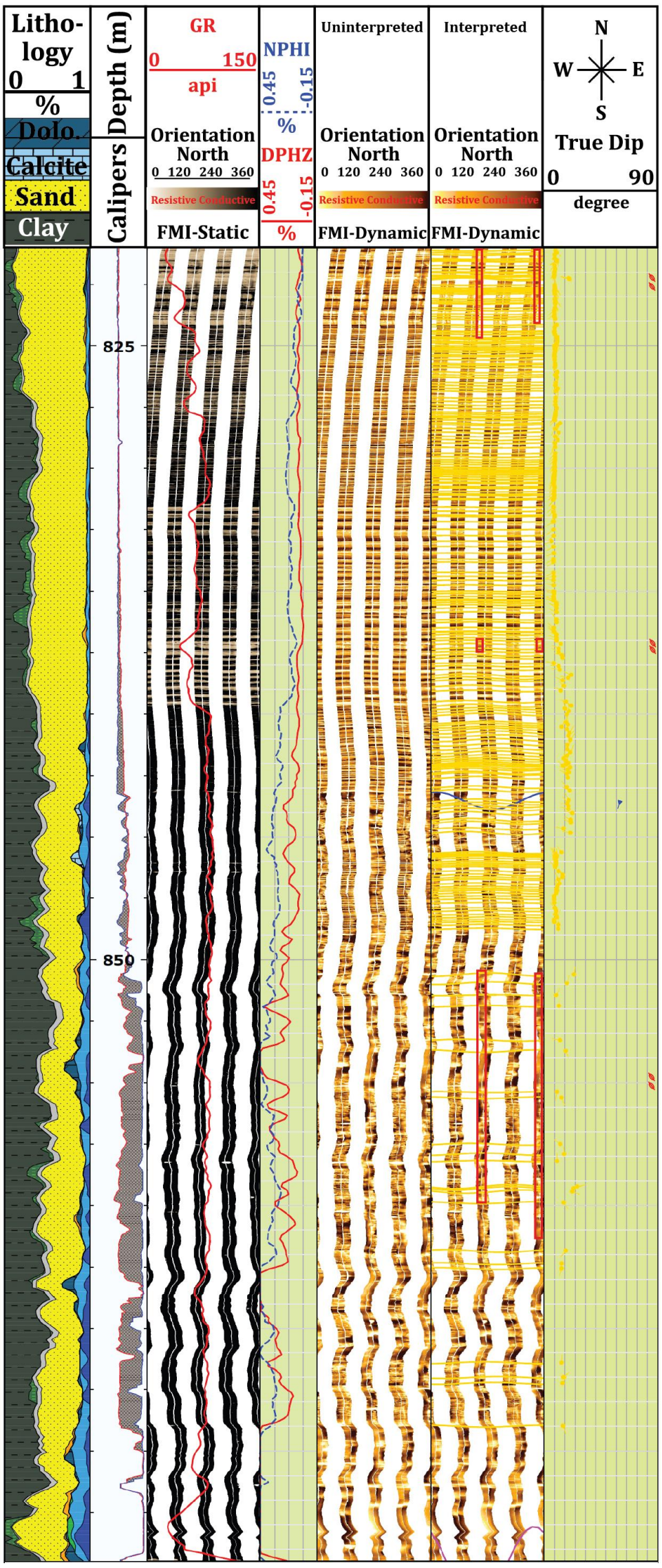

Figure 31: Interpreted log section for the Pride Mountain Formation over the depth interval 821-874.5 m (2694-2869 ft).

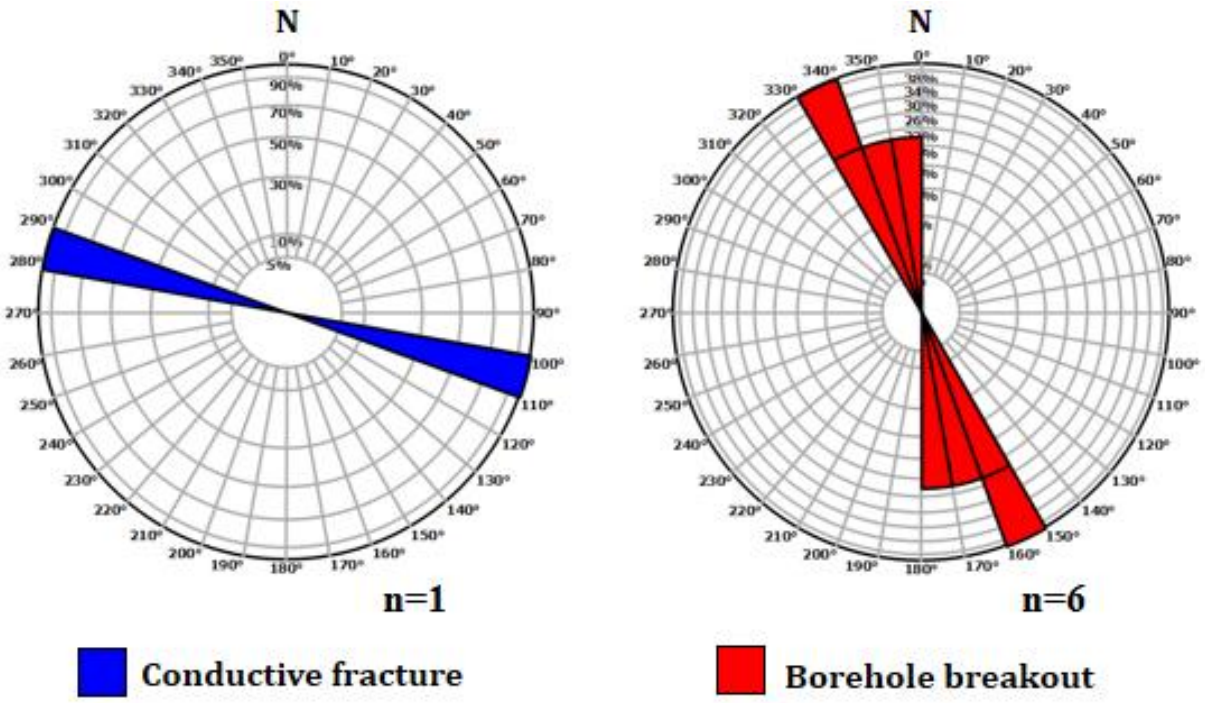

Figure 32: Rose diagrams showing the distribution of the strike orientation for the interpreted structural features in the Pride Mountain Formation.

3.1.11. Stones River Group 1143-1222 m (3750-4009 ft)

Five conductive (open) and 5 resistive (healed) fractures were observed in the Stones River Group (Figure 43). Ten sets of borehole breakouts and 15 drilling-induced tensile fractures interpreted within the formation. The distribution of the strike orientation of these fractures and faults is displayed in Figure 44.

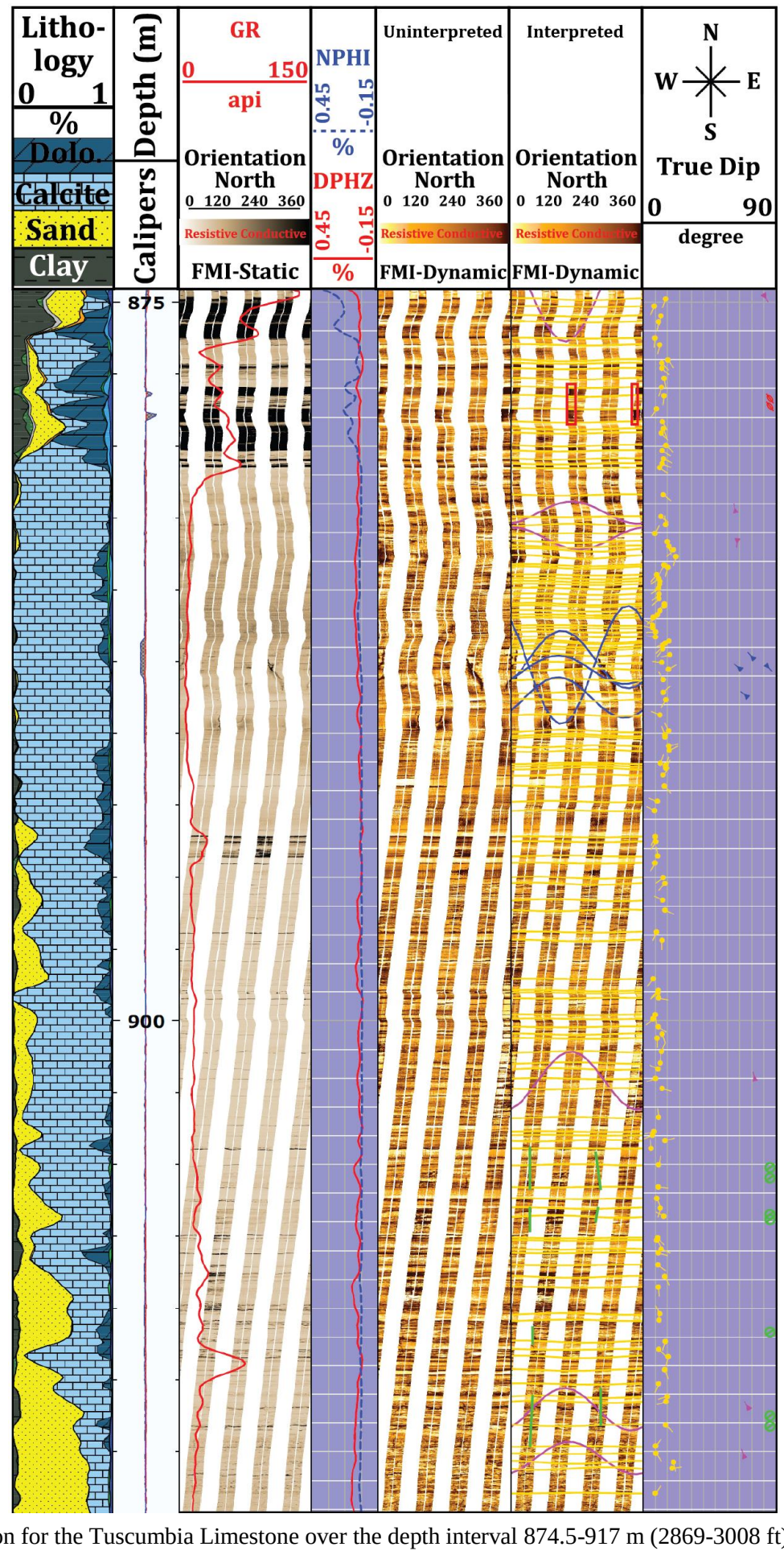

Figure 33: Interpreted log section for the Tuscumbia Limestone over the depth interval 874.5-917 m (2869-3008 ft).

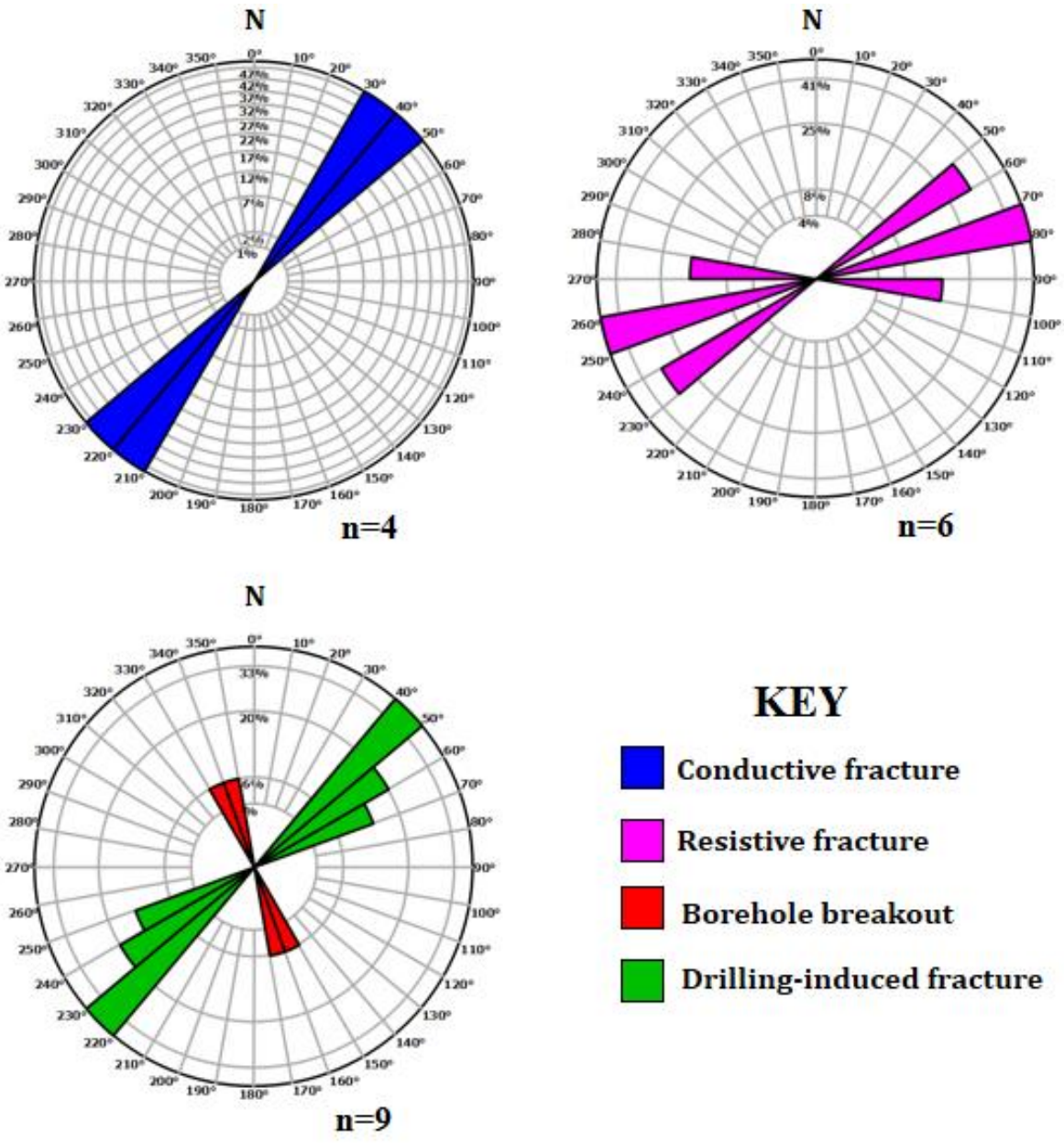

Figure 34: Rose diagrams showing the distribution of the strike orientation for the interpreted structural features in the Tuscumbia Limestone.

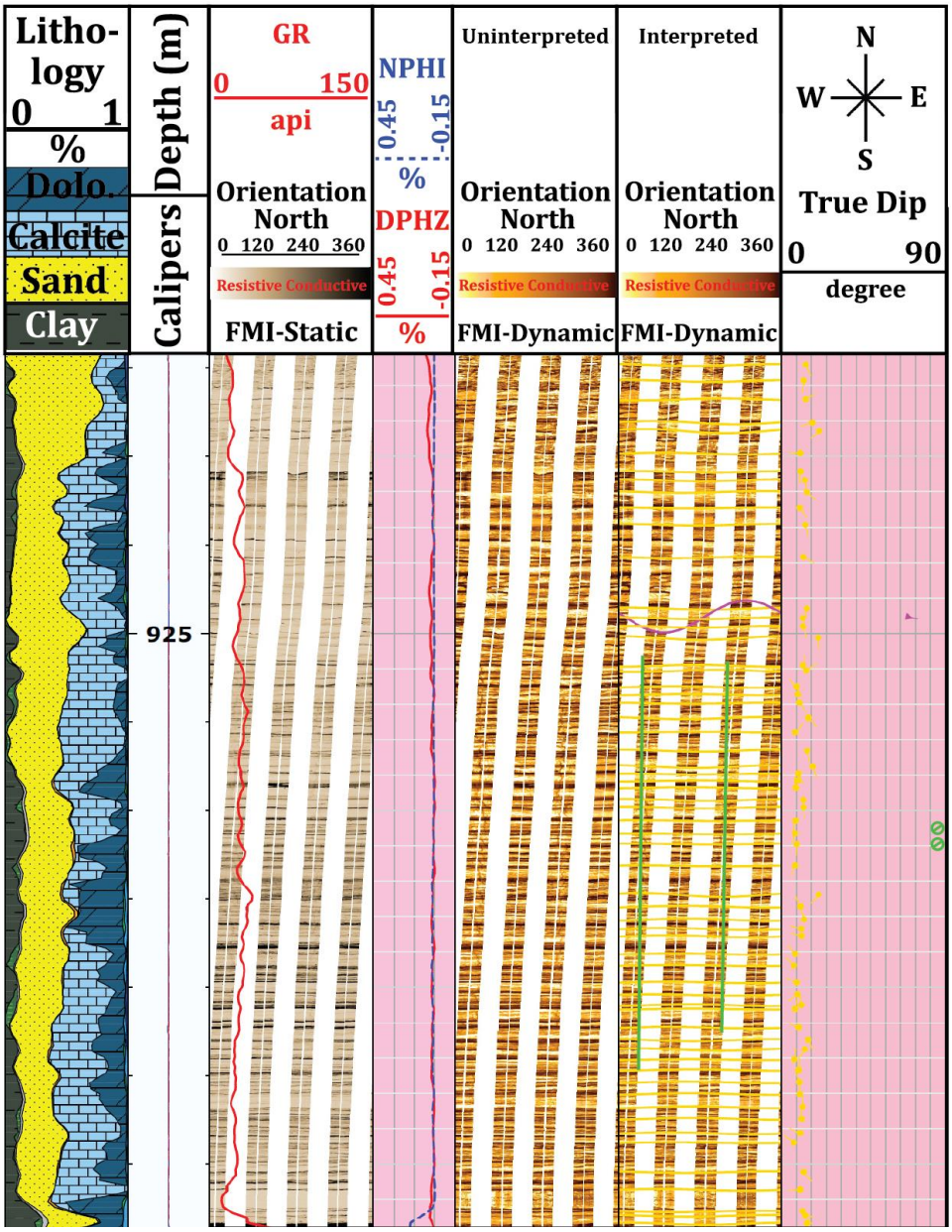

Figure 35: Interpreted log section for the Fort Payne Chert over the depth interval 917-942 m (3008-3090 ft).

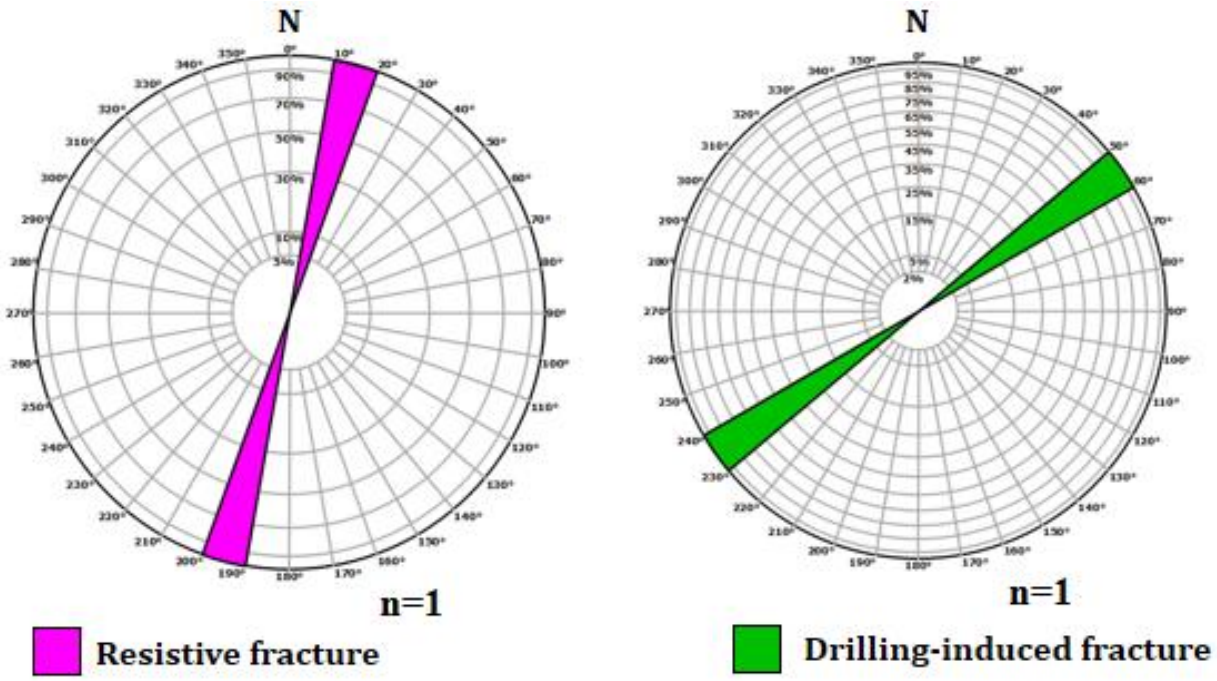

Figure 36: Rose diagrams showing the distribution of the strike orientation for the interpreted structural features in the Fort Payne Chert.

3.1.12. Knox Group 1222-1495 m (4009-4905 ft)

3.1.12.1. Chepultepec Dolomite 1222-1372 m (4009-4501 ft)

Six conductive (open) and 20 resistive (healed) fractures were observed in the Chepultepec Dolomite member of the Knox Group (Figure 45). Five sets of borehole breakouts and 29 drilling-induced tensile fractures were interpreted within the formation. The distribution of the strike orientation of these fractures and faults is displayed in Figure 46.

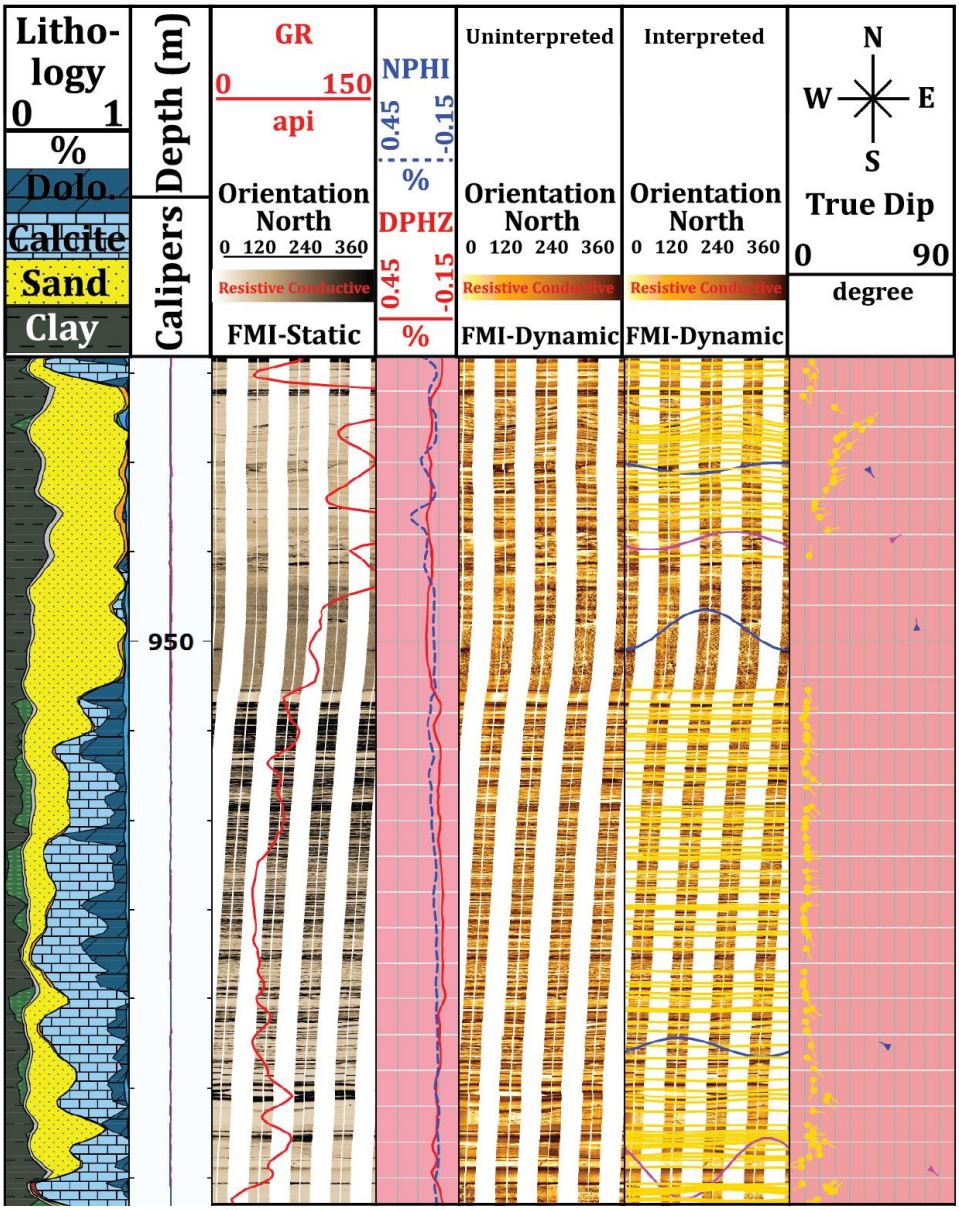

Figure 37: Interpreted log section for the Chattanooga Shale over the depth interval 942-966 m (3090-3169 ft).

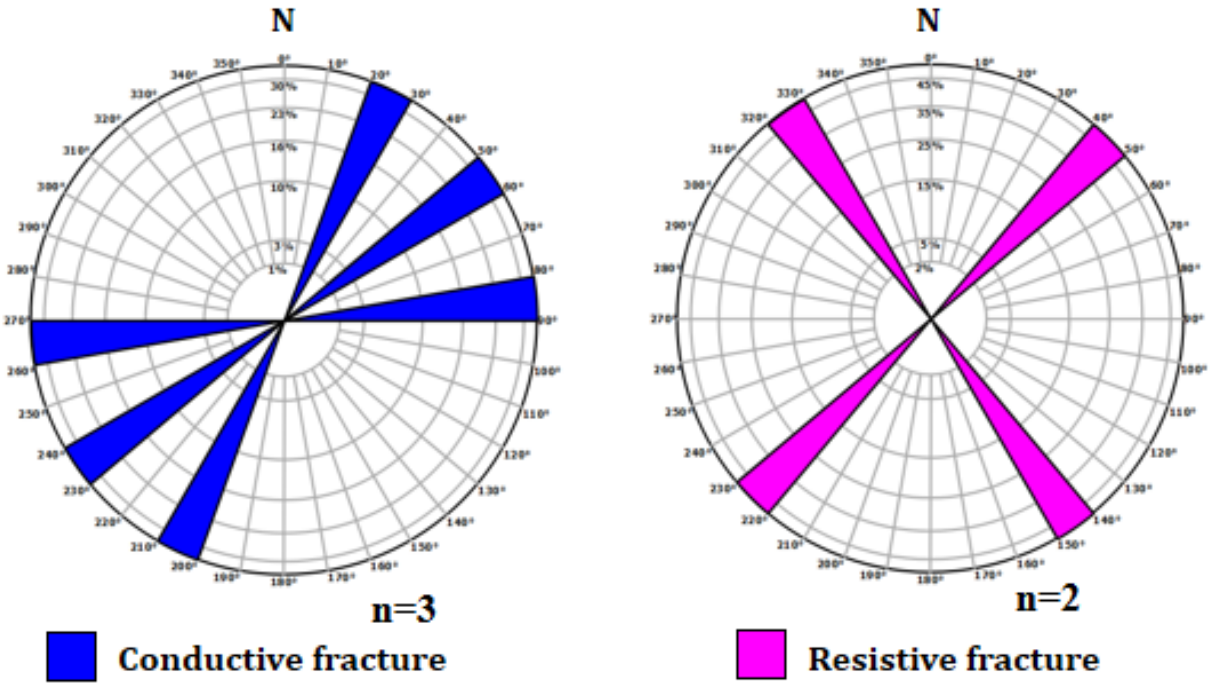

Figure 38: Rose diagrams showing the distribution of the strike orientation for the interpreted structural features in the Chattanooga Shale.

3.1.12.2. Copper Ridge Dolomite 1372-1495 m (4501-4905 ft)

Twenty four conductive (open) fractures, 45 resistive (healed) fractures, and 1 fault was observed in the Copper Ridge Dolomite member of the Knox Group (Figure 47). Both conductive and resistive fractures strike dominantly NE-SW. Two sets of borehole breakouts and 32 drilling-induced tensile fractures were interpreted within the formation. The distribution of the strike orientation of these fractures and faults is displayed in Figure 48.

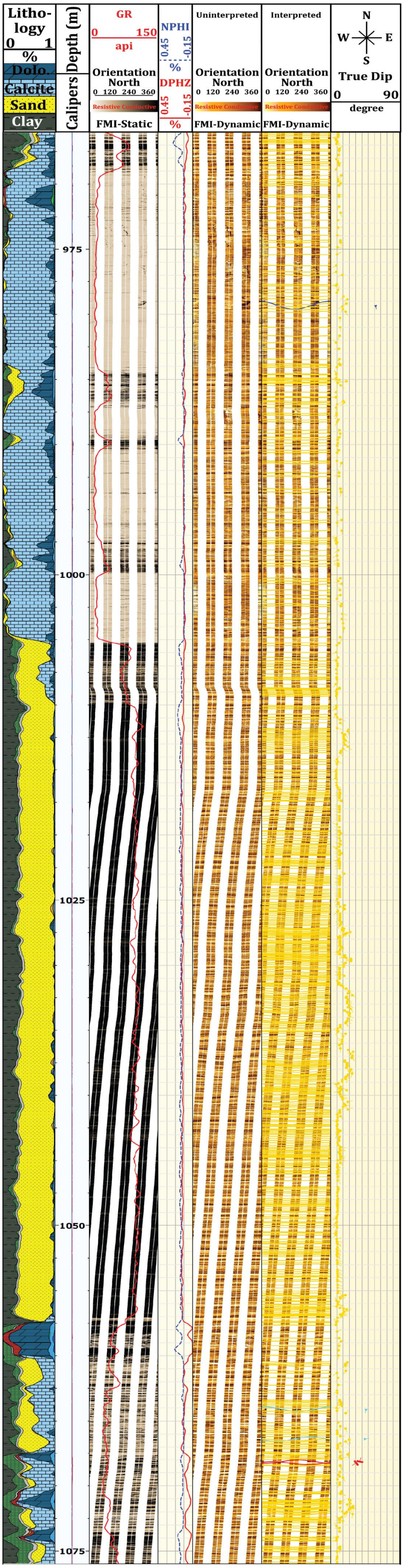

Figure 39: Interpreted log section for the Red Mountain Formation over the depth interval 966-1076 m (3169-3530 ft).

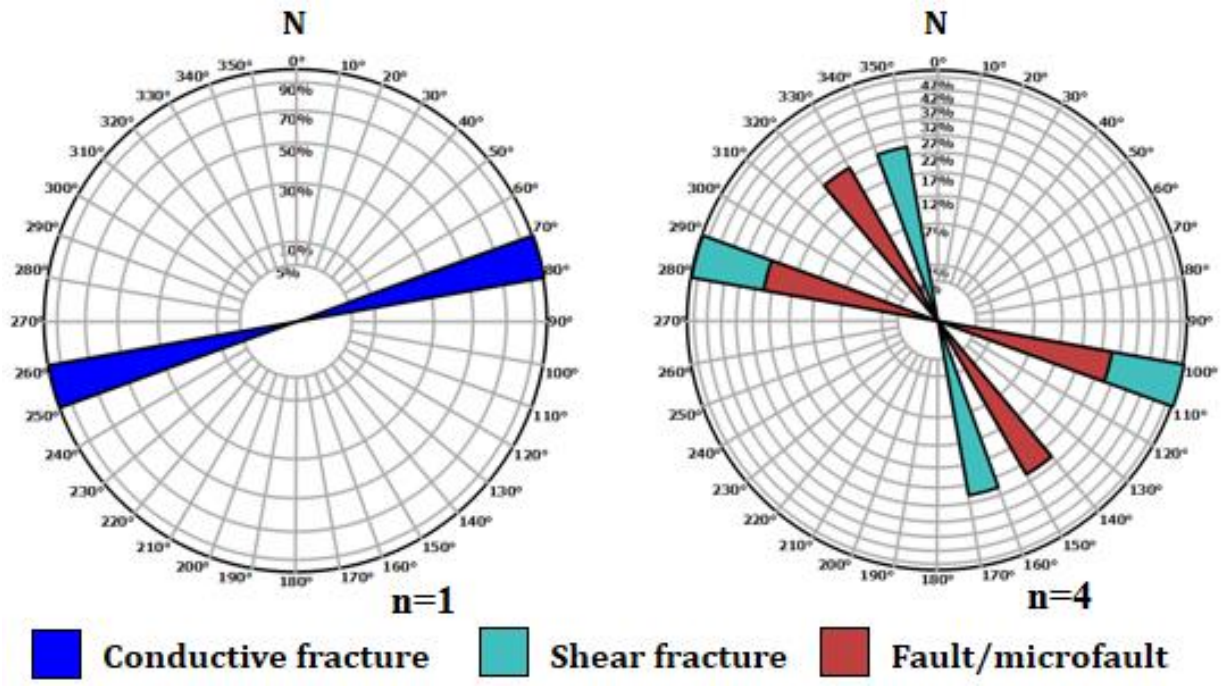

Figure 40: Rose diagrams showing the distribution of the strike orientation for the interpreted structural features in the Red Mountain Formation.

3.2. Present-day Maximum Horizontal Stress Orientation

Horizontal stress orientation was determined by interpreting borehole breakouts and drilling-induced tensile fractures (DITF) from FMI logs. A total of 64 borehole breakouts and 120 drilling-induced tensile fractures (DITF) were interpreted in the Gorgas #1 well. The mean orientation of DITFs is 50° (mode: 50°, median: 49°, standard deviation: 11°), and the borehole breakout orientation is 155° (mode: 154°, median: 154°, standard deviation: 8°). In sedimentary basins borehole breakouts provide more accurate results of horizontal stress orientations than drilling-induced fractures (Bell, 1996). The result of the interpretation indicates that the present-day maximum horizontal stress direction is oriented approximately 65° in the drilling area (Figures 49, 50).

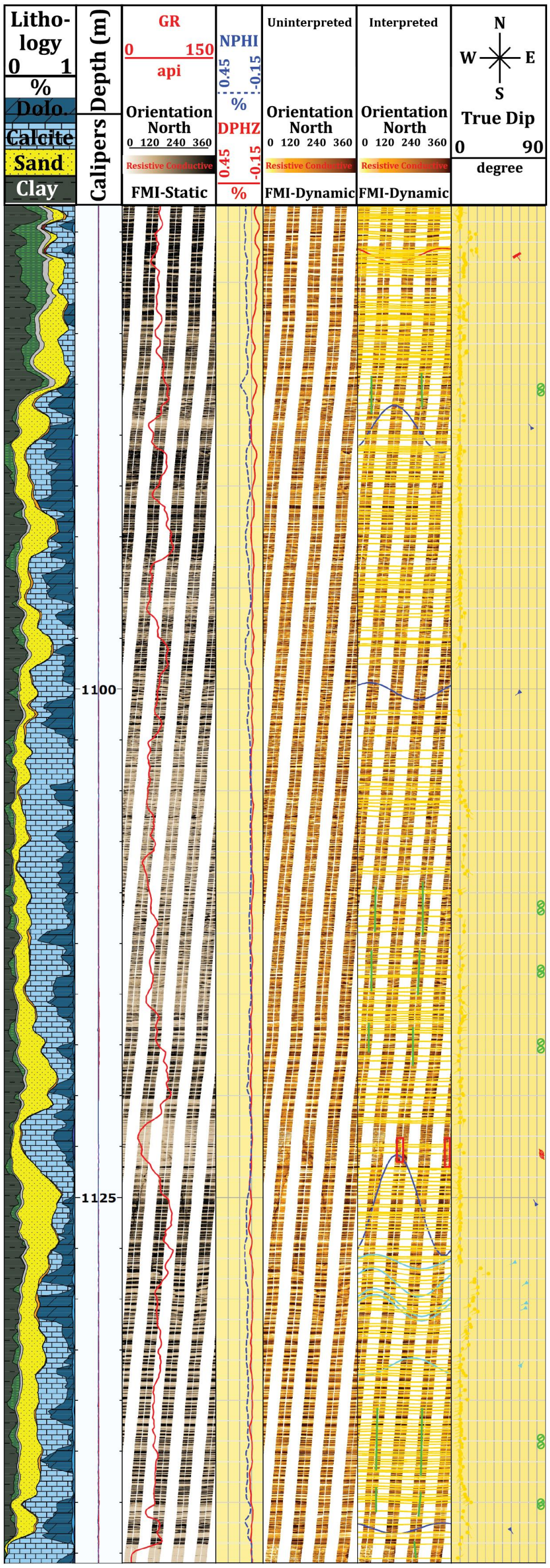

Figure 41: Interpreted log section for the Sequatchie Formation over the depth interval 1076-1143 m (3530-3750 ft).

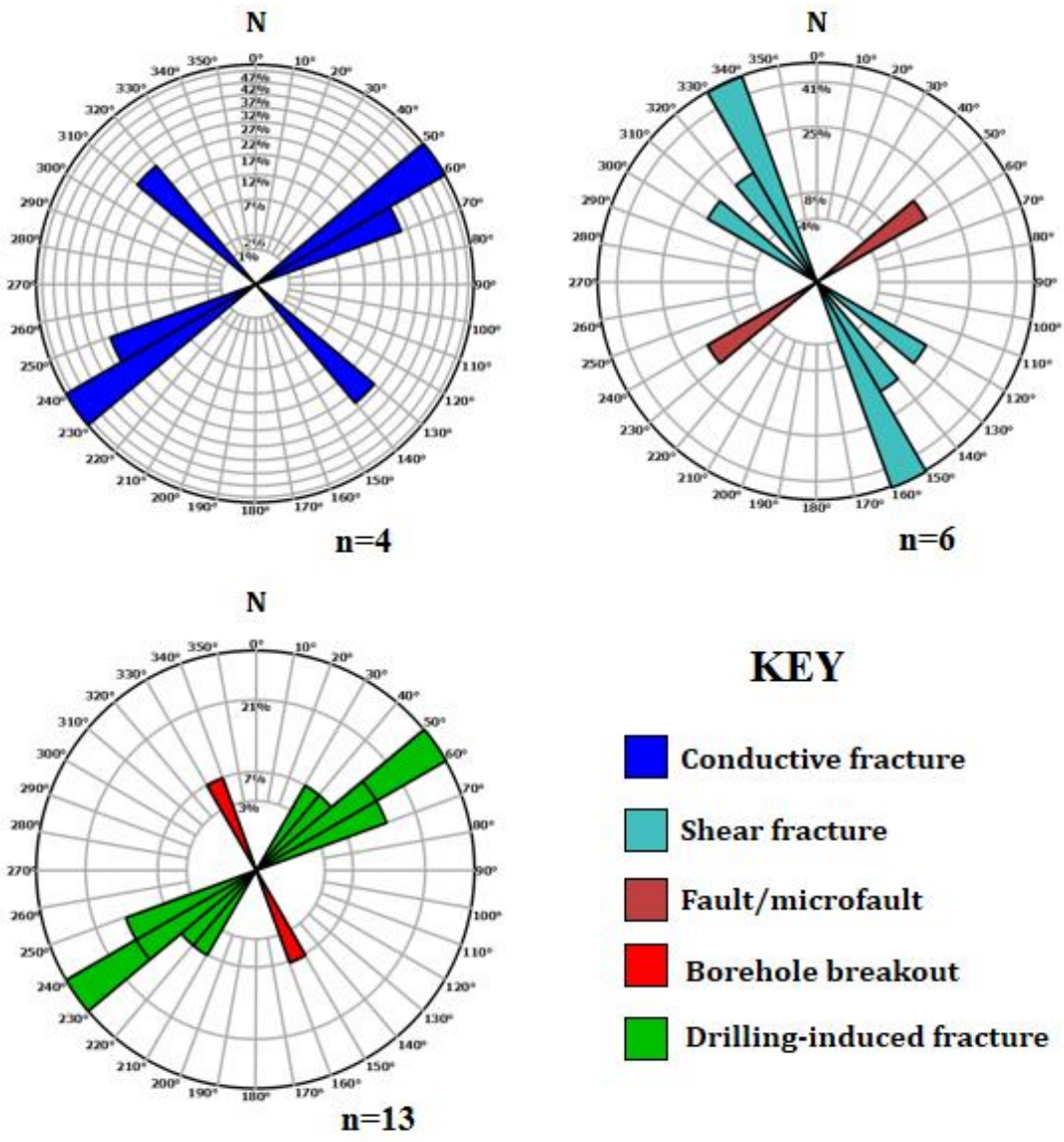

Figure 42: Rose diagrams showing the distribution of the strike orientation for the interpreted structural features in the Sequatchie Formation.

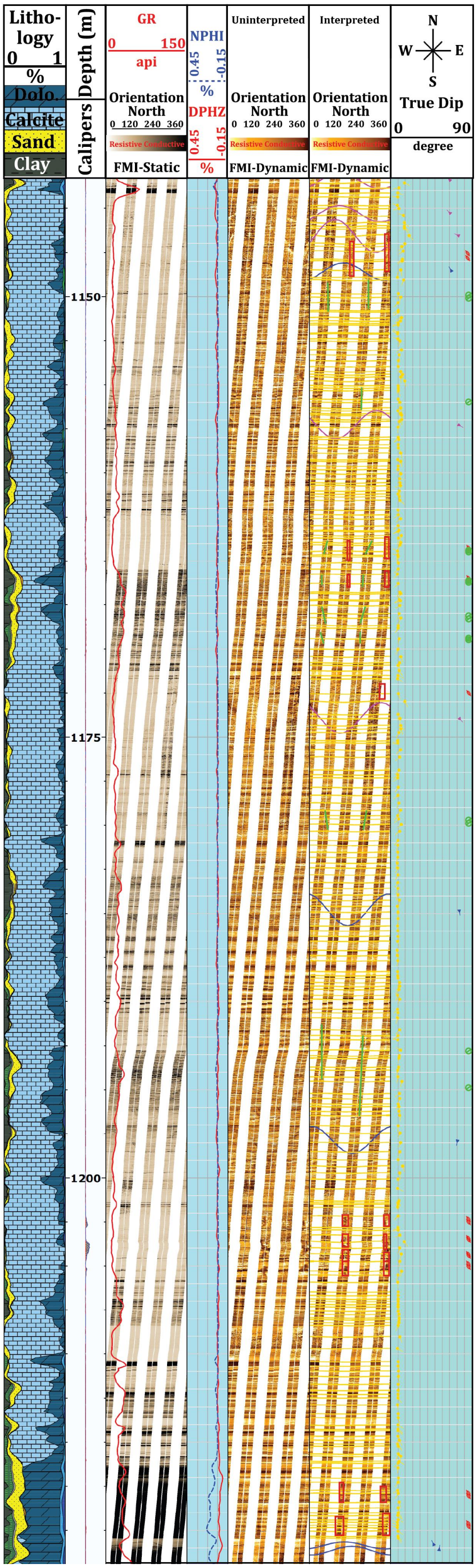

Figure 43: Interpreted log section for the Stones River Group over the depth interval 1143-1222 m (3750-4009 ft).

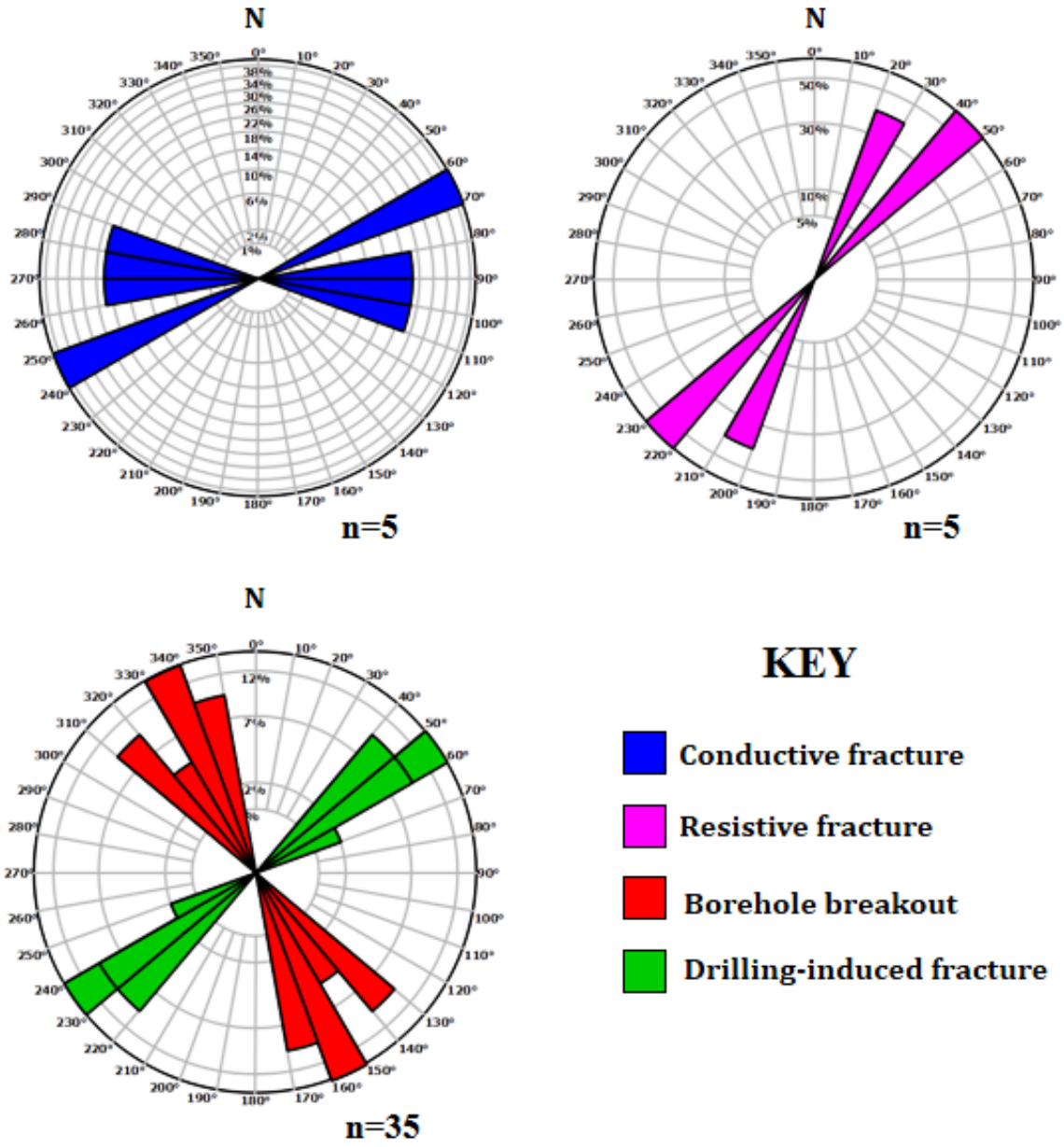

Figure 44: Rose diagrams showing the distribution of the strike orientation for the interpreted structural features in the Stones River Group.

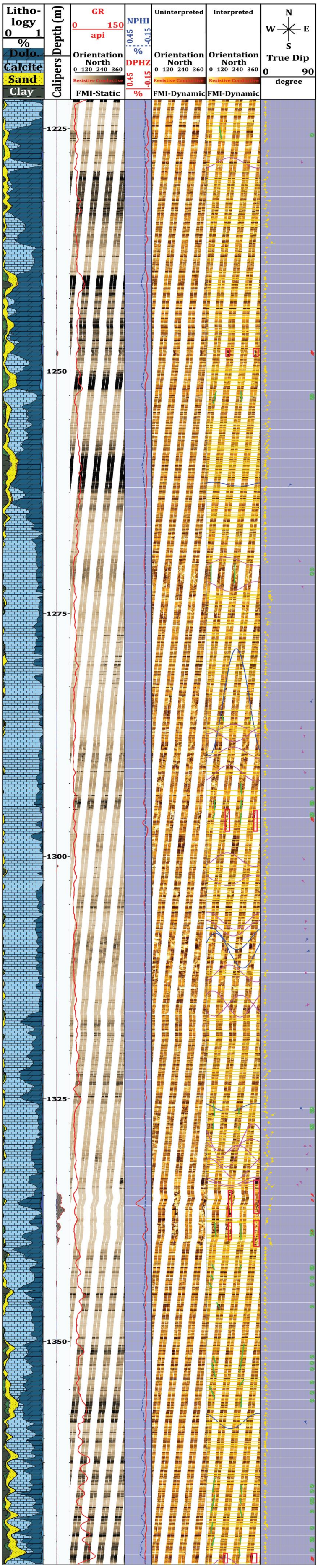

Figure 45: Interpreted log section for the Chepultepec Dolomite member of the Knox Group over the depth interval 1222-1372 m (4009-4501 ft).

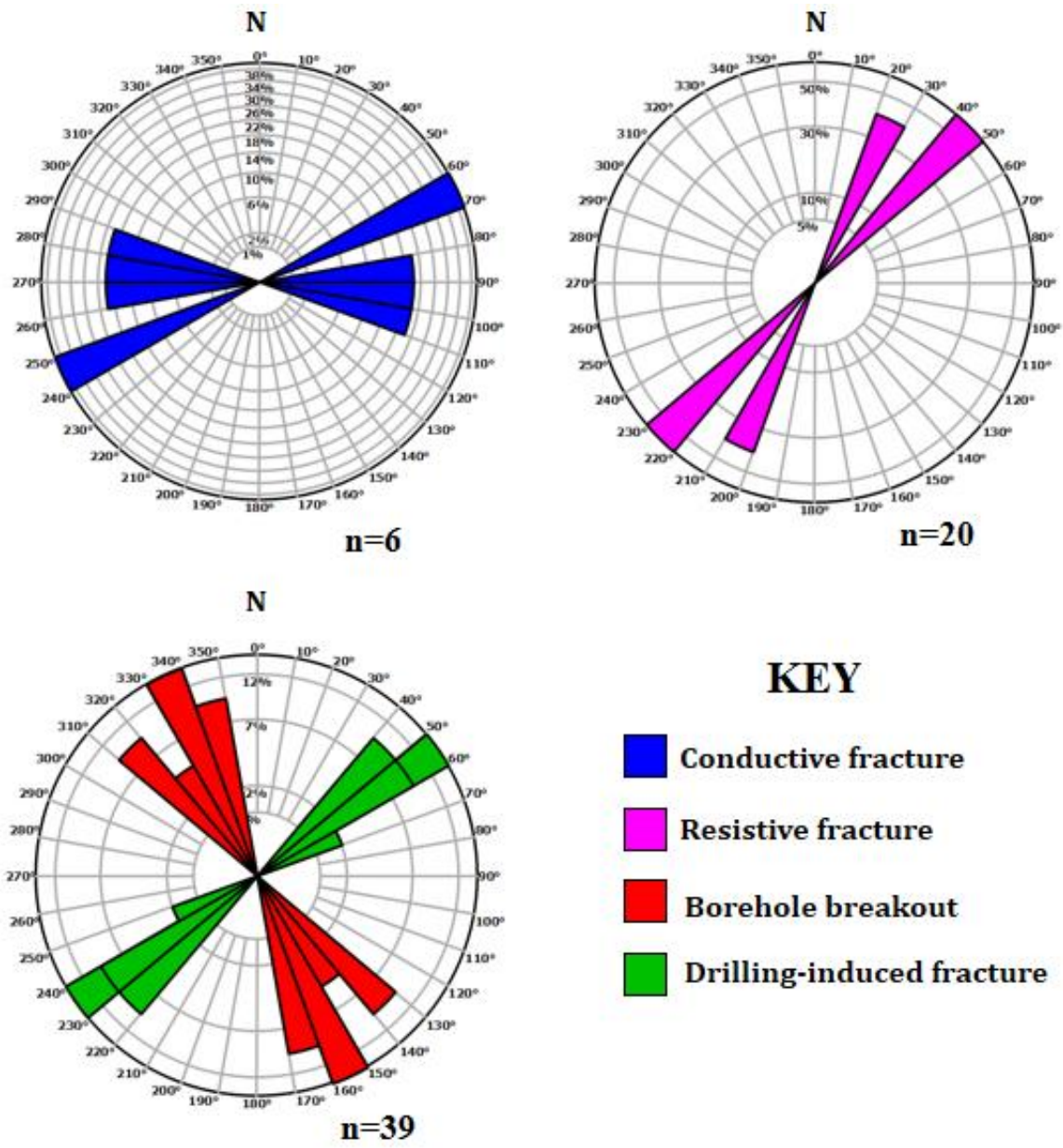

Figure 46: Rose diagrams showing the distribution of the strike orientation for the interpreted structural features in the Chepultepec Dolomite member of the Knox Group.

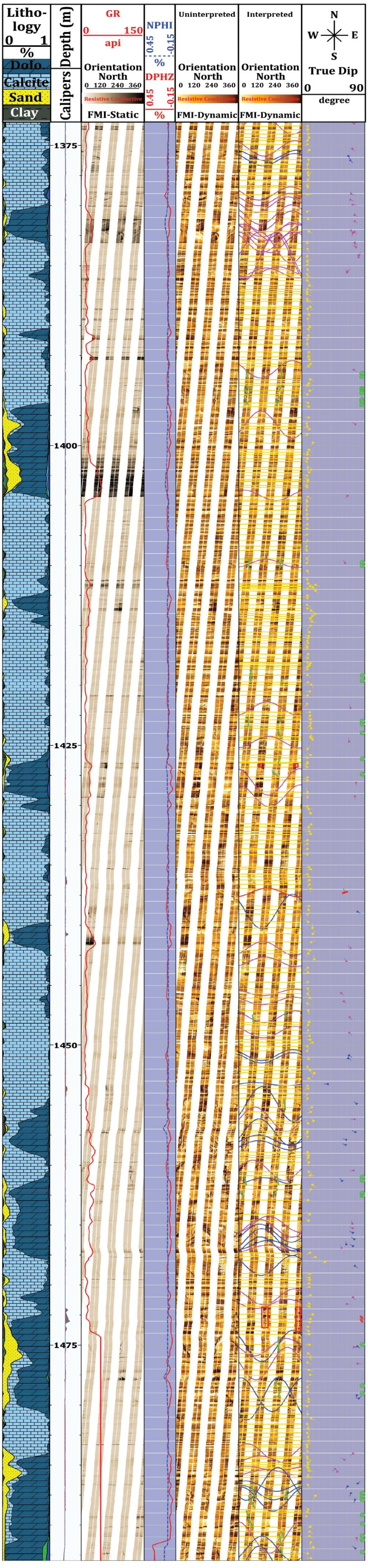

Figure 47: Interpreted log section for the Copper Ridge Dolomite member of the Knox Group at a depth of 1372-1495 m (4501-4905 ft).

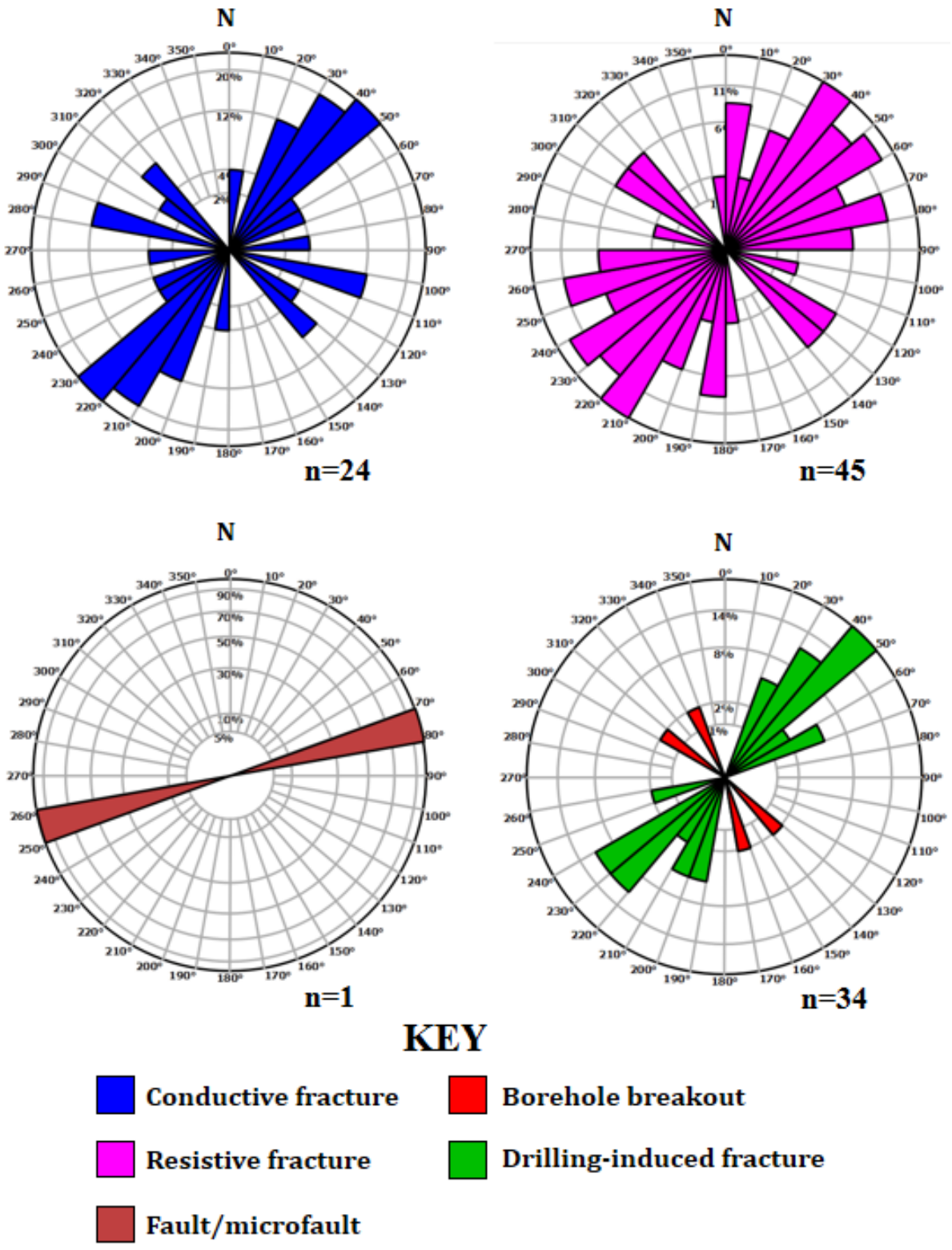

Figure 48: Rose diagrams showing the distribution of the strike orientation for the interpreted structural features in the Copper Ridge Dolomite member of the Knox Group.

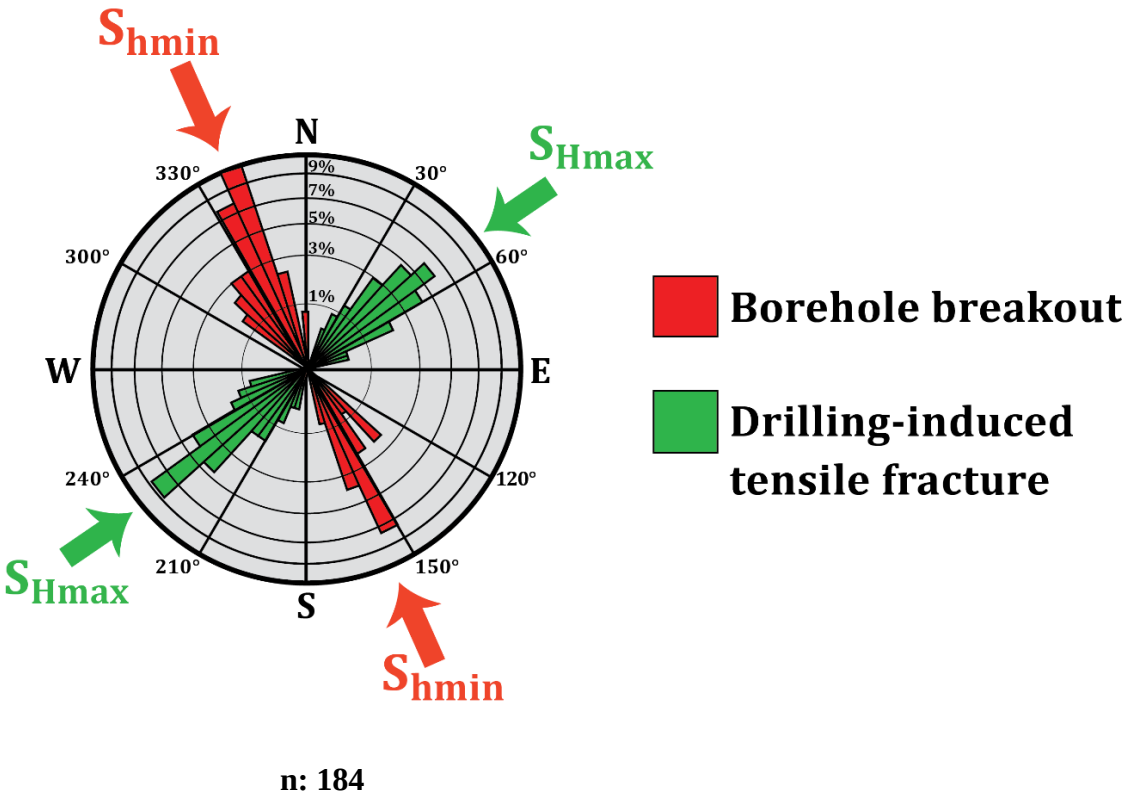

Figure 49: Strike rose diagram showing the orientation of drilling-induced tensile fractures and borehole breakouts and the interpreted horizontal stress directions for the Gorgas #1 well.

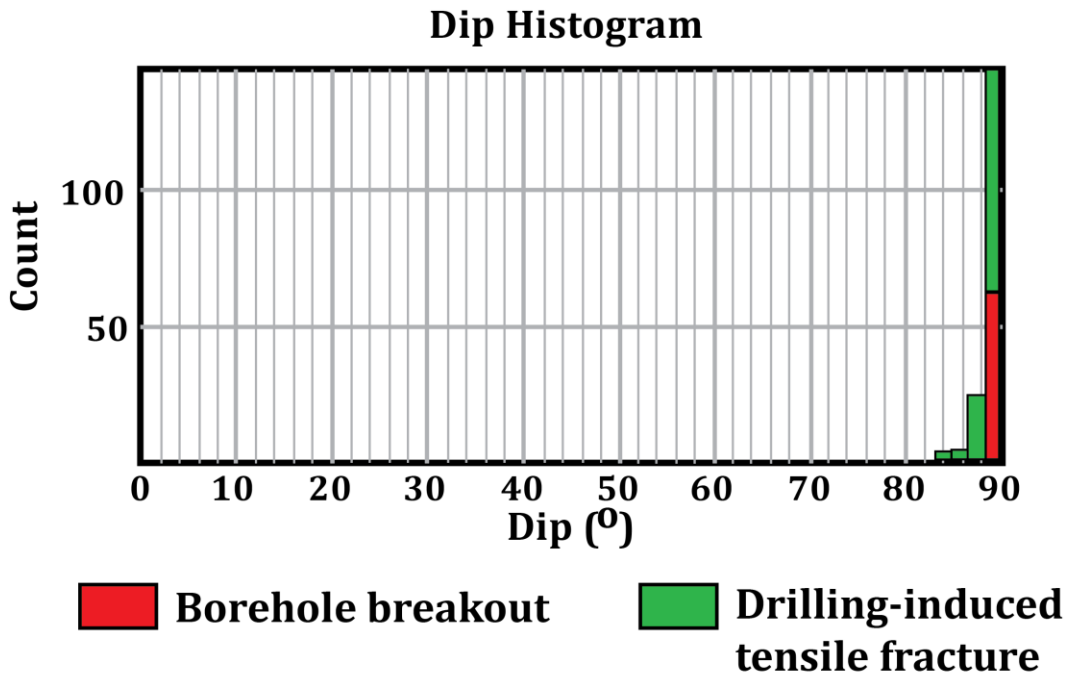

Figure 50: Dip histogram showing the dip angle distribution of drilling-induced tensile fractures and borehole breakouts in the Gorgas #1 well.

4. DISCUSSION

The origin of the modern day stress field is debated both in the Black Warrior and Appalachian basins (Sbar and Sykes, 1973; Richardson, 1992; Engelder *et al.*, 2009). In the 2008 World Stress Map (WSM) project database, the orientation of the present-day maximum horizontal stress (S_{Hmax}), as derived from nearby earthquake focal mechanism solutions and other borehole breakout and drilling-induced fracture interpretations, was determined to be N 75° E for the Black Warrior Basin and in the ENE direction for the Appalachian Basin (Zoback and Zoback, 1989; Zoback, 1992; Figure 51A). The S_{Hmax} orientation as observed herein (65°) is comparable, indicating that the same tectonic forces affect almost all of the foreland area on the western side of the Appalachian Mountains.

Based on the direction of borehole breakouts and the strike of drilling-induced fractures, there are small differences in the mean orientation of the horizontal principle stresses across the logged section of the Gorgas well. Previous studies (e.g., Haghi et al., 2013) show that these small differences in the direction of borehole breakouts and drilling-induced fractures are related to the geological heterogeneity as influence by faults, folds, and salt diapirs. In our study area, small rotations in the direction of breakouts and/or drilling-induced fractures were detected along the wellbore and might be influenced by faults and/or related to the effect of anomalies in magnetic declination measurements by the FMI tool. The FMI interpretation shows the presence of minor faults throughout the Gorgas #1 well. A major washout in the Pride Mountain Formation between 850 m (2785 ft) and 875 m (2875 ft) is the result of a fault.

The tectonic stress field is closely related to the driving mechanism of plate tectonics on a global scale. The correlations between observed tectonic stress directions and the geometry of plate boundaries has led previous workers to conclude that ridge push and/or slab pull might be the primary forces causing the present-day stress field (Solomon *et al.*, 1975; Zoback 1992). Later studies considered that topography and variations in crustal thickness and density might influence lithospheric stress (Coblentz and Richardson, 1996; Meijer *et al.*, 1997). The effect of these contributions remains hard to constrain because of the incomplete knowledge of crustal structure and its relative importance as compared to other contributions (Steinberger *et al.*, 2001). Steinberger *et al.* (2001) examined stress in the lithosphere due to tractions from mantle flow induced by density heterogeneity and found a good fit to the global stress field. Lithgow-Bertelloni and Guynn (2004) compared the findings of Steinberger *et al.* (2001) to observations of intraplate stresses from the World Stress Map (WSM) using a finite element model of the Earth's lithosphere (Figures 51B, 51C). Their model interpretations revealed that the stress field is significantly influenced by lateral variations in the viscosity of the mantle, which indicates variable amounts of decoupling between lithosphere and mantle, allowing the mantle signature to dominate in some areas and crustal signature to dominate in others.

The overwhelming majority of both conductive and resistive fractures strike NE (set i; Figures 13, 15). Set (i) is interpreted as a part of the regional ENE joint set since it is nearly parallel with the Appalachian-wide stress field (Figure 52). The ENE joints propagated within a far field stress field that affected most of the southeastern edge of Laurentia early in the Allehanian orogeny (Engelder and Whitaker, 2006). This joint set and S_{Hmax} of the observed contemporary tectonic stress field are parallel in the Black Warrior Basin (Figure 52). Engelder (1982) established that the orientation of the planar systematic joints was controlled by the

modern S_{Hmax} in the North American lithosphere. Later studies showed that the parallelism of S_{Hmax} and the ENE regional joint set is a geologic coincidence (Engelder and Whitaker, 2006). In the late Paleozoic, this joint set formed in the ENE direction as a consequence of plate-boundary tractions arising from late-stage oblique convergence, where maximum horizontal stress of the AWSF was parallel to the direction of closure between Gondwana and Laurentia (Hatcher, 2002; Engelder and Whitaker, 2006). The modern eastern edge of Laurentia has been interpreted to be oriented ~45° clockwise from its present orientation such that this same edge of Laurentia faced south (modern coordinates; Engelder *et al.*, 2009). However, post-Paleozoic continental drift carried these joints into their present orientation parallel to the S_{Hmax} of the contemporary stress field (Engelder *et al.*, 2009). This situation makes it difficult to separate neotectonic joints from the regional ENE joints.

The second dominant orientation observed in both conductive and resistive fractures is the NW-SE trending fractures (set ii, Figures 13, 15). This fracture set is perpendicular to the NE-SW trending frontal structures of the Appalachian fold and thrust belt. They are interpreted herein to represent the cross-fold joints restricted to Alleghanian folds (Figure 52).

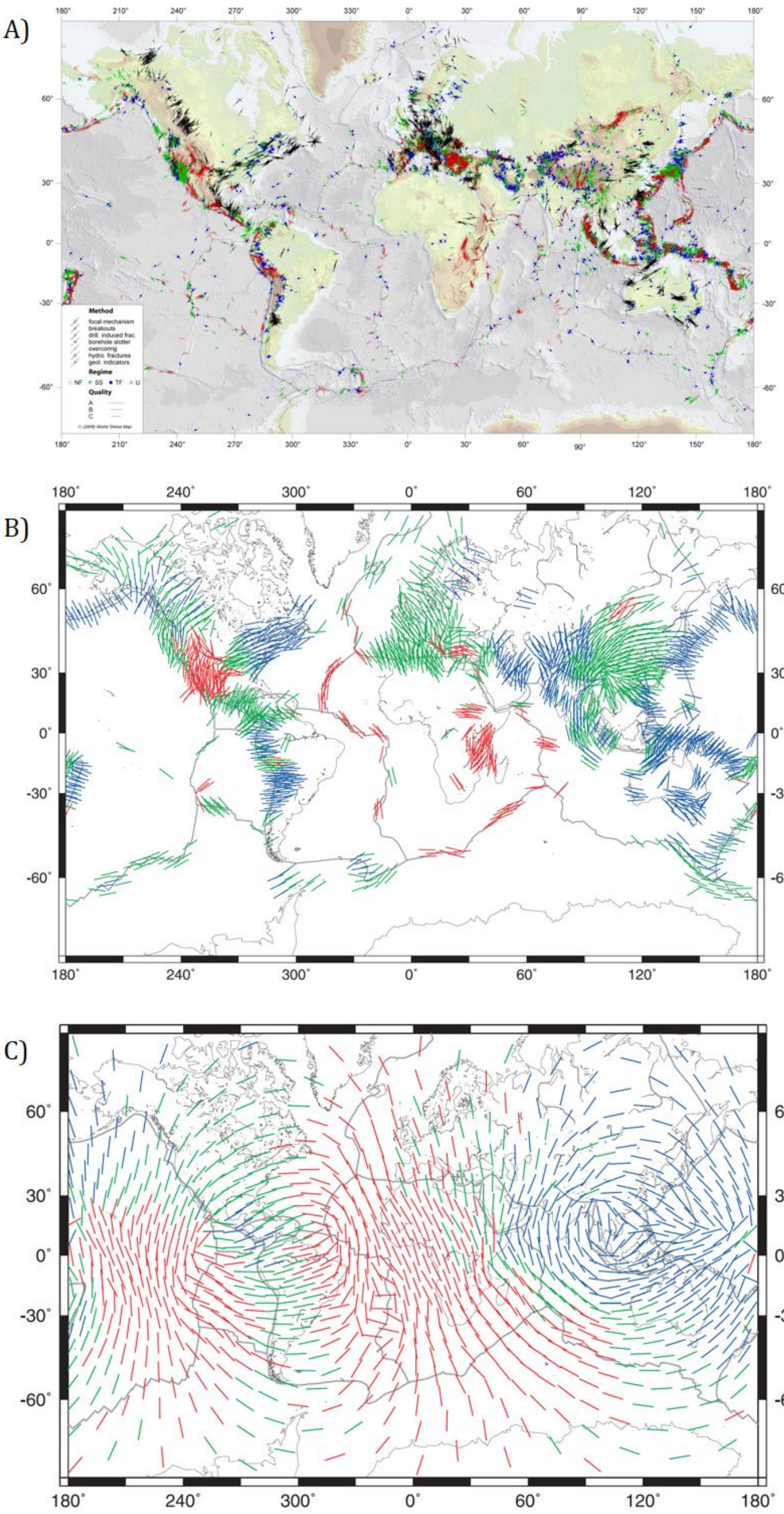

Figure 51: Comparison of the findings in the World Stress Map (WSM) project with Lithgow-Bertelloni and Guynn (2004). A) World Stress Map, release 2008 (Heidbach *et al.*, 2008); B) Interpolated S_{Hmax} directions from WSM used in the finite element model (Lithgow-Bertelloni and Guynn, 2004); and C) The result of global computational model of stresses produced by mantle tractions and crustal contributions (Lithgow-Bertelloni and Guynn, 2004). Lines are oriented in the direction of the most compressive horizontal stress. Red indicates a normal stress regime, green indicates strike-slip, and blue indicates thrust.

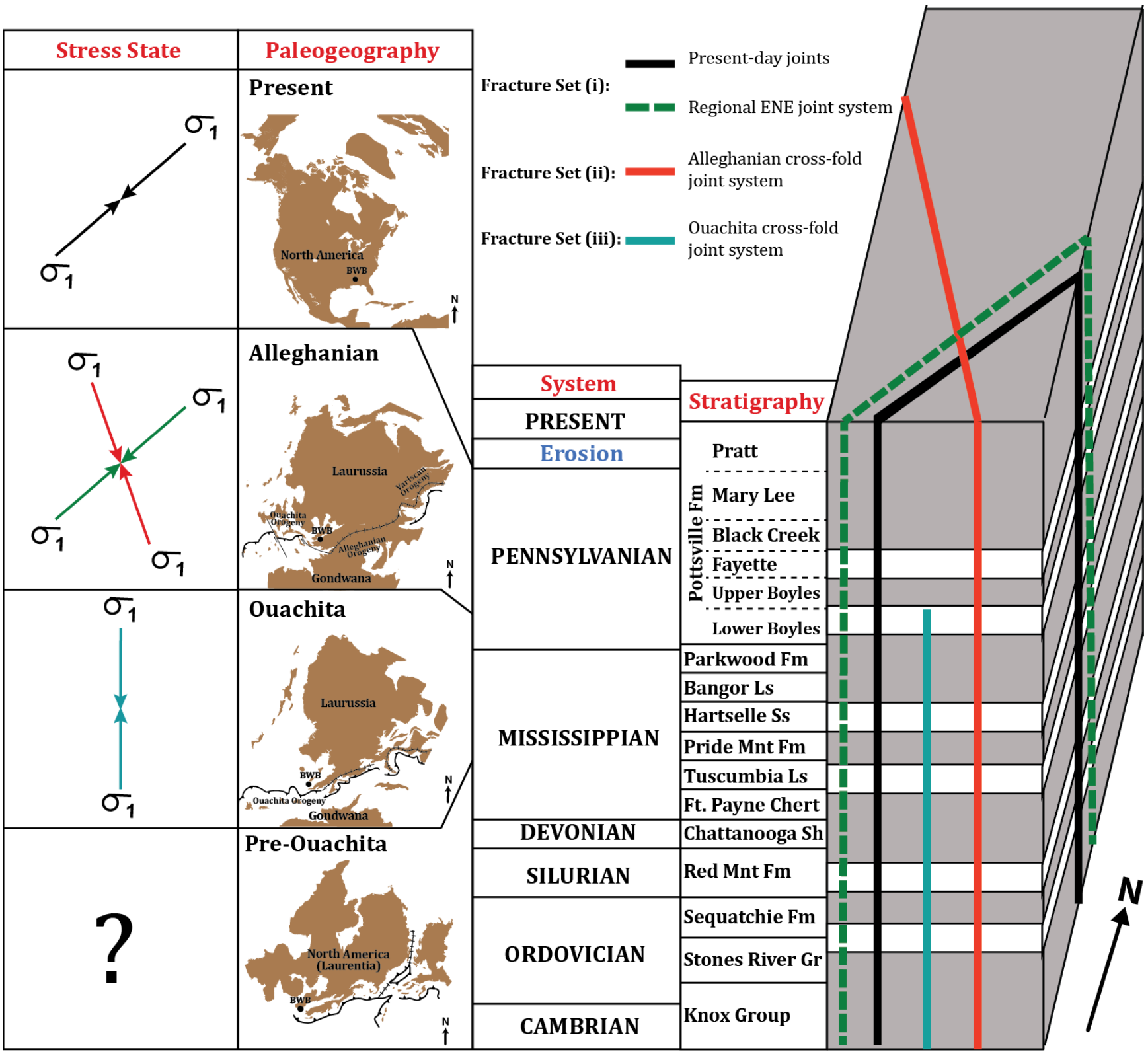

Figure 52. A cartoon showing the interpreted fracture systems and related stress orientations in the Gorgas #1 well.

Any structural influence from the Ouachita thrust belt is observed in the basin based on the conductive (open) fracture interpretation. The most significant finding in this study is the existence of N-S oriented resistive (healed) fractures (set iii; Figure 15). Because of their potential importance, these N-S oriented resistive fractures (set iii) have been intensively investigated. The resistive fractures aligned in the N-S direction are seen first in the Early Pennsylvanian lower Boyles section and persist down through the Knox Group, in the Gorgas #1 well (Figure 52). This interpretation is significant because the orientation of resistive fractures can be used to identify past stress field orientations if they are different from the present day environment. Two rose diagrams were used to demonstrate the differences of interpreted orientation distributions between the upper Boyles and younger strata (Figure 53A), and the lower Boyles and older strata (Figure 53B). The orientation of N-S trending resistive fractures (set iii) is different from the present day environment and indicates an older stress field environment.

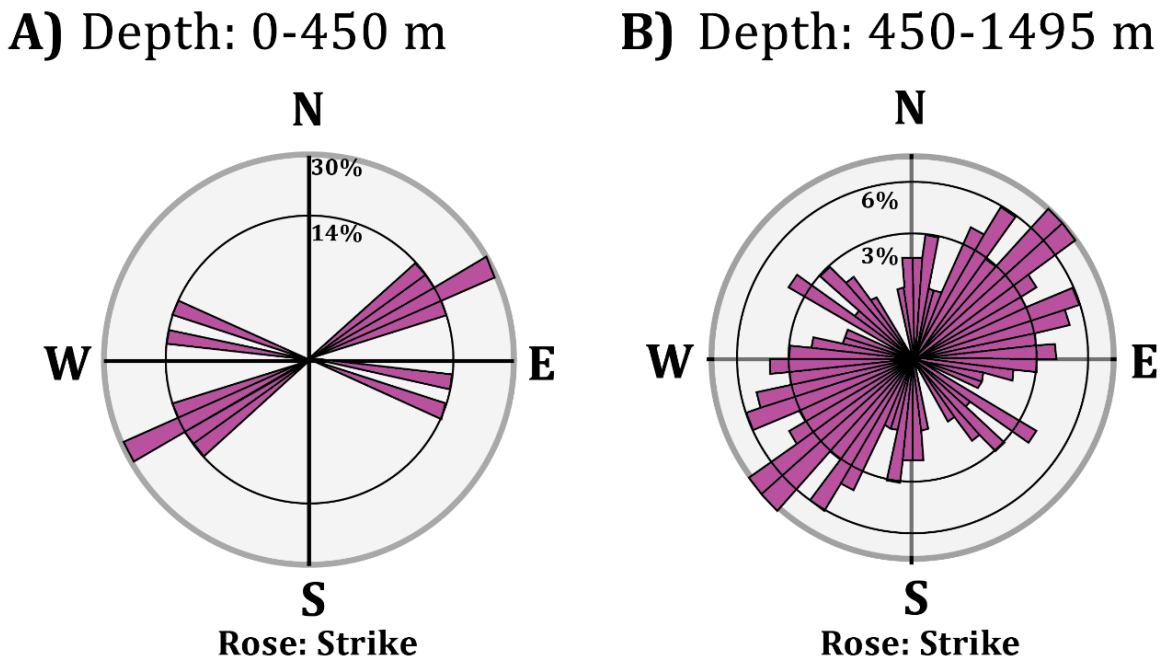

Figure 53: Strike rose diagrams of resistive (healed) fractures interpreted in A) upper Pottsville Formation, and B) lower Pottsville Formation and older strata.

Pashin (2004) presented a similar change in subsidence patterns and depocenters between the upper Boyles and younger strata, and the lower Boyles and older strata in the Black Warrior Basin. Pashin (2004) revealed the different cycles in the Pennsylvanian strata in the Black Warrior Basin related to tectonic and eustatic changes. Pashin (2004) showed that the south-southwestward increasing subsidence pattern of the upper Parkwood Formation indicates the existence of a Ouachita foreland basin. At that time, Appalachian tectonism appears to have had no significant effect. The lower Boyles cycle subsidence pattern indicates a transition between the upper Parkwood Formation and the younger cycles. The upper Boyles and younger cycles in the Pottsville Formation have a southeastward increasing subsidence pattern and have been interpreted as a result of the Appalachian orogeny.

Whitaker and Engelder (2006) documented the orientation of cross-fold jointing related to northward-verging thrusting in the Ouachita fold belt. Their mean joint orientation interpretations showed differences among the structural provinces, but they maintained a N-S orientation (Figure 54). In the central thrust belt, the mean cross-fold joint set strikes range from N 5° W to N 20° E, in the frontal imbricate zone, range from N 20° W to N 25° E, and in the Arkoma Basin, range from N 20° W to N.

Based on the fracture analysis results, the subsidence pattern documented by Pashin (2004), and the regional joint pattern observed in the Ouachita fold belt and the Arkoma Basin, the N-S oriented resistive (healed) fractures in the Gorgas well are interpreted to be related to a pre-Alleghanian origin, most likely the effect of NNE converging thrust and sediment loads of the Ouachita orogeny in the Black Warrior Basin (Figure 52).

The results indicate that the previous explanations about the origin of NW-SE trending thin-skinned normal faults in the Pottsville Formation may be misleading. These faults were interpreted to be result of Ouachita flexural extension (Bradley and Kidd, 1991; Cates *et al.*, 2004). However, the structural and stratigraphic effects of the Ouachita orogeny are seen only in the lower part of the Pottsville Formation in the Black Warrior Basin. The proposed NE-SW extension direction for the Pottsville thin-skinned normal faults conflict with the NNE convergence direction for the Ouachita orogeny documented in this study. Therefore, one scenario to explain these thin-skinned normal faults in the basin would be the northwest-converging Alleghanian orogeny creating NW-SE trending compression, and related NE-SW extensional stress field perpendicular to the compression in the foreland basin.

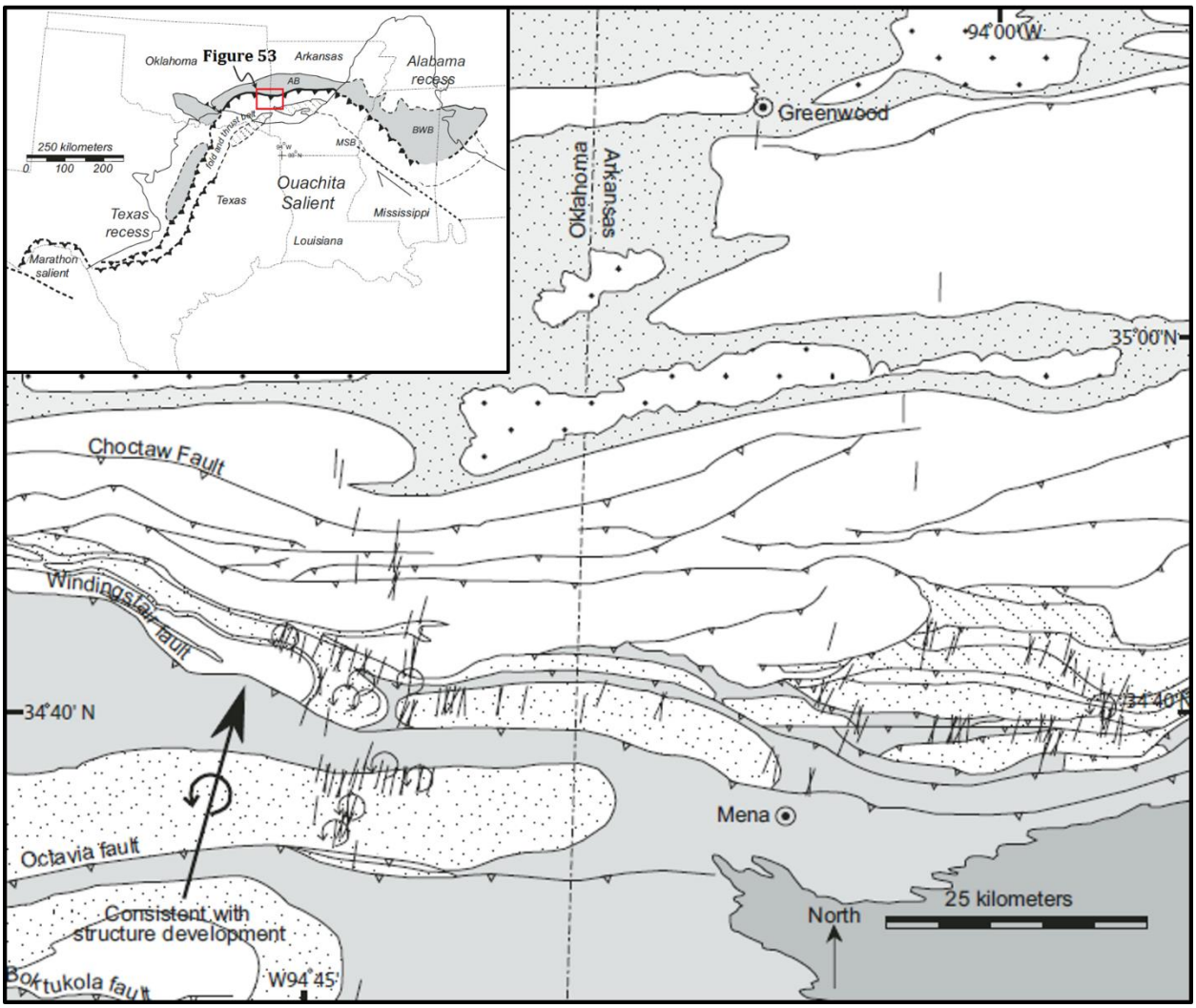

Figure 54: Simplified geological map of the central Ouachita fold and thrust belt and Arkoma Basin with the NNE-striking cross-fold joints and the tectonic compression direction proposed by joints in the area (modified after Whitaker and Engelder, 2006).

5. CONCLUSION

This study details the subsurface natural and induced fracture systems interpreted using FMI logs collected from the Gorgas #1 well, in the Black Warrior Basin.

1) Analysis of drilling-induced tensile fractures and borehole breakouts in the Gorgas well indicates the present-day maximum horizontal stress direction is oriented at approximately N 65° E in the drilling area.

2) Fracture set (i) has a 45°-75° strike orientation interpreted as a part of the regional ENE joint set related to the Appalachian-wide stress field and/or neotectonic joints system. Because both the regional joint system and the contemporary stress field share the same orientation, it is impossible to separate the origin of these fractures in FMI log.

3) Fracture set (ii) has a 120°-140° strike orientation interpreted herein to represent the cross-fold joints in the Black Warrior Basin.

4) Fracture set (iii) has a 0°-10° strike orientation. The fracture set consists of only resistive fractures, and is observed in the lower Pottsville and older strata. These fractures are interpreted as being related to the NNE-converging Ouachita thrust belt. The N-S oriented resistive fractures, the subsidence pattern of the Pennsylvanian strata in the Black Warrior Basin, and the similarity in orientation with the regional joint system observed in the Arkoma Basin, leads to the conclusion that the thin-skinned normal faults in the Pottsville strata could be related to the NE-SW oriented extensional stress field associated with the Alleghanian orogeny as opposed to the Ouachita orogeny.

REFERENCES

Ameen, M., 2003, Fracture and In-Situ Stress Characterization of Hydrocarbon Reservoirs: Definitions and Introduction: Geological Society, London, Special Publication 209, 217 p.

Anderson, E. M., 1951, The Dynamics of Faulting and Dyke Formation with Application to Britain. 2nd edn., Oliver & Boyd, Edinburgh, 206 p.

Angelier, I., Tamntola, A., Valette, B., and Manoussis, S., 1982, Inversion of field data in fault tectonics to obtain the regional stress, I, Single phase fault populations. A new method of computing the stress tensor: Geophysical Journal of the Royal Astronomical Society, v. 69, p. 607–621.

Angelier, J., 1990, Inversion of field data in fault tectonics to obtain the regional stress. 3. A new rapid direct inversion method by analytical means: Geophysical Journal International, v. 103, p. 363-376.

Angelier, J., 1994, Fault-slip analysis and paleostress reconstruction, in Hancock, P. L., eds., Continental Deformation, Pergamon, Oxford, p. 101–120.

Bayona, G., Thomas, W. A., and Van der Voo, R., 2003, Kinematics of thrust sheets within transverse zones: a structural and paleomagnetic investigation in the Appalachian thrust belt of Georgia and Alabama: Journal of Structural Geology, v. 25, p. 1193-1212.

Bell, J. S., 1996, In situ stresses in sedimentary rocks (part 1): measurement techniques: Geoscience Canada, v. 23, p. 85–100.

Bell, J.S., and Gough, D.I., 1979, Northeast–southwest compressive stress in Alberta: evidence from oil wells: Earth Planet. Science Letters, v. 45, p. 475–482.

Bradley, D. C., and Kidd, W. S. F., 1991, Flexural extension of the upper continental crust in collisional foredeeps: Geological Society of America Bulletin, v. 103, p. 1416-1483.

Branan, C. B., Jr., 1968, Natural gas in Arkoma basin of Oklahoma and Arkansas, *in* B. Rascoe, Jr, and N. J. Hyne, eds., Petroleum geology of the Mid-continent: Tulsa Geological Society Special Publication 3, Oklahoma. Reprinted and edited from B. W. Bebee and B. F. Curtis, eds., 1968, Natural gas of North America: American Association of Petroleum Geologists Memoir 9, v. 2, Tulsa, Oklahoma, p. 1616–1635.

Brandes C., Schmidt, C., Tanner, D. C., and Winsemann, J., 2013, Paleostress pattern and salt tectonics within a developing foreland basin (north-western Subhercynian Basin, northern Germany): International Journal of Earth Sciences, v. 102, p. 2239-2254.

Cates, L. M., and Groshong, R. H., Jr., 1999, Confirmation of regional thin-skinned extension in the eastern Black Warrior Basin, Alabama, *in* Pashin, J. C., and Carroll, R. E., eds., Geology of the Cahaba Coalfield: 36th Annual Field Trip Guidebook: Tuscaloosa, Alabama, Alabama Geological Society, p. 49-57.

Cates, L. M., McIntyre, M.R., Hawkins, W. B., and Groshong, R. H., Jr., 2004, Structure and oil & gas production in the Black Warrior Basin, *in* University of Alabama College of Continuing Studies, 2004 Proceedings of the International Coalbed Methane Symposium: Tuscaloosa, University of Alabama Paper 0440, 34 p.

Coblentz, D. D., and Richardson, R. M., 1996, Analysis of the South American intraplate stress field: Journal of Geophysical Research: Solid Earth, v. 101, p. 8643-8657.

Delvaux, D., Moeys, R., Stapel, G., Melkinov, A., and Erminow, V., 1995, Paleostress reconstructions and geodynamics of the Baikal region, Central Asia, Part 1. Paleozoic and Mesozoic pre-rift evolution, Tectonophysics, v. 252, p. 61-101.

Delvaux, D., Moeys, R., Stapel, G., Petit, C., Levi, K., Miroshnichenko, A., Ruzhich, V., and San'kov, V., 1997, Paleostress reconstructions and geodynamics of the Baikal region Central Asia, Part 2. Cenozoic rifting: Tectonophysics, v. 282 p. 1–38.

Donselaar, M. E., and Schmidt, J. M., 2005, Integration of outcrop and borehole image logs for high-resolution facies interpretation: example from a fluvial fan in the Ebro Basin, Spain: Sedimentology, v. 52, no. 5, p. 1021-1042.

Driese, S. G., Srinivasan, K., Mora, C. I., and Stapor, F. W., 1994, Paleoweathering of Mississippian Monteagle Limestone preceding development of a Lower Chesterian transgressive systems tract and sequence boundary, middle Tennessee and northern Alabama: Geological Society of America Bulletin, v. 106, no. 7, p. 866-878.

Engelder, T., 1982, Is there a relationship between regional joints and contemporary stress within the lithosphere of North America?: Tectonics, v. 1, p. 161-177.

Engelder, T., 1993, Stress Regimes in the Lithosphere: Princeton, Princeton University Press, New Jersey, U.S.A. 475 p.

Engelder, T., and Whitaker, A., 2006, Early jointing in coal and black shale: Evidence for an Appalachian-wide stress field as a prelude to the Alleghanian orogen: Geology, v. 34, p. 581–584.

Engelder, T., Lash, G. G., and Uzcátegui, R. S., 2009, Joint sets that enhanced production from Middle and Upper Devonian gas shales of the Appalachian basin: American Association of Petroleum Geologists Bulletin, v. 95, p. 857-889.

Etchecopar, A., Vasseur, G., and Daignieres, M., 1981, An inverse problem in microtectonics for the determination of stress tensors from fault striation analysis: Journal of Structural Geology, v. 3, p. 51–56.

Ettensohn, F.R., 2008,Chapter 4,The Appalachian foreland basin in the eastern United States, *in* Miall, A., eds., The Sedimentary basins of the United States and Canada: Sedimentary Basins of the World, Amsterdam, Elsevier, p. 105–179.

Ferrill, B. A, 1989, Middle Cambrian to Lower Mississippian Synsedimentary Structures in the Appalachian Fold-Thrust Belt in Alabama and Georgia, Ph.D. dissertation, The University of Alabama, Tuscaloosa, AL, 270 p.

Groshong, R.H., Jr., Hawkins, W.B., Jr., Pashin, J.C., and Harry, D.L., 2010, Extensional structures of the Alabama Promontory and Black Warrior foreland basin: Styles and relationship to the Appalachian fold-thrust belt, *in* Tollo, R.P., Bartholomew, M.J., Hibbard, J.P., and Karabinos, P.M., eds., From Rodinia to Pangea: The Lithotectonic Record of the Appalachian Region: Geological Society of America Memoir, v. 206, p. 579-605.

Groshong, R.H., Jr., Pashin, J.C., and McIntyre, M.R., 2009, Structural controls on fractured coal reservoirs in the southern Appalachian Black Warrior foreland basin: Journal of Structural Geology, v. 31, p. 874–886.

Haase, C. S., Walls, E. C., and Stow, S.H., 1985, Stratigraphic and structural data for the Conasauga Group and the Rome Formation on the Copper Creek fault block near Oak Ridge, Tennessee: Preliminary results for test borehole ORNL-JOY No. 2. ORNL/TM-9159: Oak Ridge National Laboratory, 88 p.

Haghi, A. H., Kharrat, R., Asef, M. R., and Rezazadegan, H., 2013, Present-day stress of the central Persian Gulf: implications for drilling and well performance: Tectonophysics, v. 608, p. 1429-1441.

Hatch, J. R., and Pawlewicz, M. J., 2007, Geologic assessment of undiscovered oil and gas resources of the Black Warrior Basin Province, Alabama and Mississippi: U.S. Geological Survey Digital Data Series DDS–69–I.

Heidbach, O., Tingay, M., Barth, A., Reinecker, J., Kurfeß, D., and Müller, B., 2008. The 2008 Release of the World Stress Map available online atwww.world-stress-map.org

Hines, R. A., Jr., 1988, Carboniferous evolution of the Black Warrior foreland basin, Alabama and Mississippi: Ph.D. thesis: University of Alabama, Tuscaloosa, Alabama, 231 p.

Horsey, C. A., 1981, Depositional environments of the Pennsylvanian Pottsville Formation in the Black Warrior basin of Alabama: Journal of Sedimentary Petrology, v. 51, no. 3, p. 799-806.

Huerta, A. D., and Harry, D. L., 2012, Wilson cycles, tectonic inheritance, and rifting of the North American Gulf of Mexico continental margin: Geosphere, v. 8, no. 2, p. 374-385.

Hurley, N. F., 1994, Recognition of faults, unconformities and sequence boundaries using cumulative dip plots: American Association of Petroleum Geologists Bulletin, v. 78, p. 1173-1185.

Lithgow-Bertelloni, C., and Guynn, J. H., 2004, Origin of the lithospheric stress field: Journal of Geophysical Research, v. 109, B01408, doi: 10.1029/ 2003JB002467.

Mancini, E. A., Bearden, B. L., Holmes, J. W., and Shepard, B. K., 1983, Geology of Alabama's Black Warrior Basin: Oil and Gas Journal, v.81, p. 147-154.

Meijer, P. T., Govers, R., and Wortel, M. J. R., 1997, Forces controlling the present-day state of stress of the Andes: Earth and Planetary Science Letters, v. 148, p. 157-170.

Mellen, F. F., 1947, Black Warrior Basin, Alabama and Mississippi: American Association of Petroleum Geologists Bulletin, v. 31, p. 1801-1816.

Miall, A. D., and Blakey, R. C., 2008, The Phanerozoic tectonic and sedimentary evolution of North America, *in* Miall, A. D. eds., Sedimentary Basins of United States and Canada: Elsevier, Amsterdam p. 1-29.

Michael, A. J., 1984, Determination of stress from slip data: Faults and folds: Journal of Geophysical Research: Solid Earth, v. 89, no. B13, p. 2156-2202.

Nance, R. D., and Linnemann, U., 2008, The Rheic ocean: Origin, evolution, and significance: GSA Today, v. 18, no. 12, p. 4–12.

Narr, W., Schechter, D. S., and Thompson, L. B., 2006, Naturally Fractured Reservoir Characterization. Society of Petroleum Engineers, Richardson, Texas, USA, 115 p.

Neathery, T. L., and Copeland, C. W., 1983, New information on the basement and lower Paleozoic stratigraphy of north Alabama: Geological Survey of Alabama Open-File Report, Tuscaloosa, 28 p.

Pashin, J. C., 1991, Subsurface models of coal occurrence, Oak Grove field, Black Warrior basin, Alabama: Tuscaloosa, Alabama, The University of Alabama, College of Continuing Studies, 1991 Coalbed Methane Symposium Proceedings, p. 275-291.

Pashin, J. C., 2004, Cyclothems of the Black Warrior basin, Alabama, U.S.A.: Eustatic snapshots of foreland basin tectonism, *in* J. C. Pashin and R. A. Gastaldo, eds., Sequence stratigraphy, paleoclimate, and tectonics of coal–bearing strata: American Association of Petroleum Geologists Studies in Geology 51, Tulsa, Oklahoma, p. 199–217.

Pashin, J. C., and Groshong, R. H., Jr., 1998, Structural control of coalbed methane production in Alabama: International Journal of Coal Geology, v. 38, p. 89–113.

Pashin, J. C. and R. A. Gastaldo, 2009, Carboniferous of the Black Warrior basin, *in* Greb., S. F., and Chesnut, D. R., eds., Carboniferous Geology and Biostratigraphy of the Appalachian Basin: Kentucky Geological Survey Special Publication 10, p. 10-21.

Pashin, J. C., Carroll, R. E., Hatch, J. R., and Goldhaber, M. B., 1999, Interplay among cleating, maturation, and mineralization in coalbed methane reservoirs of the Black Warrior basin: Tuscaloosa, Alabama, University of Alabama, College of Continuing Studies, 1999 International Coalbed Methane Symposium Proceedings, p. 367-375.

Pashin, J. C., Groshong, R. H., Jr., and Wang, S., 1995, Thin-skinned structures influence gas production in Alabama coalbed methane fields, *in* Intergas'95, International Unconventional Gas Symposium: Tuscaloosa, Alabama, University of Alabama College of Continuing Studies, p. 39-52.

Pashin, J. C., Jin, G., and Payton, J. W., 2004, Three-dimensional computer models of natural and induced fractures in coalbed methane reservoirs of the Black Warrior basin: U.S. Geological Survey of Alabama Bulletin, v. 174, 66 p.

Pashin, J. C., Ward, W. E., II, Winston, R. B., Chandler, R. V., Bolin, D. E., Richter, K. E., Osborne, W. E., and Sarnecki, J. C., 1991, Regional analysis of the Black Creek-Cobb coalbed-methane target interval, Black Warrior basin, Alabama: Alabama Geological Survey Bulletin, v. 145, 127 p.

Pitman, J. K., Pashin, J. C., Hatch, J. R., and Goldhaber, M. B., 2003, Origin of minerals in joint and cleat systems of the Pottsville Formation, Black Warrior basin, Alabama: implications for coalbed methane generation and production: American Association of Petroleum Geologists Bulletin, v. 87, p. 713-731.

Pollard, D. D., Saltzer, S. D., and Rubin, A. M., 1993, Stress inversion methods: are they based on faulty assumptions?: Journal of Structural Geology, v. 15, p. 1045-1054.

Raymond, D. E., 1991, New subsurface information on Paleozoic stratigraphy of the Alabama fold and thrust belt and the Black Warrior basin: Geological Survey of Alabama Bulletin 143, 185 p.

Raymond, D. E., Osborne, W. E., Copeland, C. W., and Neathery , T. L., 1988, Alabama stratigraphy: Alabama Geological Survey Circular 140, 97 p.

Reinecker, J., Tingay, M., and Müller, B., 2003, Borehole breakout analysis from four-arm caliper logs. Guidelines: Four-arm Caliper Logs: World Stress Map Project, 5 p.

Richardson, R.M., 1992. Ridge forces, absolute plate motions, and the intraplate stress field, Journal of Geophysical Research, v. 97, p. 11739-11748.

Robinson, D. M., Bailey, R. M., and Goodliffe, A. M., 2012, Structure of the Alleghanian thrust belt under the Gulf Coastal Plain of Alabama: Gulf Coast Association of Geological Societies Journal, v. 1, p. 44-54.

Rutter, R. S., 2012, A geophysical characterization of stratigraphy in the eastern Black Warrior Basin underlying Gorgas Power Generation Plant, Walker county, Alabama: M.S. thesis, The University of Alabama, Tuscaloosa, AL, 80 p.

Sbar, M. L., and Sykes, L. R., 1973, Contemporary compressive stress and seismicity in eastern North America: an example of intra-plate tectonics: Geologic Society of America Bulletin, v. 84, p.1861-1882.

Schlumberger (Schlumberger), 2002, FMI Borehole Geology, Geomechanics and 3D Reservoir Modeling, 12 p.

Solomon, S. C., Sleep, N. H., and Richardson, R. M., 1975, On the forces driving plate tectonics: Inferences from absolute plate velocities and intraplate stress: Geophysical Journal of the Royal Astronomical Society, v. 42, no. 2, p. 769-801.

Soroush, H., 2010, Importance of Petrophysical logging data to geomechanical analysis: 2010 Annual SPWLA presentation, 46 p.

Steinberger, B., Schmeling, H., and Marquart, G., 2001, Large-scale lithospheric stress field and topography induced by global mantle circulation: Earth and Planetary Science Letters, v. 186, p. 75-91.

Thomas, W. A., 1972, Mississippian stratigraphy of Alabama: Alabama Geological Survey Monograph, v. 12, 121 p.

Thomas, W. A., 1976, Evolution of Ouachita-Appalachian continental margin: American Journal of Science, v. 277, p. 1233–1278.

Thomas, W. A., 1977, Evolution of Appalachian-Ouachita salient and recesses from reentrants and promontories in the continental margin: American Journal of Science, v. 277, p. 1233–1278.

Thomas, W. A., 1985, The Appalachian-Ouachita connection: Paleozoic orogenic belt at the southern margin of North America: Annual Review of Earth and Planetary Sciences, v. 13, p. 175–199.

Thomas, W. A., 1988, The Black Warrior basin, *in* Sloss, L. L., eds., Sedimentary cover—North American craton: U. S. Geological Society of America, The Geology of North America, v. D-2, p. 471-492, Plate 8.

Thomas, W. A., 1989, The Appalachian-Ouachita orogen beneath the Gulf Coastal Plain between the outcrops in the Appalachian and Ouachita Mountains, *in* Hatcher, R. D. Jr., W. A. Thomas, and Viele, G. W., eds., The Appalachian-Ouachita Orogen in the United States. Boulder, Colorado, Geological Society of America, The Geology of North America, v. F-2, p. 537-554.

Thomas, W. A., 1991, The Appalachian-Ouachita rifted margin of southeastern North America: Geological Society of America Bulletin, v. 103, p. 415–431.

Thomas, W.A., 2004, Genetic relationship of rift-stage crustal structure, terrane accretion, and foreland tectonics along the southern Appalachian-Ouachita orogen: Journal of Geodynamics, v. 37, p. 549-563.

Thomas, W. A., 2011, The Iapetan rifted margin of southern Laurentia: Geosphere, v. 7, p. 97 – 120.

Thomas, W. A., and Bayona, G., 2002, Palinspastic restoration of the Anniston transverse zone in the Appalachian thrust belt, Alabama: Journal of Structural Geology, v. 24, no. 4, p. 797-826.

Thomas, W. A., and Mack, G. H., 1982, Paleogeographic relationship of a Mississippian barrier island and shelf-bar system (Hartselle Sandstone) in Alabama to the Appalachian-Ouachita orogenic belt: Geological Society of America Bulletin, v. 93, p. 6-19.

Tingay, M. R. P., Hillis, R. R., Morley, C. K., King, R. C., Swarbrick, R. E. and Damit, A. R., 2009, Present-day stress and neotectonics of Brunei: implications for petroleum exploration and production: American Association of Petroleum Geologists Bulletin, v. 93, p. 75-100.

Tripathy, V., and Saha, D., 2013, Plate margin paleostress variations and intracontinental deformations in the evolution of the Cuddapah basin through Proterozoic: Precambrian Research, v. 235, p. 107-130.

Viele, G. W., and Thomas, W. A., 1989, Tectonic synthesis of the Ouachita orogenic belt, in R.D. Hatcher, Jr., W. A. Thomas, and B.W. Viele, eds., The geology of North America, v. F-2: The

Appalachian-Ouachita orogeny in the United States: Geological Society of America, Boulder, Colorado, p. 695-728.

Wang, S., 1994, Three-dimensional geometry of normal faults in southeastern Deerlick Creek coalbed methane field, Black Warrior Basin, Alabama [M.S. thesis]: Tuscaloosa, University of Alabama, 77 p.

Wang, S., Groshong, R. H., Jr., and Pashin, J. C., 1993, Thin-skinned normal faults in Deerlick Creek coalbed-methane field, Black Warrior Basin, Alabama, *in* Pashin, J. C., eds., New Perspectives on the Mississippian System of Alabama: Guidebook for the 30th Annual Field Trip: Alabama Geological Society, p. 69-78.

Ward, W. E., Drahovzal, J. A., and Evans, F. E., Jr., 1984, Fracture analyses in a selected area of the Warrior coal basin, Alabama: Alabama Geological Survey Circular v. 111, 78 p.

Whitaker, A. E., and Engelder, T., 2006, Plate-scale stress fields driving the tectonic evolution of the central Ouachita salient, Oklahoma and Arkansas, Geological Society of America Bulletin, v. 118, no. 5/6, p. 710-723.

Whiting, B. M., and Thomas, W. A., 1995, Three-dimensional controls on subsidence of a foreland basin associated with a thrust-belt recess: Black Warrior basin, Alabama and Mississippi: Geology, v. 22, p. 727-730.

Zoback, M.L., 1992. First and second order patterns of stress in the lithosphere: The World Stress Map Project, Journal of Geophysical Research, v. 97, p. 11703-11728.

Zoback, M.D., Moos, D., Mastin, L.G., and Anderson, R.N., 1985, Well bore breakouts and in situ stress: Journal of Geophysical Research, v. 90, p. 5523-5530.

Zoback M. L., and Zoback, M. D., 1989, Tectonic stress field of the continental U.S., *in* Pakiser, L., and Mooney, W., eds., Geophysical framework of the continental United States: Geological Society of America Memoir, v. 172, p. 523-539.